# Application of Hilbert Transform in Geophysics

by

Abdurrazag M. Ali Ushah

A thesis
presented to the University of Manitoba
in partial fulfillment of the
requirements for the degree of
Master Of Science In Geophysics
in
Earth Science Department

Winnipeg, Manitoba

ISBN 0-315-34002-9

# APPLICATION OF HILBERT TRANSFORM IN GEOPHYSICS

BY

ABDURRAZAG M. ALI USHAH

A thesis submitted to the Faculty of Graduate Studies of
the University of Manitoba in partial fulfillment of the requirements
of the degree of

MASTER OF SCIENCE

I hereby declare that I am the sole author of this thesis.

I authorize the University of Manitoba to lend this thesis to other institutions or individuals for the purpose of scholarly research.

Abdurrazag M. Ali Ushah

I further authorize the University of Manitoba to reproduce this thesis by photocopying or by other means, in total or in part, at the request of other institutions or individuals for the purpose of scholarly research.

Abdurrazag M. Ali Ushah

The University of Manitoba requires the signatures of all persons using or photocopying this thesis. Please sign below, and give address and date.

## ABSTRACT

This thesis presents an analytical and numerical study of the one and two-dimensional Hilbert transform method, three-dimensional potential field data interpretation ( gravity and magnetic ), and two-dimensional seismic signal analysis, applied to selected geophysical problems such as filtering.

In the one-dimensional case the basic relations of Hilbert transforms are reviewed and derived. The data processing techniques using Hilbert transforms have been proved to be very useful, especially in magnetic, gravity and seismic data processing and, in some cases, modeling.

The theory of the two-dimensional Hilbert transform and three dimensional potential field data ( gravity and magnetic ) are reviewed and numerical algorithm package developed. Applications of 2-D Hilbert transform in quantitative interpretation of magnetic and gravity anomalies as well as their derivatives are also investigated.

The vertical derivatives of magnetic anomaly and gravity effects due to prismatic and multiprismatic bodies are used to test the 2-D Hilbert transform techniques and horizontal derivative approach. An excellent result was achieved by using these relatively new techniques in comparison with the

traditional methods. The Hilbert transformed digital maps of both gravity and magnetic data from the Sudbury area of Canada identify some of the real geological boundaries as reported in the previously published geological maps of the area. The results with theoretical and real data indicate that the 2-D Hilbert transform techniques can, in a robust fashion, be utilized, as a first step towards the 3-D geophysical imaging.

ACKNOWLEDGEMENTS

The author is greatly indebted to Dr. W. Moon for proposal of the point of study, supervision, and continuous encouragement during the course of this work.

Appreciation should also be extended to my fellow students Mr. Allan Carswell and Mr. Chris Dillistone for their help. Also I would like to express my appreciation to Dr. D.H. Hall, Head of the Department of Earth Sciences.

## LIST OF SYMBOLS

$j = (-1)^{1/2}$, ( and also represents an integer ).
$\omega$ = angular frequency ( = $2\pi f$ ).
$\mathcal{F}$ = Fourier transform operator.
$f_c$ = cut-off frequency.
$\omega c$ = cut-off angular frequency ( = $2\pi f_c$ ).
fc = complex function.
tc = complex time .
$\mathcal{P}$ = the Cauchy principle value.
P(i) = finite causal pulse.
Pe(i) = even part of P(i).
Po(i) = odd part of P(i).
sgn = signum function.
$\mathcal{I}$ = instantaneous frequency.
$\mathcal{O}$ = instantaneous phase.
$\mathcal{M}$ = minimum phase angle
DFT = Discrete Fourier transform.
IDFT = Inverse Discrete Fourier transform.
$\delta$ = delta function.
$\mathcal{S}$ = complex sequence in frequency domain.
$\mathcal{s}$ = complex sequence in time domain
H = Hilbert transform in frequency domain.
ht = continuous Hilbert transform in time domain.
Dht = discrete Hilbert transform in time domain.
DH = discrete Hilbert transform in frequency domain.
htr = truncation of Hilbert transform by box-car function in time domain.
Htr = htr in frequency domain.
$\dot{w}$ = time window function.
V = vertical magnetic effect.
Q = the polarization angle.
$\mathcal{Q}(\omega)$ = Fourier transform of real function q(t).
$h_1$ = depth to the top of the body ( H1 ) ( finite depth extent ).
$h_2$ = depth to the bottom of the body ( H2 ) ( finite depth extent ).
h = depth to the top of the body ( H1 ) ( infinite depth extent ).
$\bar{I}$ = the intensity of magnetization.
d = the dip angle
$\Delta F$ = the total field of magnetic anomaly.
$\emptyset$ = strike angle.
Ph = phase angle.
I = the inclination of the normal geomagnetic field.
K = magnetic susceptibility contrast.
G = the gravitational constant.
$\rho$ = the density contrast.
Fig. = figure.

Figs. = figures.
$I_p$ = the polarization magnitude.

TABLE OF CONTENTS

# CHAPTER 1

## INTRODUCTION

This thesis is concerned with application of Hilbert integral transform and associated problems on two and three-dimensional potential field data ( gravity and magnetic ) and on the two-dimensional (2-D) seismic signal analysis.

After the development of one-dimensional (1-D) Hilbert transform was made by Gold and Read (1969); Cizek (1970), this transform has found more and more applications in theory and practice of digital signal processing. The fundamental relations of 1-D Hilbert transform are reviewed and derived. These relations have become very significant, especially, in Geophysics applications.

In 2-D magnetic data application, I am going to discuss two methods; the first one ( Mohan et al., 1982 ) uses the point of intersections between the vertical magnetic effect of anomalous bodies and its Hilbert transform, several models are tested with different polarization angle (Q), and the second method (Green and Stanley 1975 ; Izzeldin, 1983 ) deals with the magnetic anomaly and its Hilbert transform, envelope and phase of such an anomaly.

In gravity data processing, the physical parameters of a dipping fault can be easily obtained by using Fourier trans-

form, second horizontal derivative of the gravity effect of the dipping fault and its Hilbert transform. I have extended this method from the theoretical models to the field data using 1-D discrete Hilbert transform and cubicspline method. The gravity effect of a vertical fault will also be analysed as a special case of the dipping fault.

In seismic application, I will try to construct a seismic signal by using the complex envelope ( amplitude and phase ) of the same signal, which can be obtained by using a discrete Hilbert transform algorithm. The pulse I will discuss is the Berlage function ( Kulhanek and Klima, 1970 ), which has approximately the same characteristics of seismic wavelets. The minimum phase characteristics of a wavelet, which can be calculated by using Hilbert transform, has many uses. It may be used for feedback filtering such as inverse and recursive filtering. The discussion will also be extended to lowpass and bandpass filtering which can be directly expressed in terms of Hilbert transforms.

The extension of the 1-D Hilbert transform to 2-D case was probably first reported by Read and Treitel( 1973 ). Bose and Prabhu( 1979 ) derived another expression for 2-D Hilbert transform in cotangent, sine and matrix forms. Nabighian ( 1984 ) derived yet another form of 2-D case using 2-D signum function and he generalized the 1-D Cauchy-Riemann relations between the potential function and its Hilbert transform for the 2-D case. In the 2-D case, the Hilbert

transform is composed of two parts; one part acting on the X component and the other one on the Y component.

Development of 1-D Hilbert transform concept to the 2-D case is considered as a first step toward automatic interpretation of 3-D potential field data. One of the advantages of this approach is based on the fact that the horizontal and vertical derivatives of 3-D potential field data are the Hilbert transforms of each other ( Nabighian, 1983 ).

The Hilbert transform algorithm developed in this study was first tested with theoretical potential field data.

A closed expression developed for the gravitational attraction of a prism was derived by Nagy ( 1966a-b ) which is valid for any point outside of or on the boundary of the prism , and this was later modified by Goodacre ( 1972 ). The magnetic examples tested in this thesis were computed using the expressions of magnetic total field of a prism and multiprismatic bodies ( Bhattacharyya, 1964, 1980 )

The first and second vertical derivatives of the magnetic total field and gravity effects due to prismatic bodies were computed using the new techniques of 2-D Hilbert transform, and several examples were studied for various different situations. The application of these techniques was extended and tested with real data sets, where the digitized magnetic and gravity contour maps of the Sudbury area were studied in detail.

# CHAPTER 2

# ONE-DIMENSIONAL (1-D) HILBERT TRANSFORM

## 2.1 INTRODUCTION

The development of the one-dimensional(1-D) Hilbert transform is closely patterned after Gold and Rader (1969); Cizek (1970). The 1-D Hilbert transform is often defined as a quadrature filter which introduces a $90^0$ phase shift. In a complex function the real and imaginary parts are related together through the Hilbert transform.

In almost every field where Fourier transform techniques are used to represent and analyze physical processes, one finds that there are situations where there exist relationships between the real and imaginary parts or the magnitude and phase of the Fourier transform. These relationships are frequently represented by one form or other of the Hilbert transform relations.

In this chapter we shall derive and review a number of such relationships that are important in both the theory and application of digital geophysical data processing. We shall see, for example, that if a sequence is causal, then the real and imaginary part of its Fourier transform or the even and odd components of the function are related by a Hilbert transform. Such a transform can be used in constructing the envelope and phase of a time function.

The task of designing a 1-D Hilbert transform with different length operators and several windows such as Hamming, Triangular, and Blackman windows is always to obtain the best approximation to the exact transform.

## 2.2 1-D HILBERT TRANSFORM EQUATIONS

In this section we will review some relations before attempting to derive Hilbert transform equation in integral form which is considered as a starting point of discrete Hilbert transform algorithm. Recent years, the Hilbert transform has found more and more applications in theory and practice of digital signal processing.

As we know the Fourier transform of a function f(t) is $F(\omega)$, then;

$$F(\omega) = \int_{-\infty}^{\infty} f(t)\, \exp(-j\omega t)\, dt \quad \text{for all } \omega \qquad 2.2\text{-}1$$

and

$$f(t) = (1/2\pi) \int_{-\infty}^{\infty} F(\omega)\, \exp(j\omega t)\, d\omega \quad \text{for all } t \qquad 2.2\text{-}2$$

but equation ( 2.2-1 ) may also be written as;

$$F(\omega) = \int_{-\infty}^{\infty} f(t)(\cos \omega t - j \sin \omega t)dt \qquad 2.2\text{-}3$$

where;

$$\exp(-j\omega t) = \cos \omega t - j \sin \omega t.$$

Then

$$F(\omega) = \int_{-\infty}^{\infty} f(t) \cos \omega t\, dt - j \int_{-\infty}^{\infty} f(t) \sin \omega t\, dt \qquad 2.2\text{-}4a$$

So equation ( 2.2-4a ) takes the following form;

$$F(\omega) = Fr(\omega) - j\, Fi(\omega)$$

where, $Fr(\omega)$ and $Fi(\omega)$ are the real and imaginary parts of the equation ( 2.2-4a ), such that

$$Fr(\omega) = \int_{-\infty}^{\infty} f(t) \cos \omega t \, dt \quad \text{and}$$

$$Fi(\omega) = \int_{-\infty}^{\infty} f(t) \sin \omega t \, dt. \qquad 2.2\text{-}4b$$

It also follows that

$$F(-\omega) = Fr(\omega) + j\, Fi(\omega) \qquad 2.2\text{-}5$$

because

$$Fr(-\omega) = Fr(\omega) \quad ( \text{ even function } )$$

$$\text{and} \quad Fi(-\omega) = - Fi(\omega) \quad ( \text{ odd function } )$$

Therefore we should be able to write

$$Fr(\omega) = (F(\omega) + F(-\omega))/2 \qquad 2.2\text{-}6a$$

$$Fi(\omega) = j(F(\omega) - F(-\omega))/2 \qquad 2.2\text{-}6b$$

From equation ( 2.2-2 ), the inverse Fourier transform may be divided into regions of positive and negative frequency,

$$f(t)=(1/2\pi) \int_{-\infty}^{0} F(\omega) \exp(j\omega t) \, d\omega + (1/2\pi) \int_{0}^{\infty} F(\omega) \exp(j\omega t) \, d\omega$$

$$=(1/2\pi) \int_{0}^{\infty} F(-\omega) \exp(-j\omega t) \, d\omega + (1/2\pi) \int_{0}^{\infty} F(\omega) \exp(j\omega t) \, d\omega \qquad 2.2\text{-}7$$

upon substituting equation (2.2-6), we have equations with positive frequency only

$$f(t) = (1/\pi) \int_{0}^{\infty} Fr \cos \omega t \, d\omega + (1/\pi) \int_{0}^{\infty} Fi \sin \omega t \, d\omega \qquad 2.2\text{-}8$$

This may be written in terms of a complex time $tc = t + j\sigma$

$$\lim_{\sigma \to 0} f(t) = \lim_{\sigma \to 0} \pi^{-1} \int_0^{\infty} (Fr \cos \omega t + Fi \sin \omega t) \exp(-\sigma\omega)\, d\omega \qquad 2.2\text{-}9$$

Next let us define a complex function;

$$fc = f(t,\sigma) - j\, f_H(t,\sigma) \qquad 2.2\text{-}10$$

such that the complex function is made of the original real part, f(t), and a part called the quadrature function, $f_H(t)$, which will be shown to be the Hilbert transform of f(t). The quadrature is defined so that it introduces a $90^0$ phase shift because we will sometimes want to use it to obtain the envelope of the real time function. Therefore, sines are converted to cosines and cosines are converted to negative sines in equation (2.2-8);

$$f_H(t,0) = (1/\pi) \int_0^{\infty} (Fi \cos \omega t - Fr \sin \omega t)\, d\omega \qquad 2.2\text{-}11$$

and

$$fc(t,\sigma) = (1/\pi) \int_0^{\infty} [Fr(\omega) - j\, Fi(\omega)] \exp(j\omega t) \exp(-\sigma\omega)\, d\omega \qquad 2.2\text{-}12$$

Substitution of Fr and Fi from equation (2.2-4b) into the equation (2.2-11) will relate $f_H$ and f more clearly.

$$f_H(t) = (1/\pi) \int_0^{\infty} \int_{-\infty}^{\infty} [f(T) \sin \omega T \cos \omega t - f(T) \cos \omega T \sin \omega t\, ]\, dT\, d\omega$$

$$= \lim_{\omega' \to \infty} (1/\pi) \int_0^{\omega'} \int_{-\infty}^{\infty} f(T) \sin \omega(T-t)\, dT\, d\omega \qquad 2.2\text{-}13$$

Integrating first with respect to dω we obtain;

$$f_H(t) = \lim_{\omega' \to \infty} (1/\pi)\, \mathbb{P} \int_{-\infty}^{\infty} f(T)((1-\cos \omega'(T-t))/(T-t))\, dT \qquad 2.2\text{-}14$$

where, $\mathbb{P}$ indicates the Cauchy principal value. It can be shown that;

$$\lim_{\omega' \longrightarrow \infty} (1/\pi)\ \mathbb{P} \int_{-\infty}^{\infty} f(T)(\cos \omega'(T-t))/(T-t)\ dT = 0 \qquad 2.2\text{-}15$$

Using the Riemann-Lebesque Lemma we have;

$$f_H(t) = -\ (1/\pi)\ \mathbb{P} \int_{-\infty}^{\infty} f(T)/(t - T)\ dT \qquad 2.2\text{-}16$$

Equation (2.2-16) is known as the Hilbert transform in integral form. Substitution of Fr and Fi from equation (2.2-6) into equation (2.2-11) gives

$$f_H(t) = (j/2\pi) \int_{0}^{\infty} [F(\omega) - F(-\omega)] \cos \omega t\ d\omega$$

$$- (1/2\pi) \int_{0}^{\infty} [F(\omega) + F(-\omega)] \sin \omega t\ d\omega$$

$$= (j/2\pi) \int_{0}^{\infty} [F(\omega) \exp(j\omega t) - F(-\omega) \exp(-j\omega t)]\ d\omega \qquad 2.2\text{-}17$$

$$= (1/2\pi) \int_{0}^{\infty} j\ F(\omega) \exp(j\omega t)\ d\omega$$

$$- (1/2\pi) \int_{-\infty}^{\infty} j\ F(\omega) \exp(j\omega t)\ d\omega. \qquad 2.2\text{-}18$$

If we let

$$F_H(\omega) = j\ F(\omega)\ \text{sgn}\ \omega \qquad 2.2\text{-}19$$

where sgn is a signum function

$$\text{sgn}\ \omega = \begin{pmatrix} 1 & \omega > 0 \\ 0 & \omega = 0 \\ -1 & \omega < 0 \end{pmatrix} \qquad 2.2\text{-}20$$

Then equation (2.2-18) shows that $f_H$ and $F_H$ are inverse Fourier transforms

$$f_H(t) = \int F_H(\omega) \exp(j\omega t)\ d\omega \qquad 2.2\text{-}21$$

From equations (2.2-19) and (2.2-11) it is also possible to obtain the inverse Hilbert transform.

$$f(t) = (1/\pi)\ \mathbb{P} \int_{-\infty}^{\infty} [f_H(T)/(t-T)]\ dT \qquad 2.2\text{-}22$$

In equation (2.2-19) we can define a Fourier transform, $Q(\omega)$ as

$$Q(\omega) = j\ \text{sgn}\ \omega \qquad 2.2\text{-}23$$

The Fourier series of $Q(\omega)$ is $q_n$

$$q_n(n\Delta t) = (1/2\pi) \int_{-\pi}^{\pi} Q(\omega)\ \exp(-j\omega n\Delta t)\ d\omega$$

$$= j(1/2\pi) \int_{-\pi}^{0} \exp(-j\omega n\Delta t) - j(1/2\pi) \int_{0}^{\pi} \exp(-j\omega n\Delta t)\ d\omega$$

$$= (1/2\pi)\ (-1 + \exp(jn\pi\Delta t) + \exp(-jn\pi\Delta t) - 1)$$

$$q_n(n\Delta t) = \begin{cases} 0 & n \text{ even} \\ -1/(\pi n\Delta t) & n \text{ odd} \end{cases} \qquad 2.2\text{-}24$$

As $\Delta t \longrightarrow 0$ the Fourier series becomes a Fourier integral and $n\Delta t$ becomes the continuous time variable t, i.e.,

$$q(t) = -1/(\pi t) \qquad 2.2\text{-}25$$

The function q(t) and its Fourier transform, $Q(\omega)$, are plotted in Fig. 2.1. By equation (2.2-19) the Hilbert transform in the frequency domain is given by the product of $F(\omega)$ and $Q(\omega)$.

$$F_H(\omega) = F(\omega)\ Q(\omega) \qquad 2.2\text{-}26$$

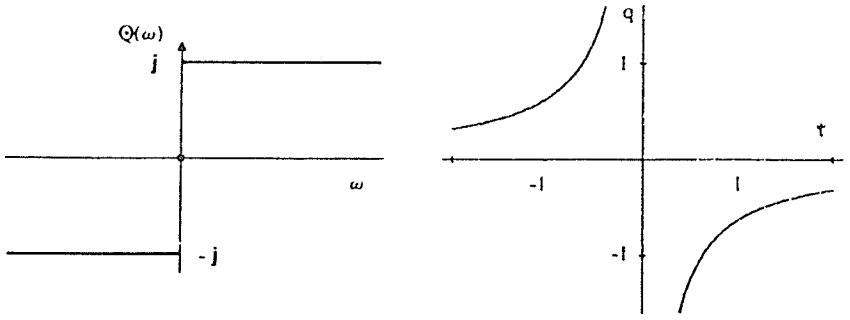


Fig. 2.1 Represents the function $Q(\omega)$ and its inverse transform, $q(t)$.

Table 1. Some simple functions and their Hilbert transforms.

| Function | Hilbert transform |
|---|---|
| $f(t)$ | $F_H(t)$ |
| $\delta(t)$ | $-1/(\pi t)$ |
| $f(t) = 1 \quad -1/2 \leq t \leq 1/2$ | $(1/\pi)$ Log $\lvert(t-1/2)/(t+1/2)\rvert$ |
| $= 0$ otherwise | |
| ( Box-car function ) | |
| sin t | cos t |
| cos t | - sin t |
| (sin t)/t | (cos t -1)/t |

By the convolution theorem it is possible to obtain the Hilbert transform in the time domain by convolving q(t) with f(t).

$$f_H(t) = q(t)*f(t) = (-\pi t)^{-1} * f(t) \qquad 2.2\text{-}27$$

Writing out the convolution indicated by the star in equation (2.2-27) we can obtain the equation (2.2-16) again. It can be also shown that if Hilbert transform is applied twice successively we should reverse all the phases in the Fourier harmonics and obtain the original function back

$$f(t) = -(-\pi t)^{-1} * f_H(t) = -(-\pi t)^{-1} * (-\pi t)^{-1} * f(t) \qquad 2.2\text{-}28$$

Hilbert transforms of few simple functions are listed in Table 1.

## 2.3 1-D HILBERT TRANSFORM RELATIONS IN WAVE ENVELOPE AND PHASE STUDY

The envelope, E, of any real function, f(t), can be obtained by taking the modulus of equation (2.2-10)

$$E(t) = [f^2(t) + f_H^2]^{1/2} = [fc\ fc^*]^{1/2} \qquad 2.3\text{-}1$$

The instantaneous phase, $\phi$,can be also given as a function of time( Bracewell, 1965).

$$\phi(t) = \arctan[f_H(t)/f(t)]\ . \qquad 2.3\text{-}2$$

The instantaneous frequency, $\phi(t)$, is obtained from the rate of change of phase. The complex function fc may then be written as follows:

$$fc = E(t)\ \exp[-j\phi(t)]. \qquad 2.3\text{-}3$$

Solving for the phase we have

$$\phi = j\ \log\ fc/E(t). \qquad 2.3\text{-}4$$

Letting

$$Fc = fc/E \qquad 2.3\text{-}5$$

and differentiating with respect to t, yields the instantaneous frequency

$$\phi(t) = d\phi/dt = j(dFc/dt)/Fc \qquad 2.3\text{-}6$$

Following Claerbout ( 1976 ) this may be approximated by the imaginary part, Im, of the difference equation;

$$\phi(t_i) \equiv Im[2\{Fc(t_i)-Fc(t_{i-1})\}/\{\Delta t\ (Fc(t_i)+Fc(t_{i-1})\}] \qquad 2.3\text{-}7$$

where, $i = 0, 1, 2, 3, \ldots\ldots\ldots\ldots$

The instantaneous frequency is useful for functions that show dispersion. It is often used in reflection seismology to detect zones of interference indicating rapid changes in the elastic impedance in the earth.

## 2.4 THE MINIMUM PHASE CONCEPT

A linear system is said to be physically realizable and its impulse response is said to be causal if it vanishes for negative time

$$f(t) = 0 \qquad t < 0 \qquad 2.4\text{-}1$$

As we know, any function can be expressed as the sum of an even and odd function.

$$f(t) = fe(t) + fo(t) \qquad 2.4\text{-}2$$

$$= [f(+t) + f(-t)]/2 + [f(+t) - f(-t)]/2 \qquad 2.4\text{-}3$$

But from equation (2.4-1), we have

$$fe(t)=-fo(t) \text{ for } t < 0 \text{ and } fe(t)=fo(t) \text{ for } t > 0 \qquad 2.4\text{-}4$$

for a physically realizable linear system. Therefore, for causal signals, we can introduce the signum function such that

$$fe(t) = fo(t) \operatorname{sgn} t \text{ and } fo(t) = fe(t) \operatorname{sgn} t \qquad 2.4\text{-}5$$

Similarly, the real part of the Fourier transform of $F(\omega)$ is even while the imaginary part is odd;

$$Fe(\omega) = (-j/\pi)\ \mathbb{P} \int_{-\infty}^{\infty} [Fo(W)/(\omega-W)]\ dW = Fr(\omega)$$
$$Fo(\omega) = (-j/\pi)\ \mathbb{P} \int_{-\infty}^{\infty} [Fe(W)/(\omega-W)]\ dW = j\ Fi(\omega) \qquad 2.4\text{-}6$$

Thus as a result of (2.4-5) and because of the similarity between $F(\omega)$ in equation (2.2-19) and the even and odd properties of $F(\omega)$, the real and imaginary parts of a causal function are indeed Hilbert transforms;

$$Fr(\omega) = (1/\pi)\ \mathbb{P} \int_{-\infty}^{\infty} [Fi(W)/(\omega-W)]\ dW \qquad 2.4\text{-}7$$

$$Fi(\omega) = (1/\pi)\ \mathbb{P} \int_{-\infty}^{\infty} [Fr(W)/(\omega-W)]\ dW. \qquad 2.4\text{-}8$$

The transfer function may be written as

$$Y(\omega) = |Y(\omega)|\ \exp[j\emptyset(\omega)]. \qquad 2.4\text{-}9$$

Taking log of both sides, we have

$$\text{Log}\ Y(\omega) = \text{Log}\ |Y(\omega)| + j\emptyset(\omega). \qquad 2.4\text{-}10$$

If the impulse response is a causal function it follows that we can compare Log $Y(\omega)$ to $F(\omega)$ in equation (2.2-4b). Thus Log $|Y(\omega)|$ and $\emptyset(\omega)$ are Hilbert transforms just as $Fr(\omega)$ and $Fi(\omega)$ in equations (2.4-7) and (2.4-8).

$$\text{Log}\ |Y(\omega)| = -(1/\pi)\ \mathbb{P} \int [\emptyset(T)/(T-\omega)]\ dT \qquad 2.4\text{-}11$$

$$\emptyset(\omega) = (1/\pi)\ \mathbb{P} \int [\text{Log}\ |Y(\omega)|/(T-\omega)]\ dT \qquad 2.4\text{-}12$$

The Log of the transfer function, $Y(\omega)$, must be analytical and bounded in the lower half of the z-plane. That is , the lower half plane must have no poles or zeros so that it will be a minimum phase system.

## 2.5 1-D DISCRETE HILBERT AND FOURIER TRANSFORM RELATIONS

The discrete Fourier transform( DFT ) has played an important role in many aspects of geophysical data processing. Thus $P(i) = P(i + kN)$ for any integer k, where i is a running index, and $P(i)$ is the ith sampled value of a discrete pulse series.

A finite discrete pulse series $P(i)$ $(i = 0,1,.....,N-1)$ is causal if over one period of length N,

$$P(i) = 0 \quad \text{for} \quad i \geq N/2 \qquad 2.5\text{-}1$$

Then any finite discrete pulse can be made to satisfy this condition by choosing an appropriate N and appending zeros. As an example we shall study a pulse $P(i)$ which has the form of Berlage function often used to simulate seismic signals ( Kulhanek and Klima, 1970)

$$P(i) = \begin{cases} 0, & 0 > i \geq N/2 \\ i^2 \exp(2-2i)\sin(2\pi i) & 0 \leq i < N/2 \end{cases} \qquad 2.5\text{-}2$$

This pulse is given in Fig. 2.2a for the case N = 120. The even and odd parts of a finite discrete function are given by

$$\begin{cases} Pe(i) = (1/2)[P(i) + P(N-i)] \\ Po(i) = (1/2)[P(i) - P(N-i)] \end{cases} \qquad 2.5\text{-}3$$

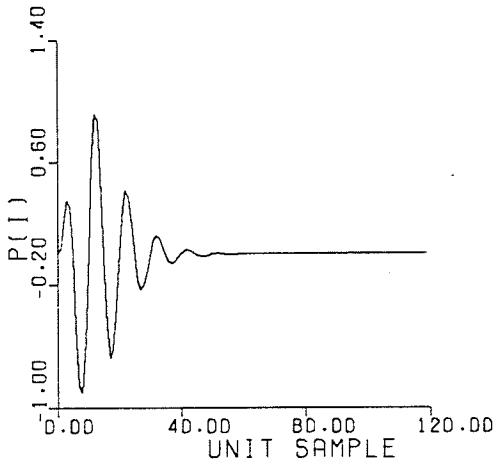


a

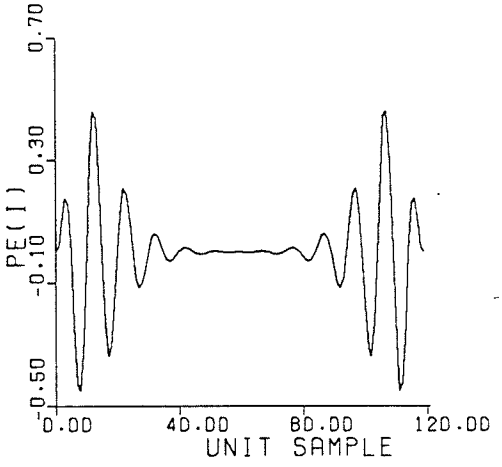


b

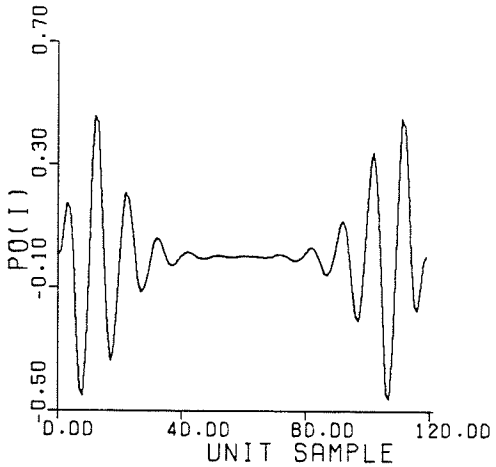


c

Fig. 2.2 (a) The Berlage function as impulse response, (b) and (c) are the even and odd parts of the Berlage function, respectively.

The even and odd parts of Berlage function are shown in Fig. 2.2b-c, Thus for a finite discrete causal pulse, one has

$$Pe(i) = Pe(N - i) \quad (\text{ even symmetry }) \qquad 2.5\text{-}4$$

$$Po(i) = - Po(N - i) \quad (\text{ odd symmetry }) \qquad 2.5\text{-}5$$

From these equations, it follows that the odd and even parts of the pulse P(i) are related by

$$Pe(i) = sgn(i)\ Po(i) + P(i)\delta_N(i) \qquad 2.5\text{-}6$$

$$Po(i) = sgn(i)\ Pe(i) \qquad 2.5\text{-}7$$

where $\delta_N(i)$ is the modulo $N$ Kronecker delta,

$$\delta_N(i) = \begin{pmatrix} 1 & \text{for} \quad i = kN, \quad k = \text{any integer} \\ 0 & \text{otherwise} \end{pmatrix} \qquad 2.5\text{-}8$$

and where

$$sgn(i) = \begin{pmatrix} 0 & i = 0,\ N/2 \\ 1 & 0 < i < N/2 \\ -1 & N/2 < i < N \end{pmatrix}. \qquad 2.5\text{-}9$$

Table 2. Transform Relations

| P(i) | <——> | DFT(P(i)) |
|---|---|---|
| even | | even |
| odd | | odd |
| even and real | | even and real |
| odd and real | | odd and imaginary |
| real | | real part even, imaginary part odd |
| imaginary | | real part odd, imaginary part even |
| even and imaginary | | even and imaginary |
| odd and imaginary | | odd and real |

The above equations can be used to relate the real and imaginary parts of the Fourier transform of a finite discrete causal pulse. In order to do so, we require the symmetry relations given in Table 2 (see e.g. Gold and Rader, 1969, p.169).

The relations given in the Table 2 and equations (2.5-6) and (2.5-7) allow us to derive the relation between the real and imaginary parts of the discrete Fourier transform of the finite discrete causal pulse, P(i). The letters DFT and IDFT will be used to denote the discrete Fourier transform and the inverse discrete Fourier transform, respectively;

$$DFT(P(i)) = \sum_{n=0}^{N-1} W^{ni} P(n) \qquad 2.5\text{-}10a$$

where

$$W = \exp[j(2\pi/N)], \text{ and } j = (-1)^{1/2}.$$

$$IDFT[DFT(P(i))] = (1/N)[\sum_{n=0}^{N-1} W^{-ni} P(n)]. \qquad 2.5\text{-}10b$$

From equation (2.5-3) we obtain

$$P(i) = Po(i) + Pe(i) \qquad 2.5\text{-}11$$

Transforming this equation we have

$$DFT(P(i)) = DFT(Po(i)) + DFT(Pe(i)). \qquad 2.5\text{-}12$$

Both Po(i) and Pe(i) are real. From Table 2, we see that DFT(Po(i)) is odd and imaginary, while DFT(Pe(i)) is even and real. Thus

$$PR(i) = DFT(Pe(i)) \qquad 2.5\text{-}13a$$

$$PI(i) = -j\ DFT(Po(i)) \qquad 2.5\text{-}13b$$

where PR(i) and PI(i) are the real and imaginary parts of DFT[P(i)], respectively. Since the result of transforming a real and odd pulse Po(i) is purely imaginary ( see Table 2 ), the multiplication by -j in equation (2.5-13b) results in a real quantity PI(i). Inverse transformation of these equations yields:-

$$Pe(i) = IDFT(PR(i)), \text{ and } Po(i) = IDFT(jPI(i)). \qquad 2.5\text{-}14$$

Inserting equation (2.5-14) into the right-hand sides of equation (2.5-6) we obtain:-

$$Pe(i) = sgn(i)\ IDFT(jPI(i)) + P(i)\ \delta_N(i) \qquad 2.5\text{-}15a$$

$$Po(i) = sgn(i)\ IDFT(PR(i)). \qquad 2.5\text{-}15b$$

Direct transformation of both sides of equation (2.5-15a) together with use of equations (2.5-13a-b) gives

$$PR(i) = DFT(sgn(i)\ IDFT(jPI(i)) + P(i)\ \delta_N(i) \qquad 2.5\text{-}16a$$

$$PI(i) = -j\ DFT(sgn(i)\ IDFT(PR(i)) \qquad 2.5\text{-}16b$$

Equations (2.5-16a-b) relate the real and imaginary parts of the DFT of a finite causal pulse. In this respect, equations (2.5-16a-b) are similar to the Integral Hilbert transform equations that relate the real and imaginary parts of the integral.

## 2.6 1-D HILBERT TRANSFORM RELATIONS FOR COMPLEX SEQUENCES

In the proceeding sections we have considered Hilbert transform relations for the Fourier transform of causal sequences and the discrete Fourier transform of periodic sequences which are "causal" in the sense that they are zero in the second half of each period. In this section we will investigate complex sequences for which the real and imaginary components can be related through a convolution similar to the Hilbert transform relations derived in the previous sections.

It is possible to base the derivation of the Hilbert transform relations on the notion of causality as in the previous discussions. Since we are interested in relating the real and imaginary parts of a complex sequence, "causality" will be applied to the Fourier transform of the sequence. If we assume a discrete complex sequence $s(n)$ and its Fourier transform $S(\bar{\omega})$ where $\bar{\omega} = \exp(j\omega)$, then, the "causality" can be defined as

$$S(\bar{\omega}) \equiv 0, \quad -\pi \leq \omega < 0 \quad \text{( Oppenheim, 1975 ).} \qquad 2.6\text{-}1$$

We can express $s(n)$ as

$$s(n) = sr(n) + j\, si(n) \qquad 2.6\text{-}2$$

where $sr(n)$ and $si(n)$ are real sequences. The Fourier transform of $s(n)$ is denoted by $S(\bar{\omega})$, then;

$$S(\bar{\omega}) = Sr(\bar{\omega}) + j\, Si(\bar{\omega}) \qquad 2.6\text{-}3$$

where

$$\$r(\bar{\omega}) = [\$(\bar{\omega}) + \$^*(-\bar{\omega})]/2 \qquad 2.6\text{-}4$$

$$j\ \$i(\bar{\omega}) = [\$(\bar{\omega}) - \$^*(-\bar{\omega})]/2. \qquad 2.6\text{-}5$$

The complex transforms $\$r(\bar{\omega})$ and $\$i(\bar{\omega})$ play a role similar to even Pe and odd Po parts of a given pulse P as in previous section, where $\$r(\bar{\omega})$ is not an even function but is conjugate even; i.e., $\$r(\bar{\omega}) = \$r^*(-\bar{\omega})$, and similarly, $j\ \$i(\bar{\omega})$ is conjugate odd; i.e.; $\$i(\bar{\omega}) = -\ j\ \$i^*(-\bar{\omega})$.

If $\$(\bar{\omega})$ is 0 for $-\pi \leq \omega < 0$, then there is no overlap between the nonzero portions of $\$(\bar{\omega})$ and $\$^*(-\bar{\omega})$. Thus $\$(\bar{\omega})$ can be obtained from $\$i(\bar{\omega})$ or $\$r(\bar{\omega})$.

In particular,

$$\$(\bar{\omega}) = \begin{pmatrix} 2\ \$r(\bar{\omega}) & 0 \leq \omega < \pi \\ 0\ , & -\pi \leq \omega < 0 \end{pmatrix} \qquad 2.6\text{-}6$$

$$\$(\bar{\omega}) = \begin{pmatrix} 2\ j\ \$i(\bar{\omega}) & 0 \leq \omega < \pi \\ 0 & -\pi \leq \omega < 0 \end{pmatrix} \qquad 2.6\text{-}7$$

Therefore for $0 \leq \omega < \pi$, $2\ j\ \$i(\bar{\omega}) = 2\ \$r(\bar{\omega})$ or $\$i(\bar{\omega}) = -j\ \$r(\bar{\omega})$ and for $-\pi \leq \omega < 0$, $\$(\bar{\omega}) = 0$, which means from equations (2.6-4) and (2.6-5) $\$i(\bar{\omega}) = j\ \$r(\bar{\omega})$;

$$\$i(\bar{\omega}) = \begin{pmatrix} -\ j\ \$r(\bar{\omega}) & 0 \leq \omega < \pi \\ j\ \$r(\bar{\omega}) & -\pi \leq \omega < 0 \end{pmatrix} \qquad 2.6\text{-}8$$

In the other form $\$i(\bar{\omega}) = H(\bar{\omega})\ \$r(\bar{\omega})$, where:

$$H(\bar{\omega}) = \begin{pmatrix} -j, & 0 \leq \omega < \pi \\ j, & -\pi \leq \omega < 0 \end{pmatrix} \qquad 2.6\text{-}9$$

Thus according to the fact that we can obtain $si(n)$ from $sr(n)$ by using the operator ht(n), the frequency response of a system ht(n) has unity magnitude, a phase angle of $-\pi/2$ for $\omega$ between 0 and $\pi$, and $+\pi/2$ for $\omega$ between 0 and $-\pi$. Such a system is sometimes called Hilbert Transformer. To derive the impulse response ht(n) from $H(\bar{\omega})$ we have to use the inverse Fourier integral formula as follows

$$ht(n) = (1/2\pi)\left[\int_{-\pi}^{0} j\exp(j\omega n)\,d\omega - \int_{0}^{\pi} j\exp(j\omega n)\,d\omega\right]$$

$$= (2/\pi n)\sin^2(\pi n/2) \qquad n \neq 0$$

$$= 0 \qquad n = 0 \qquad \text{2.6-10}$$

From equation (2.6-8), we obtain the following relations

$$si(n) = \sum_{m=-\infty}^{\infty} sr(n-m)\,ht(m) \qquad \text{2.6-11}$$

$$sr(n) = -\sum_{m=-\infty}^{\infty} si(n-m)\,ht(m) \qquad \text{2.6-12}$$

The equations (2.6-11) and (2.6-12) represent 1-D Hilbert transform relations between real and imaginary parts of discrete-time analytic signal. And from section 2.4 we can represent $s(n)$ in terms of its magnitude and phase

$$|A(n)| = [sr^2(n) + si^2(n)]^{1/2} \qquad \text{2.6-13a}$$

$$\text{and} \quad Ph(n) = \arctan[si(n)/sr(n)] \qquad \text{2.6-13b}$$

where; $|A(n)|$ and Ph(n) are called the envelope and phase of a complex sequence $s(n)$, respectively.

## 2.7 TRUNCATION AND WINDOW EFFECTS

In the previous section, we introduced impulse response of 1-D Hilbert transform, which has a spectral distortion. In order to minimize distortion we can truncate the impulse response with a box-car function $\dot{w}(n)$ whose values is 1 over the required length (2N) and zero elsewhere. The function $\dot{w}(n)$, normally called the time window is defined by:-

$$\dot{w}(n) = \begin{pmatrix} 1 & -N < n < N \\ 0 & \text{elsewhere} \end{pmatrix} \qquad 2.7\text{-}1$$

If we assume htr(n) is truncated function, then;

$$htr(n) = ht(n)\ \dot{w}(n) \qquad 2.7\text{-}2$$

where ht(n) is the normalized impulse response of 1-D Hilbert transform. Using the convolution theorem, the Fourier transform $Htr(\omega)$ of the truncated function htr(n) is given by:

$$Htr(\omega) = (1/2\pi)\ H(\omega)*\dot{W}(\omega) \qquad 2.7\text{-}3$$

where $H(\omega)$ and $\dot{W}(\omega)$ are the Fourier transforms of ht(n) and $\dot{w}(n)$, respectively. However, since $\dot{W}(\omega) = (2/\omega)\ \sin(\omega N)$ we may write:

$$Htr(\omega) = (1/2\pi)\ H(\omega)*(2/\omega)\ \sin\ (\omega N) \qquad 2.7\text{-}4a$$

or

$$Htr(\omega) = (N/\pi) \int_{-\infty}^{\infty} H(p)[\sin N(\omega-p)/(N(\omega-p))]\ dp \qquad 2.7\text{-}4b$$

This means that truncating a signal brings about a spectrum modification which can be expressed by the convolution operation between the two functions $H(\omega)$ and $\dot{W}(\omega)$. This im-

plies that truncation introduces a smoothing effect of severity which depends on the window length. The shorter the window length is, the greater the degree of smoothing will be. The function $Htr(\omega)$ , is sometimes called average or the weighted spectrum ( Blackman and Tukey, 1959).

The truncation will introduce ripples of approximately the same height into the amplitude characteristics. This phenomenon is the well known Gibbs' phenomenon. To eliminate the ripples which is introduced by using a box-car function( rectangular window), the following different types of windows can be used:-

The triangular window;

$$Tr.\dot{w}(n) = \begin{pmatrix} 1 - |n|/N & \text{for } |n| \leq N \\ 0 & \text{for } |n| > N \end{pmatrix} \qquad 2.7\text{-}5$$

The Hamming window;

$$Hm.\dot{w}(n) = \begin{pmatrix} 0.54+0.46\cos(n\pi/N) & \text{for } |n| \leq N \\ 0 & \text{for } |n| > N \end{pmatrix} \qquad 2.7\text{-}6$$

The Blackman window;

$$Bl.\dot{w}(n) = \begin{pmatrix} 0.42+0.5\cos(n\pi/N)+0.08\cos(2\pi n/N) & \text{for } |n| \leq N \\ 0 & \text{for } |n| > N \end{pmatrix} \qquad 2.7\text{-}7$$

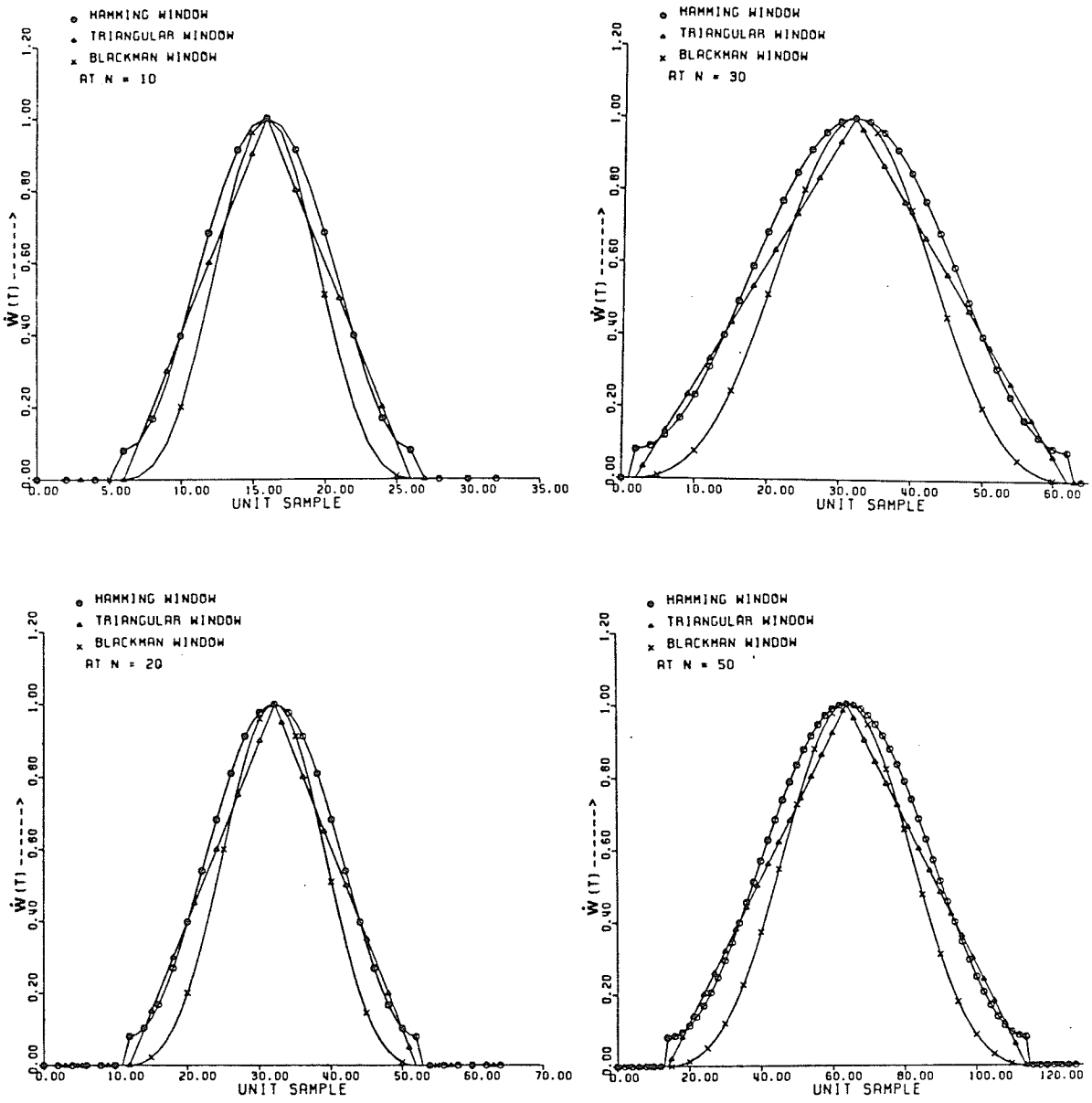


Fig. 2.3 Envelopes of various digital windows such as Triangular, Hamming and Blackman windows truncated at N = 10, 20, 30, and 50.

The envelopes of these windows are shown in Fig. 2.3 for different values of N. From the spectra of various digital windows, one can see that the triangular window has no negative lobe, and that the total area of the negative lobes in the Hamming or Blackman windows is very small compared with that of the positive lobes. In general, a time-window which tapers off gradually towards both ends of the signal, introduces less distortion than a window which has near-vertical ends. A least-distortive window should possess the following properties:-

1)- The time-interval must be as long as possible. This implies that the corresponding spectral window has its energy concentrated to its main lobe.

2)- The shape of the time-window must be as smooth as possible and free of sharp corners. The more smooth the window is, the smaller the side lobes of the corresponding spectral window become.

In addition to the effect introduced by the shape of the time-window, its length 2N plays an important role in the accuracy of the computed spectrum. Since the length of the time-window is equal to the length of the signal, the larger the signal length is, the better the resolution and the closer the computed spectrum to the true spectrum becomes. In fact, it is known that the entire (infinite ) length( i.e. $|2N| \longrightarrow \infty$) is required in order to obtain the full resolution.

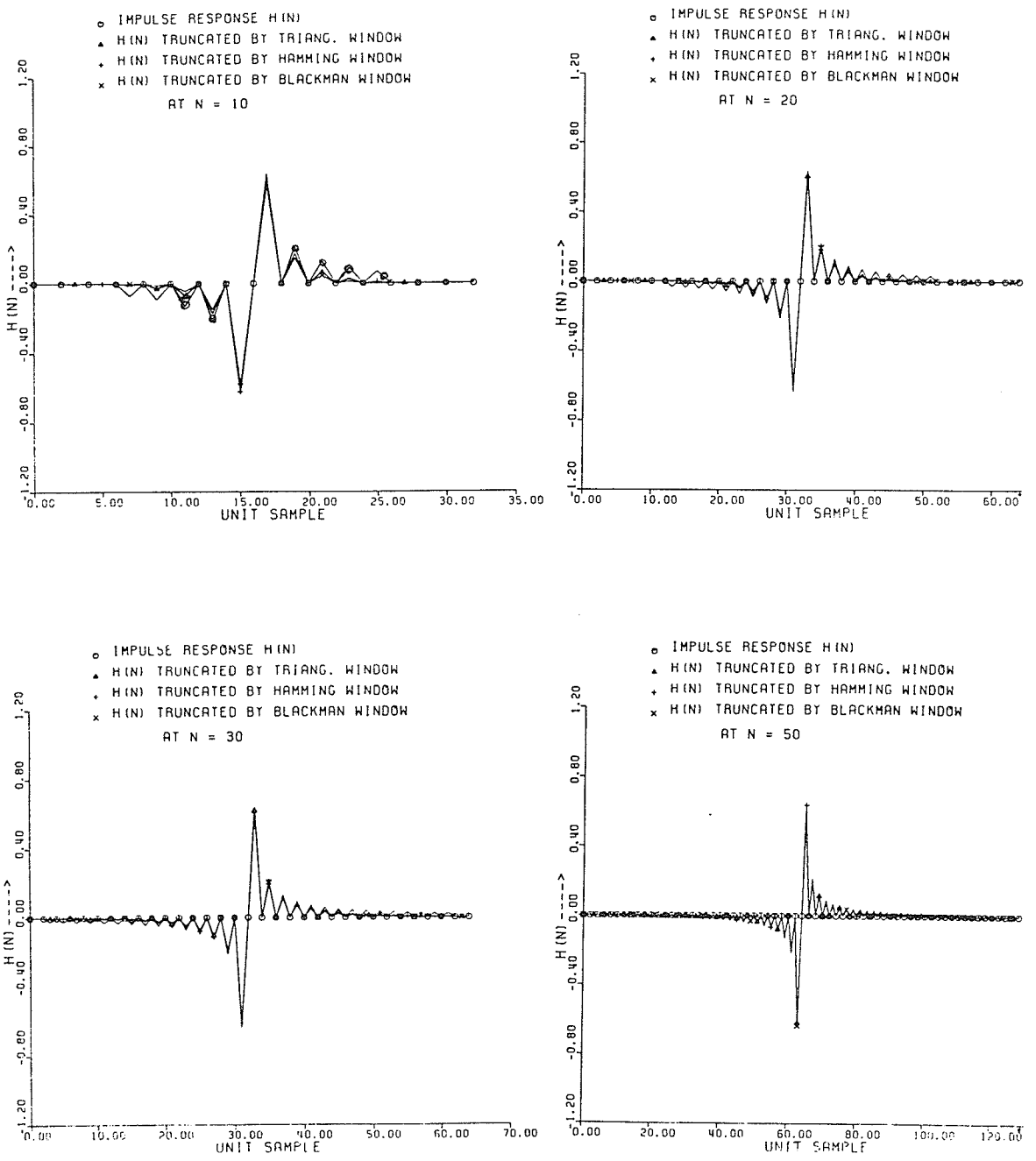


Fig. 2.4 Impulse response of 1-D Hilbert transform approximation in time domain with Triangular, Hamming and Blackman windows at N = 10, 20, 30, and 50.

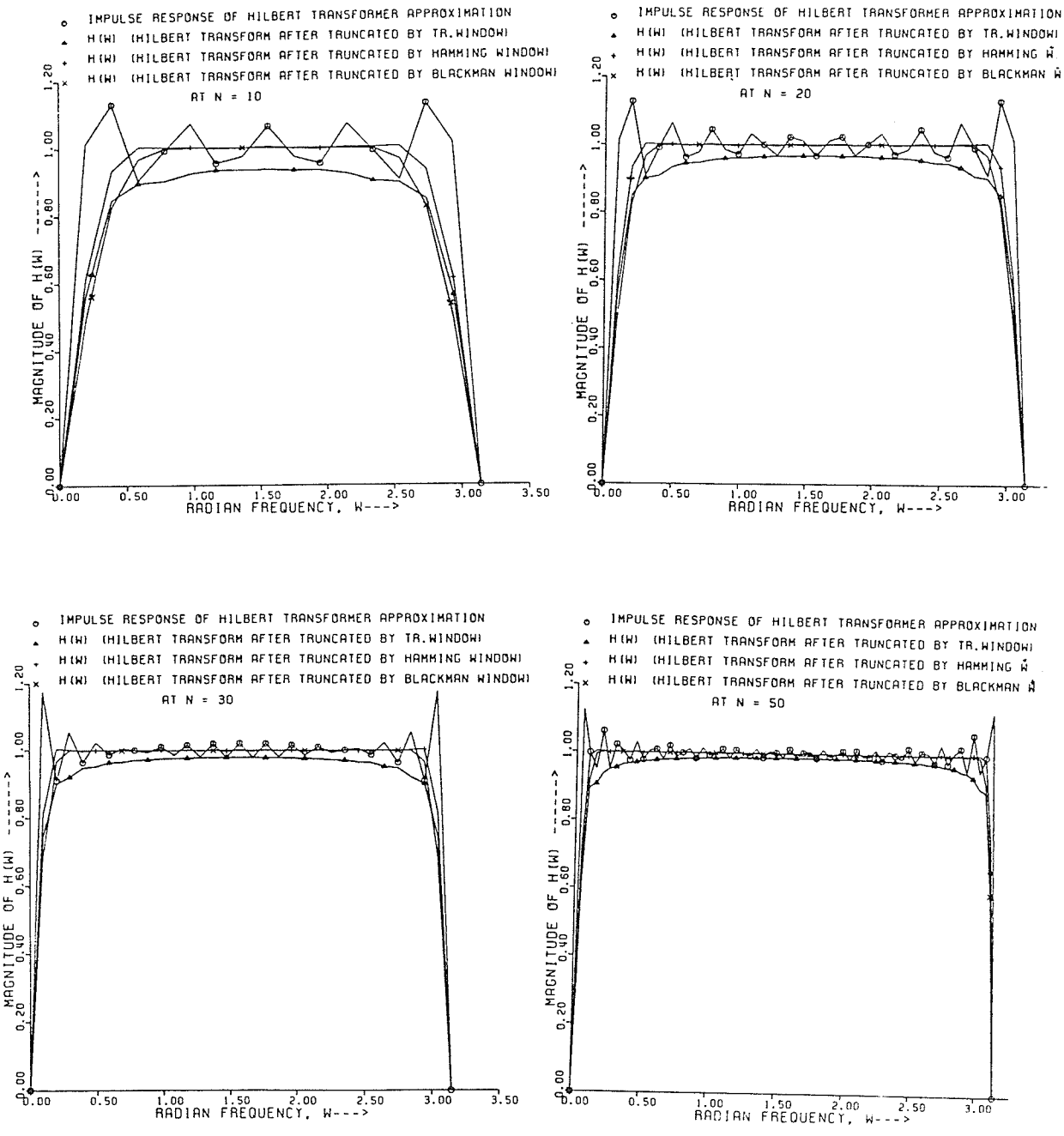


Fig. 2.5 Represents the magnitude of the spectral analysis of 1-D Hilbert transform, which is given in figure 2.4

## 2.8 DESIGN OF 1-D HILBERT TRANSFORM OPERATOR

Approximations to the ideal Hilbert transform can numerically be obtained in the case of finite-duration approximations, the standard techniques of windowing, frequency sampling, and equi-ripple approximation can be applied in approximating the characteristics of the ideal Hilbert transformer (equation 2.6-9).

In this section the Hilbert transformer (equation 2.6-10) with Triangular, Hamming and Blackman windows with different length operators ( N ) is computed and presented as given in Fig. 2.4. The magnitude of the frequency response $H(\omega)$ is shown in Fig. 2.5 for $0 \leq \omega \leq \pi$.

In case of N = 10 the impulse response appears to contains more than usual ripples in both sides of the main lobe and these ripples which appear in ht(n) have affected on the magnitude of $H(\omega)$. Also these ripples are seen in the magnitude spectrum of the frequency response.

The benefit of using the windows is to reduce or attenuate the ripples, which in turn leads one to obtain a smooth ht(n) and $H(\omega)$. Therefore, we have to know which window is more suitable in obtaining the best approximation to the ideal Hilbert transform.

When we truncated ht(n) by Triangular window with N = 10, it gives better resolution than the impulse response itself (truncated by a boxcar). The $|H(\omega)|$ obtained with a

triangular window is better because no ripples are noticeable when compare with $|H(\omega)|$ which is initially truncated by a boxcar.

In the case of Hamming window with $N = 10$ , the ripples are decreased in both sides of main lobe of $ht(n)$ but the $H(\omega)$ is not smooth as we wish, and the $|H(\omega)| \neq 1$. Therefore, it is found that if we want to use the operator length of $N = 10$, the window which will give the best resolution for $ht(n)$ and $H(\omega)$ is the Blackman window.

In this method we have tested the operator length of $N = 10, 20, 30,$ and 50. From these experiments we have found that the smaller the N is, the wider the ripples, and as N increases the ripples or the lobes become narrower. But the amplitude remains almost constant. In other words, as N increases, the main lobe of $ht(n)$ approaches to a spike and $|H(\omega)|$ approaches to true values.

In conclusion we can therefore say that for any value of N the best approximation can be obtained when the Blackman window is incorporated in designing the Hilbert transformer.

A computer program in standard FORTRAN language for designing 1-D Hilbert transform was written ( see program No.1 in Appendix A ).

# CHAPTER 3

# APPLICATION OF 1-D HILBERT TRANSFORM IN MAGNETIC AND GRAVITY DATA INTERPRETATION

## 3.1 INTRODUCTION

In recent years, Hilbert transform techniques have found more and more applications in magnetic and gravity data interpretation ( Shuey, 1972; Nabighian, 1972; Stanley and Green, 1975; and Stanley, 1977) particularly in fast quantitative interpretation of gravity and magnetic data. The works done by Shuey( 1972 ) and Nabighian( 1972 ) were more or less confined to the transformation of vertical gradients (vertical magnetic field) into horizontal gradients( horizontal magnetic field) and vice-versa with the help of the Hilbert transform.

Mohan et al.( 1982 ) derived simple relations between the vertical magnetic anomalies of sheets ( finite and infinite depth extent ) and their Hilbert transforms. Similar relations were also extended to simple dikes and horizontal circular cylindrical bodies.

In 1983, Izzeldin described a simple automatic direct method of interpretation which is intended for determining uniquely the physical parameters of two dimensional structures ( eg. semi-infinite dikes and the horizontal cylin-

ders). The method is flexible enough to encompass total vertical and horizontal field measurements at all latitudes. Linear regional gradients do not hamper the application of the method. Remanent magnetization does not affect the determination of the main parameters, i.e. depth and location. Unlike most other methods no knowledge of origin or datum level is required in this method.

In this chapter I will try to review the theory of the above two methods and they will be discussed with some specific examples. Also I will try to clarify some problems which may confuse the readers in understanding the mathematical analysis.

In gravity data applications, I will illustrate the same approach, as Mohan et al. ( 1982 ) did in magnetic interpretation. The vertical fault will be considered as a special case of the dipping fault. Some of the points to be discussed include horizontal derivative, fault structure, Fourier transform, discrete Hilbert transform, points of intersection and density contrast.

## 3.2 APPLICATION OF HILBERT TRANSFORM IN MAGNETIC FIELD

In this section I am going to discuss two methods of using 1-D Hilbert transform in the interpretation of magnetic field data; one follows the method originally discussed by Mohan et al.( 1982 ) and the other by Green ( 1975 ) and Izzeldin ( 1983 ).

The first method deals with 1-D Hilbert transform ( ht(x) ) and vertical magnetic effect( V(x) ) caused by magnetic bodies of several geometrical shapes such as vertical sheets with finite and infinite depth, thick dikes, and horizontal circular cylinders. In general this method has some problems, especially when the polarization angle is $45^0$ and also any values by close approaching $45^0$ from either direction. In the following sections I am going to resolve this problem. At the same time, I will try to compare the results from the first approach( Mohan et al. 1982 ) with those of Green ( 1975 ) and Izzeldin ( 1983 ).

### 3.2.1 Review of the Relations Proposed by Mohan ( 1982 )

The interpretation procedures in this method are based mainly on certain characteristic points, i.e. x-coordinates ( $x_1$ and $x_2$ ) at which V(x) and ht(x) become zero. The location of the origin of anomaly is important in this type of interpretation method.

Numerical implementation of the theoretical procedures can be accomplished by using the discrete Fourier transform and Hilbert transform.

### 3.2.1a Hilbert Transform of the vertical magnetic effect of a Vertical Sheet( finite depth extent )

A vertical magnetic sheet of finite depth extent, extending infinitely in the direction parallel to the Y-axis is considered. The section of the sheet with the X-Z plane is shown in Fig. 3.1a. The vertical magnetic effect of such a body is given by (Grant and West, 1965).

$$V_1(x) = A\,[(\, x \sin Q - h_2 \cos Q \,)/(\, x^2 + h_2^2) - (\, x \sin Q - h_1 \cos Q \,)/(\, x^2 + h_1^2 \,)] \qquad 3.2\text{-}1$$

where, $h_1$ and $h_2$ are depths to the top and bottom of the sheet, respectively, Q the polarization angle, and A the magnetic constant of the sheet.

The Hilbert transform of the vertical magnetic field ( equation 3.2-1 ) is given as

$$ht_1(x) = A\,[(\, h_1 \sin Q - x \cos Q \,)/(\, h_1^2 + x^2 \,) + (\, x \cos Q - h_2 \sin Q \,)/(\, h_2^2 + x^2 \,) \qquad 3.2\text{-}2$$

since $x_1$ and $x_2$ are the abscissa of the points of intersection of $V_1(x)$ and $ht_1(x)$,

$$V_1(x_1) = ht_1(x_1)\ ,\ V_1(x_2) = ht_1(x_2).$$

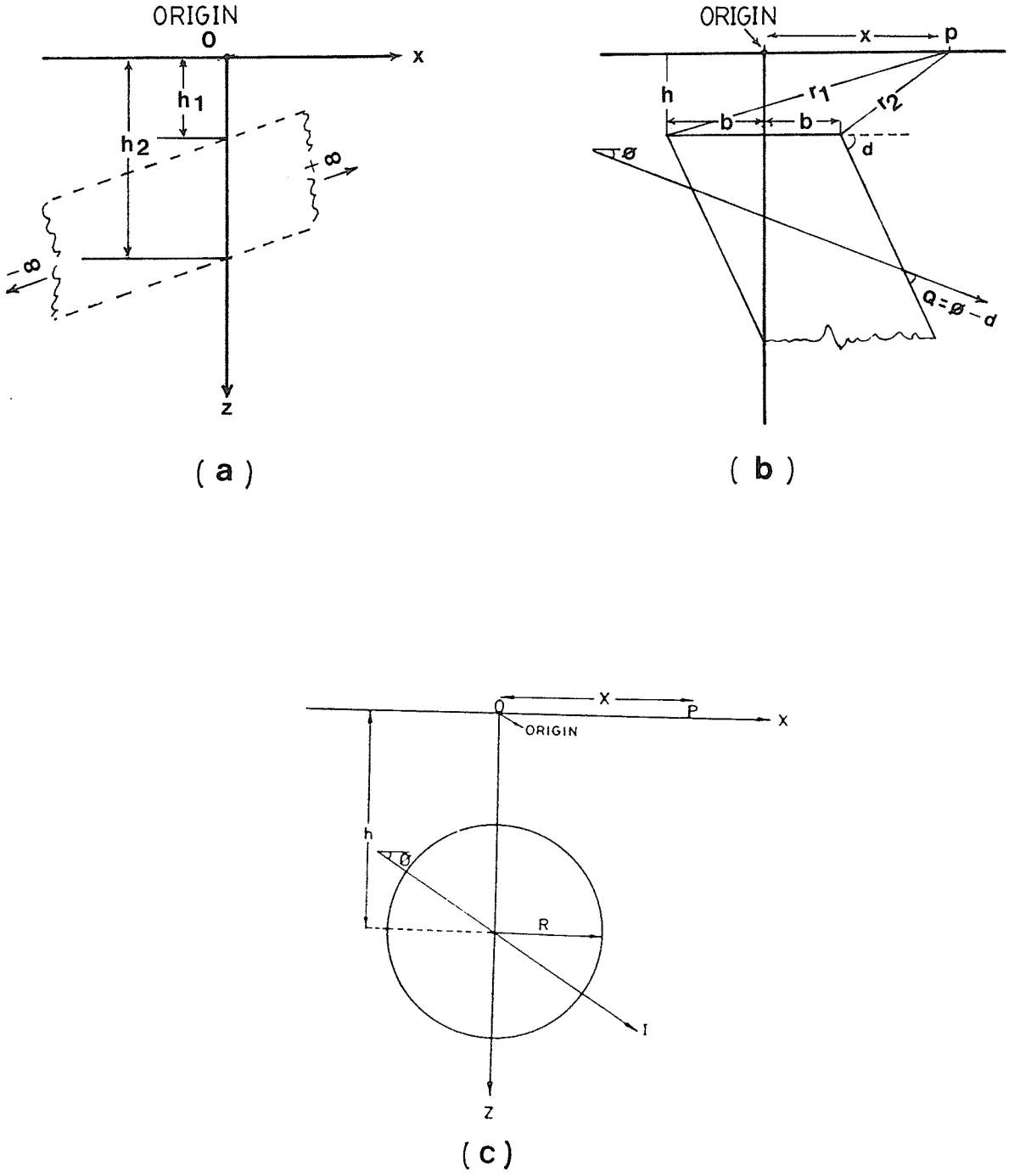


Fig. 3.1 (a) Geometry of the vertical sheet ( finite depth extent ).
(b) Geometry of the thick dike.
(c) Geometry of the horizontal circular cylinder.

From equations (3.2-1) and (3.2-2), we obtain the following relations;

$$h_1 = [(x_2 + x_1) \pm \{(x_1 + x_2) + 4x_1x_2\}^{1/2}]/2 \qquad 3.2\text{-}3$$

and

$$h_2 = 2x_1x_2/[(x_1+x_2) \pm ((x_1+x_2)^2 + 4x_1x_2)^{1/2}]. \qquad 3.2\text{-}4$$

It is evident from equations ( 3.2-1 ) and ( 3.2-2 ) that

$$Q = \arctan [( x^2ht_1(x) - h_1h_2ht_1(x) - xV_1(x)(h_1 + h_2))/ (x^2V_1(x) - h_1h_2V_1(x) - x\, ht_1(x)(h_1+ h_2))] \qquad 3.2\text{-}5$$

From equation ( 3.2-5 ), it is clear that $V_1(x)$ and $ht_1(x)$ at any x are sufficient for determining Q. In order to enhance the accuracy of Q, different values of x over a range of the body where the magnetic effect is maximum are considered, and then the average of the Q is taken. The parameter A can be obtained from

$$A = [(V_1^2(0) + ht_1^2(0))^{1/2}/\{(1/h_1) - (1/h_2)\}] \qquad 3.2\text{-}6$$

### 3.2.1b Vertical Sheet( infinite depth ) Example

The geometrical configuration of earlier section represents the body of infinite depth extent as $h_2 \longrightarrow \infty$ . The vertical magnetic effect of such a sheet is given by (Grant and West, 1965)

$$V_2 = A [( h \cos Q - x \sin Q )/( h^2 + x^2 )] \qquad 3.2\text{-}7$$

The Hilbert transform of the vertical magnetic effect ( equation 3.2-7 ) is

$$ht_2 = A\,[(\,h \sin Q - x \cos Q\,)/(\,h^2 + x^2\,)] \qquad 3.2\text{-}8$$

At the points of intersection of $V_2(x)$ and $ht_2(x)$

$$V_2(x) = ht_2(x) = h \cos Q - x \sin Q = h \sin Q - x \cos Q$$

Then

$$h = -x,$$

The parameter Q is obtained from equations ( 3.2-7) and (3.2-8) as

$$Q = \arctan\,[(h\,ht_2(x)+xV_2(x))/(h\,V_2(x)+x\,ht_2(x))] \qquad 3.2\text{-}9$$

and

$$A = h\,[V_2^2(0) + ht_2^2(0)]^{1/2}. \qquad 3.2\text{-}10$$

### 3.2.2 Thick Dike

An infinitely long, dipping dike with its normal section parallel to the X-Z plane is studied by Mohan et al., ( 1982 ). The origin of the coordinate system is taken on the ground surface such that the downward vertical. i.e., the Z-axis, bisects the upper surface of the dike ( Fig. 3.1b ).

The vertical magnetic effect of the dipping dike is given by (Grant and West 1965)

$$V(x) = 2\,\bar{I} \sin d\,[\cos Q\,\{\arctan((x+b)/h) - \arctan((x-b)/h)\} + (1/2) \sin Q\,\{\mathrm{Log}((h^2+(x+b)^2)/(h^2+(x-b)^2))\}] \qquad 3.2\text{-}11$$

Where

b = the half width of the dike,

h = the depth of the upper surface,

$\bar{I}$ = the intensity of magnetization,

d = the dip of the causative body,

Q = the inclination of the magnetic vector.

The Hilbert transform of equation ( 3.2-11 ) is given as;

$$ht(x) = 2\bar{I} \sin d \,[\sin Q \,\{\arctan((x+b)/h) - \arctan((x-b)/h)\} + (\cos(Q)/2)\,\{\mathrm{Log}((h^2 + (x+b)^2)/(h^2 + (x-b)^2))\}] \quad 3.2\text{-}12$$

Since the expression for V(x) and ht(x) involves arctan and logarithmic operations, and since the interpretation is rather complicated, their derivatives are considered in order to facilitate an easy analysis. Thus

$$V'(x) = dV/dx = 2\,\bar{I} \sin d\,[\cos Q\,\{h/((x+b)^2 + h^2) - h/((x-b)^2 + h^2)\} + \sin Q\,\{(x+b)/((x+b)^2 + h^2) - (x-b)/((x-b)^2 + h^2)\}] \quad 3.2\text{-}13$$

and

$$ht'(x) = d(ht)/dx = 2\,\bar{I} \sin d\,[\sin Q\,\{h/((x+b)^2 + h^2) - h/((x-b)^2 + h^2)\} + \cos Q\,\{(x+b)/((x+b)^2 + h^2) - (x-b)/((x-b)^2 + h^2)\}]. \quad 3.2\text{-}14$$

By solving equations (3.2-13) and (3.2-14) at points of intersection ( $x_1$ ) and ( $x_2$ ), we have

$$h = (x_1 + x_2)/2 \quad \text{and}$$

$$b = \pm\,(x_1^2 - 2x_1h - h^2)^{1/2} \quad \text{or}$$

$$b = \pm\,(x_2^2 - 2x_2h - h^2)^{1/2} \quad 3.2\text{-}15$$

Dividing the respective sides of equations ( 3.2-13 ) and ( 3.2-14 ), the Q is obtained as

$$Q = \arctan [\{(h^2+b^2-x^2)\ V'(x) + 2xh\ ht'\}/ \{(h^2+b^2 - x^2)\ ht'(x) + 2xhV'(x)\}] \qquad 3.2\text{-}16$$

The above equation yields the parameter Q for any arbitrary value of x. However, for greater accuracy with real data various estimates of Q corresponding to several values of x can be computed, and the parameter Q is determined from the saturated value. Further,

$$\bar{I} \sin d = [(b^2+h^2)(\ V'^2(0) + ht'^2(0)\ )^{1/2}]/4b \qquad 3.2\text{-}17$$

where

$$V'(0) = 2\ \bar{I} \sin d \sin Q\ (2b/(b^2+h^2)) \qquad 3.2\text{-}18$$

$$ht'(0) = 2\ \bar{I} \sin d \cos Q\ (2b/(b^2+h^2)) \qquad 3.2\text{-}19$$

It is not possible to determine $\bar{I}$ or d individually. However the above equation facilitates the determination of either d or $\bar{I}$ provided the second parameter is known.

### 3.2.3 Horizontal Circular Cylinder

The vertical magnetic effect of a horizontal circular cylinder extending infinitely along the Y-direction, and its normal section parallel to the X-Z plane, is considered ( Mohan et al., 1982 ). The origin of the coordinate system is taken on the ground surface such that the Z-axis coincides with the diameter ( Fig. 3.1c ). Then we have

$$V(x) = C\ [\{(h^2-x^2) \sin Q - 2xh \cos Q\}/(h^2+x^2)^2] \qquad 3.2\text{-}20$$

where,

$C = 2\pi R^2 \bar{I}$

R = the radius of the cylinder

$\bar{I}$ = the intensity of the magnetization

h = the depth to the center of the cylinder

The Hilbert transform of equation ( 3.2-20 ) is given as

$$ht(x) = C\ [\{(h^2-x^2)\cos Q - 2xh \sin Q\}/(h^2+x^2)^2] \qquad 3.2\text{-}21$$

At the points of intersection of V(x) and ht(x)

$$h = (x_1 + x_2)/2 \qquad 3.2\text{-}22$$

From equations (3.2-20 ) and (3.2-21 )

$$Q = \arctan[\{(h^2- x^2)V(x) + 2xh\ ht(x)\}/ \{(h^2 - x^2)ht(x) + 2xhV(x)\}] \qquad 3.2\text{-}23$$

C is determined from

$$C = h^2(V^2(0) + H^2(0))^{1/2} \qquad 3.2\text{-}24$$

where

$$V(0) = (C \sin Q)/h^2 \quad \text{and} \quad ht(0) = (C \cos Q)/h^2$$

Finally, assuming $\bar{I}$, the radius R is determined from

$$R = [\ C/(2\ \pi\ \bar{I})\ ]^{1/2} \qquad 3.2\text{-}25$$

### 3.2.4 The effect of Polarization angle ( Q )

In this section, I am going to discuss the first method ( Mohan et al., 1982 ) when the polarization angle ( Q ) has a critical value. For the simplicity, the discussion will be restricted on the first model ( finite vertical sheet ) because all the other models can be discussed with the same idea. The equations (3.2-1) and (3.2-2) are not applicable when the polarization angle ( Q ) equals $45^0$ because V(x) = ht(x) for all values of x and the "$x_1$" and "$x_2$" are not defined. To solve this problem which in fact applies to all Mohan models, when the polarization angle $Q = 45^0$, I will consider the negative of either V(x) or ht(x). Hence it could be resolved easily as follows:

$$V(x)\Big|_{Q=45^0} = A \sin Q \left[\{(x - h_2)/(x^2 + h^2_2)\} - \{(x - h_1)/(x^2 + h^2_1)\}\right] \qquad 3.2\text{-}26$$

and

$$ht(x)\Big|_{Q=45^0} = A \cos Q \left[\{(x - h_2)/(x^2 + h^2_2)\} - \{(x - h_1)/(x^2 + h^2_1)\}\right] \qquad 3.2\text{-}27$$

At the points of intersection of V(x) and -ht(x)

$$V(x_1) = - ht(x_1) \qquad \text{at } x = x_1 \qquad 3.2\text{-}28a$$

$$V(x_2) = - ht(x_2) \qquad \text{at } x = x_2 \qquad 3.2\text{-}28b$$

From the equation ( 3.2-28a ),

$$V(x_1) = -ht(x_1) = [(x_1-h_2)/(x_1^2+h_2^2)] = [(x_1-h_1)/(x_1^2+h_1^2)] \qquad 3.2\text{-}29a$$

From the equation (3.2-29a), we have

$$x_1^2(h_1-h_2)+x_1(h_1-h_2)(h_1+h_2)-h_1h_2(h_1-h_2) = 0$$

$$x_1^2 + x_1(h_1 + h_2) - h_1h_2 = 0 \qquad 3.2\text{-}29b$$

Similarly from equation (3.2-28b)

$$x_2^2 + x_2(h_1 + h_2) - h_1h_2 = 0 \qquad 3.2\text{-}30$$

and from equation (3.2-29b),

$$h_2 = -(x_1^2 + x_1h_1)/(x_1 - h_1) \qquad 3.2\text{-}31$$

By substituting equation (3.2-31) in equation (3.2-29b) we obtain,

$$h_1^2 + h_1(x_1 + x_2) - x_1x_2 = 0 \qquad 3.2\text{-}32$$

The equation (3.2-32) has the form of a quadratic equation $ax^2 + bx + c = 0$, and the solution becomes

$$h_1 = [\{-(x_1+x_2) \pm ((x_1+x_2)^2 + 4x_1x_2)^{1/2}\}/2] \qquad 3.2\text{-}33$$

Similarly;

$$h_2 = [-2x_1x_2/\{(x_1+x_2) \pm ((x_1+x_2)^2+4x_1x_2)^{1/2}\}] \qquad 3.2\text{-}34$$

From equations (3.2-3), (3.2-4), (3.2-33) and (3.2-34), we can conclude that

$$h\Big|_{Q=45^0} = -\,h\Big|_{Q\neq 45^0}$$

and the rest of derivation are applicable to any value of Q except the equation ( 3.2-15 ) which takes the following form;

$$b = \pm (-x_1^2+2x_1h - h^2)^{1/2} \quad \text{or}$$

$$b = \pm (-x_2^2+2x_2h - h^2)^{1/2} \qquad 3.2\text{-}35$$

### 3.2.5 Theoretical Examples

Several theoretical models(Tables 3, 4 and 5 ) are considered to illustrate the procedure described above. Using equations (3.2-1), (3.2-2'), (3.2-7) and (3.2-8), the vertical magnetic effect of the vertical sheet (finite and infinite depth) and its Hilbert transform are computed for different values of polarization angle ( Q ) as shown in Figs. 3.2, 3.3 and 3.4. It is observed that in each case the curves of $V_1(x)$, $V_2(x)$, $ht_1(x)$ and $ht_2(x)$ intersect on either side of the origin. From these figures the intersection points $x_1$ and $x_2$ are determined, and with the help of equations ( 3.2-3 to 3.2-10 ), $h_1$, $h_2$, Q and A can be computed. Other examples are given in Tables 3, 4 and 5. In cases of Horizontal circular cylinder and thick dike, the Figs. 3.2, 3.3 and 3.4 show the examples with model parameters and evaluated values of these parameters as well.

A computer program in FORTRAN language was written ( see program No.2 in Appendex A ) to perform the computation ( Tables 3, 4 and 5 ). The graphical representation of V(x) and ht(x) or V'(x) and ht'(x) are not necessary, since this program can be used to find the point of intersections between V(x) and ht(x) or V'(x) and ht'(x) numerically.

Table 3. Example of continuous and discrete Hilbert transforms (CH, DH) in quantitative interpretation of magnetic anomaly.

Case - 1

| 1a) Vertical finite Sheet( Fig.3.2a ) | | | | | | | | | 1b) Vertical infinite Sheet( Fig.3.2b ) | | | | | | |
|---|---|---|---|---|---|---|---|---|---|---|---|---|---|---|---|
| Model parameters | | | | H. TR. | Evaluated values | | | | Model parameters | | | H. TR. | Evaluated values | | |
| $h_1$ | $h_2$ | Q | a | | $h_1$ | $h_2$ | Q | a | h | Q | a | | h | Q | a |
| 0.75 | 2.00 | 30.00 | 1.00 | CH | 0.75 | 2.00 | 29.995 | 1.00 | 1.000 | 30.000 | 1.000 | CH | 1.000 | 29.936 | 1.000 |
| 0.75 | 2.00 | 30.00 | 1.00 | DH | 0.74 | 2.06 | 31.384 | 0.972 | 1.000 | 30.000 | 1.000 | DH | 1.058 | 31.689 | 1.053 |

| 2) Thick Dike( Fig.3.2c ) | | | | | | | | | 3) Horizontal Circular Cylinder( Fig.3.2d ) | | | | | | |
|---|---|---|---|---|---|---|---|---|---|---|---|---|---|---|---|
| Model parameters | | | | H. TR. | Evaluated values | | | | Model parameters | | | H. TR. | Evaluated values | | |
| b | h | Q | $d^0$ | | b | h | Q | $d^0$ | R | h | Q | | R | h | Q |
| 0.50 | 1.00 | 30.00 | 60.00 | CH | 0.50 | 1.00 | 29.878 | 59.307 | 1.000 | 1.000 | 30.000 | CH | 1.000 | 1.000 | 29.995 |
| 0.50 | 1.00 | 30.00 | 60.00 | DH | 0.52 | 0.98 | 28.651 | 54.141 | 1.000 | 1.000 | 30.000 | DH | 0.975 | 0.975 | 28.651 |

Table 3. ( continued )

Case - 2

| 1a) Vertical finite Sheet | | | | | | | | | 1b) Vertical infinite Sheet | | | | | | |
|---|---|---|---|---|---|---|---|---|---|---|---|---|---|---|---|
| Model parameters | | | | H. TR. | Evaluated values | | | | Model parameters | | | H. TR. | Evaluated values | | |
| $h_1$ | $h_2$ | Q | a | | $h_1$ | $h_2$ | Q | a | h | Q | a | | h | Q | a |
| 1.00 | 2.00 | 45.000 | 1.000 | CH | 1.00 | 2.00 | 44.984 | 1.00 | 1.00 | 45.000 | 1.000 | CH | 1.000 | 44.902 | 1.000 |
| 1.00 | 2.00 | 45.000 | 1.000 | DH | 1.02 | 1.92 | 43.178 | 1.087 | 1.00 | 45.000 | 1.000 | DH | 0.984 | 42.031 | 0.976 |

| 2) Thick Dike | | | | | | | | | 3) Horizontal Circular Cylinder | | | | | | |
|---|---|---|---|---|---|---|---|---|---|---|---|---|---|---|---|
| Model parameters | | | | H. TR. | Evaluated values | | | | Model parameters | | | H. TR. | Evaluated values | | |
| b | h | Q | $d^o$ | | b | h | Q | $d^o$ | R | h | Q | | R | h | Q |
| 0.50 | 1.00 | 45.00 | 60.00 | CH | 0.50 | 1.00 | 44.77 | 61.042 | 1.00 | 1.00 | 45.00 | CH | 1.00 | 1.00 | 44.990 |
| 0.50 | 1.00 | 45.00 | 60.00 | DH | 0.51 | 0.99 | 38.38 | 59.098 | 1.000 | 1.00 | 45.00 | DH | 0.992 | 0.993 | 38.482 |

Table 3. ( continued )

Case - 3

| 1a) Vertical finite Sheet | | | | | | | | | 1b) Vertical infinite Sheet | | | | | | |
|---|---|---|---|---|---|---|---|---|---|---|---|---|---|---|---|
| Model parameters | | | | H. TR. | Evaluated values | | | | Model parameters | | | H. TR. | Evaluated values | | |
| $h_1$ | $h_2$ | Q | a | | $h_1$ | $h_2$ | Q | a | h | Q | a | | h | Q | a |
| 1.00 | 2.00 | 60.00 | 1.00 | CH | 1.00 | 2.00 | 59.996 | 1.00 | 1.000 | 60.000 | 1.000 | CH | 1.000 | 59.879 | 1.000 |
| 1.00 | 2.00 | 60.00 | 1.00 | DH | 1.06 | 1.79 | 60.937 | 1.298 | 1.000 | 60.000 | 1.000 | DH | 0.921 | 60.726 | 0.909 |

| 2) Thick Dike | | | | | | | | | 3) Horizontal Circular Cylinder | | | | | | |
|---|---|---|---|---|---|---|---|---|---|---|---|---|---|---|---|
| Model parameters | | | | H. TR. | Evaluated values | | | | Model parameters | | | H. TR. | Evaluated values | | |
| b | h | Q | $d^0$ | | b | h | Q | $d^0$ | R | h | Q | | R | h | Q |
| 0.50 | 1.00 | 60.00 | 60.00 | CH | 0.50 | 1.00 | 59.762 | 59.309 | 1.000 | 1.000 | 60.000 | CH | 1.000 | 1.000 | 59.996 |
| 0.50 | 1.00 | 60.00 | 60.00 | DH | 0.49 | 1.01 | 58.449 | 61.981 | 1.000 | 1.000 | 60.000 | DH | 1.011 | 1.012 | 58.413 |

Table 4. Example of continuous and discrete Hilbert transforms (CH, DH) in quantitative interpretation of magnetic anomaly.

Case - 1

| 1a) Vertical finite Sheet( Fig.3.3a ) | | | | | | | | | | 1b) Vertical infinite Sheet( Fig.3.3b ) | | | | | | | |
|---|---|---|---|---|---|---|---|---|---|---|---|---|---|---|---|---|---|
| Model parameters | | | | H. TR. | Evaluated values | | | | | Model parameters | | | H. TR. | Evaluated values | | | |
| $h_1$ | $h_2$ | Q | a | | $h_1$ | $h_2$ | Q | a | | h | Q | a | | h | Q | a | |
| 0.75 | 2.00 | 45.000 | 1.00 | CH | 0.75 | 2.00 | 44.989 | 1.000 | | 1.000 | 45.000 | 1.000 | CH | 1.000 | 44.902 | 1.000 | |
| 0.75 | 2.00 | 45.000 | 1.00 | DH | 0.76 | 1.95 | 44.255 | 1.031 | | 1.000 | 45.000 | 1.000 | DH | 0.984 | 42.031 | 0.976 | |

| 2) Thick Dike( Fig.3.3c ) | | | | | | | | | | 3) Horizontal Circular Cylinder( Fig.3.3d ) | | | | | | | |
|---|---|---|---|---|---|---|---|---|---|---|---|---|---|---|---|---|---|
| Model parameters | | | | H. TR. | Evaluated values | | | | | Model parameters | | | H. TR. | Evaluated values | | | |
| b | h | Q | $d^o$ | | b | h | Q | $d^o$ | | R | h | Q | | R | h | Q | |
| 0.50 | 1.00 | 45.000 | 60.00 | CH | 0.50 | 1.00 | 44.770 | 61.042 | | 1.000 | 1.000 | 45.000 | CH | 1.000 | 1.000 | 44.980 | |
| 0.50 | 1.00 | 45.000 | 60.00 | DH | 0.51 | 0.99 | 38.382 | 59.098 | | 1.000 | 1.000 | 45.000 | DH | 0.992 | 0.993 | 38.482 | |

Table 4 ( continued )

Case -2

| 1a) Vertical finite Sheet( Fig.3.4a ) | | | | | | | | | 1b) Vertical infinite Sheet( Fig.3.4b ) | | | | | | |
|---|---|---|---|---|---|---|---|---|---|---|---|---|---|---|---|
| Model parameters | | | | H. TR. | Evaluated values | | | | Model parameters | | | H. TR. | Evaluated values | | |
| $h_1$ | $h_2$ | Q | a | | $h_1$ | $h_2$ | Q | a | h | Q | a | | h | Q | a |
| 0.75 | 2.00 | 60.00 | 1.00 | CH | 0.75 | 2.00 | 59.996 | 1.000 | 1.000 | 60.000 | 1.000 | CH | 1.000 | 59.879 | 1.000 |
| 0.75 | 2.00 | 60.00 | 1.00 | DH | 0.77 | 1.86 | 61.059 | 1.095 | 1.000 | 60.000 | 1.000 | DH | 0.921 | 60.726 | 0.909 |

| 2) Thick Dike( Fig.3.4c ) | | | | | | | | | 3) Horizontal Circular Cylinder( Fig.3.4d ) | | | | | | |
|---|---|---|---|---|---|---|---|---|---|---|---|---|---|---|---|
| Model parameters | | | | H. TR. | Evaluated values | | | | Model parameters | | | H. TR. | Evaluated values | | |
| b | h | Q | $d^0$ | | b | h | Q | $d^0$ | R | h | Q | | R | h | Q |
| 0.50 | 1.00 | 60.000 | 60.000 | CH | 0.50 | 1.00 | 59.762 | 59.309 | 1.00 | 1.00 | 60.00 | CH | 1.00 | 1.00 | 59.996 |
| 0.50 | 1.00 | 60.000 | 60.000 | DH | 0.49 | 1.01 | 58.449 | 61.981 | 1.00 | 1.00 | 60.00 | DH | 1.011 | 1.012 | 58.413 |

Table 4.( continued )

Case - 3

| 1a) Vertical finite Sheet | | | | | | | | | 1b) Vertical infinite Sheet | | | | | | |
|---|---|---|---|---|---|---|---|---|---|---|---|---|---|---|---|
| Model parameters | | | | H. TR. | Evaluated values | | | | Model parameters | | | H. TR. | Evaluated values | | |
| $h_1$ | $h_2$ | Q | a | | $h_1$ | $h_2$ | Q | a | h | Q | a | | h | Q | a |
| 1.00 | 2.00 | 30.00 | 1.00 | CH | 1.00 | 2.00 | 29.995 | 1.00 | 1.000 | 30.000 | 1.000 | CH | 1.00 | 29.936 | 1.000 |
| 1.00 | 2.00 | 30.00 | 1.00 | DH | 0.95 | 2.07 | 31.326 | 0.94 | 1.000 | 30.000 | 1.000 | DH | 1.058 | 31.689 | 1.053 |

| 2) Thick Dike | | | | | | | | | 3) Horizontal Circular Cylinder | | | | | | |
|---|---|---|---|---|---|---|---|---|---|---|---|---|---|---|---|
| Model parameters | | | | H. TR. | Evaluated values | | | | Model parameters | | | H. TR. | Evaluated values | | |
| b | h | Q | $d^0$ | | b | h | Q | $d^0$ | R | h | Q | | R | h | Q |
| 0.50 | 1.00 | 30.00 | 60.00 | CH | 0.50 | 1.00 | 29.878 | 59.307 | 1.000 | 1.000 | 30.000 | CH | 1.000 | 1.000 | 29.995 |
| 0.50 | 1.00 | 30.00 | 60.00 | DH | 0.50 | 1.00 | 28.651 | 54.141 | 1.000 | 1.000 | 30.000 | DH | 0.975 | 0.975 | 28.651 |

Table 5. Example of continuous and discrete Hilbert transforms (CH, DH) in quantitative interpretation of magnetic anomaly.

Case - 1

| 1a) Vertical finite Sheet | | | | | | | | | 1b) Vertical infinite Sheet | | | | | | |
|---|---|---|---|---|---|---|---|---|---|---|---|---|---|---|---|
| Model parameters | | | | H. TR. | Evaluated values | | | | Model parameters | | | H. TR. | Evaluated values | | |
| $h_1$ | $h_2$ | Q | a | | $h_1$ | $h_2$ | Q | a | h | Q | a | | h | Q | a |
| 1.00 | 3.00 | 45.000 | 1.00 | CH | 1.00 | 3.00 | 44.990 | 1.000 | 1.000 | 45.000 | 1.000 | CH | 1.000 | 44.902 | 1.000 |
| 1.00 | 3.00 | 45.000 | 1.00 | DH | 1.02 | 2.84 | 32.077 | 1.061 | 1.000 | 45.000 | 1.000 | DH | 0.984 | 42.031 | 0.976 |

| 2) Thick Dike | | | | | | | | | 3) Horizontal Circular Cylinder | | | | | | |
|---|---|---|---|---|---|---|---|---|---|---|---|---|---|---|---|
| Model parameters | | | | H. TR. | Evaluated values | | | | Model parameters | | | H. TR. | Evaluated values | | |
| b | h | Q | $d^0$ | | b | h | Q | $d^0$ | R | h | Q | | R | h | Q |
| 0.50 | 1.00 | 45.000 | 60.00 | CH | 0.50 | 1.00 | 44.77 | 61.042 | 1.000 | 1.000 | 45.000 | CH | 1.000 | 1.000 | 44.990 |
| 0.50 | 1.00 | 45.000 | 60.00 | DH | 0.51 | 0.99 | 38.382 | 59.098 | 1.000 | 1.000 | 45.000 | DH | 0.993 | 0.992 | 38.482 |

Table 5 ( continued )

Case -2

| 1a) Vertical finite Sheet | | | | | 1b) Vertical infinite Sheet | | | | |
|---|---|---|---|---|---|---|---|---|---|
| Model parameters | | | | H. TR. | Evaluated values | | | | Model parameters | | | H. TR. | Evaluated values | | |
| $h_1$ | $h_2$ | Q | a | | $h_1$ | $h_2$ | Q | a | h | Q | a | | h | Q | a |
| 1.00 | 2.50 | 45.00 | 1.00 | CH | 1.00 | 2.50 | 44.906 | 1.00 | 1.000 | 45.000 | 1.000 | CH | 1.000 | 44.902 | 1.000 |
| 1.00 | 2.50 | 45.00 | 1.00 | DH | 1.02 | 2.39 | 39.641 | 1.067 | 1.000 | 45.000 | 1.000 | DH | 0.984 | 42.031 | 0.976 |

| 2) Thick Dike | | | | | 3) Horizontal Circular Cylinder | | | | |
|---|---|---|---|---|---|---|---|---|---|
| Model parameters | | | | H. TR. | Evaluated values | | | | Model parameters | | | H. TR. | Evaluated values | | |
| b | h | Q | $d^0$ | | b | h | Q | $d^0$ | R | h | Q | | R | h | Q |
| 0.70 | 1.00 | 45.00 | 45.00 | CH | 0.70 | 1.00 | 44.925 | 46.836 | 0.800 | 1.000 | 45.00 | CH | 0.800 | 1.000 | 44.990 |
| 0.70 | 1.00 | 45.00 | 45.00 | DH | 0.70 | 0.99 | 38.450 | 46.109 | 0.800 | 1.000 | 45.00 | DH | 0.794 | 0.993 | 38.482 |

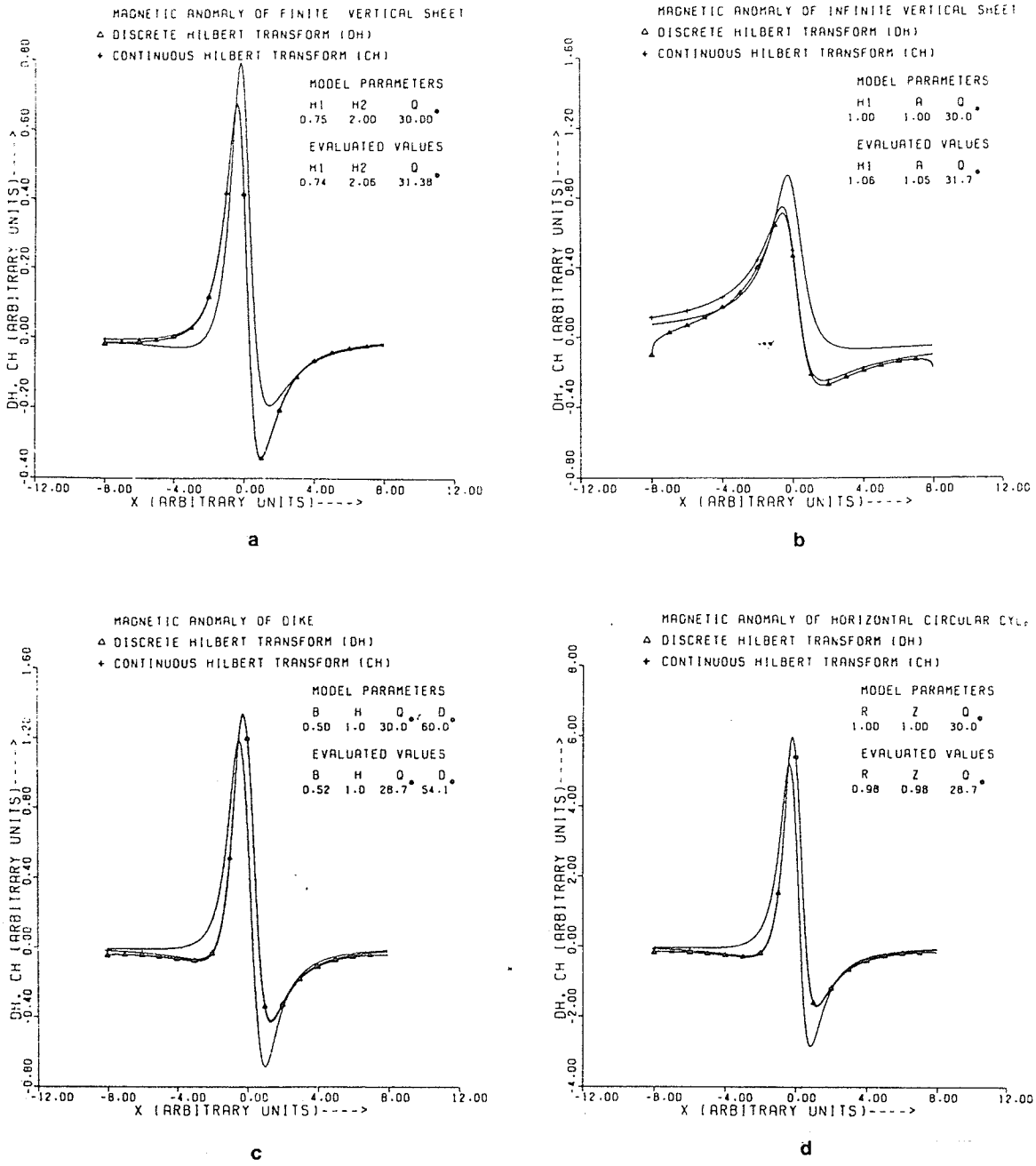


Fig. 3.2 Example of using the 1-D Hilbert transforms in quantitative interpretation of 2-D magnetic bodies, the polarization angle ( Q ) = $30^0$.

(a) Computed vertical magnetic effect of the vertical sheet ( finite depth extent ) and the Hilbert transforms.

(b) Computed vertical magnetic effect of the vertical sheet ( infinite depth extent ) and the Hilbert transforms.

(c) Computed first horizontal derivative of the vertical magnetic effect of the dike and the Hilbert transforms.

(d) Computed vertical magnetic effect of the horizontal circular cylinder and the Hilbert transforms.

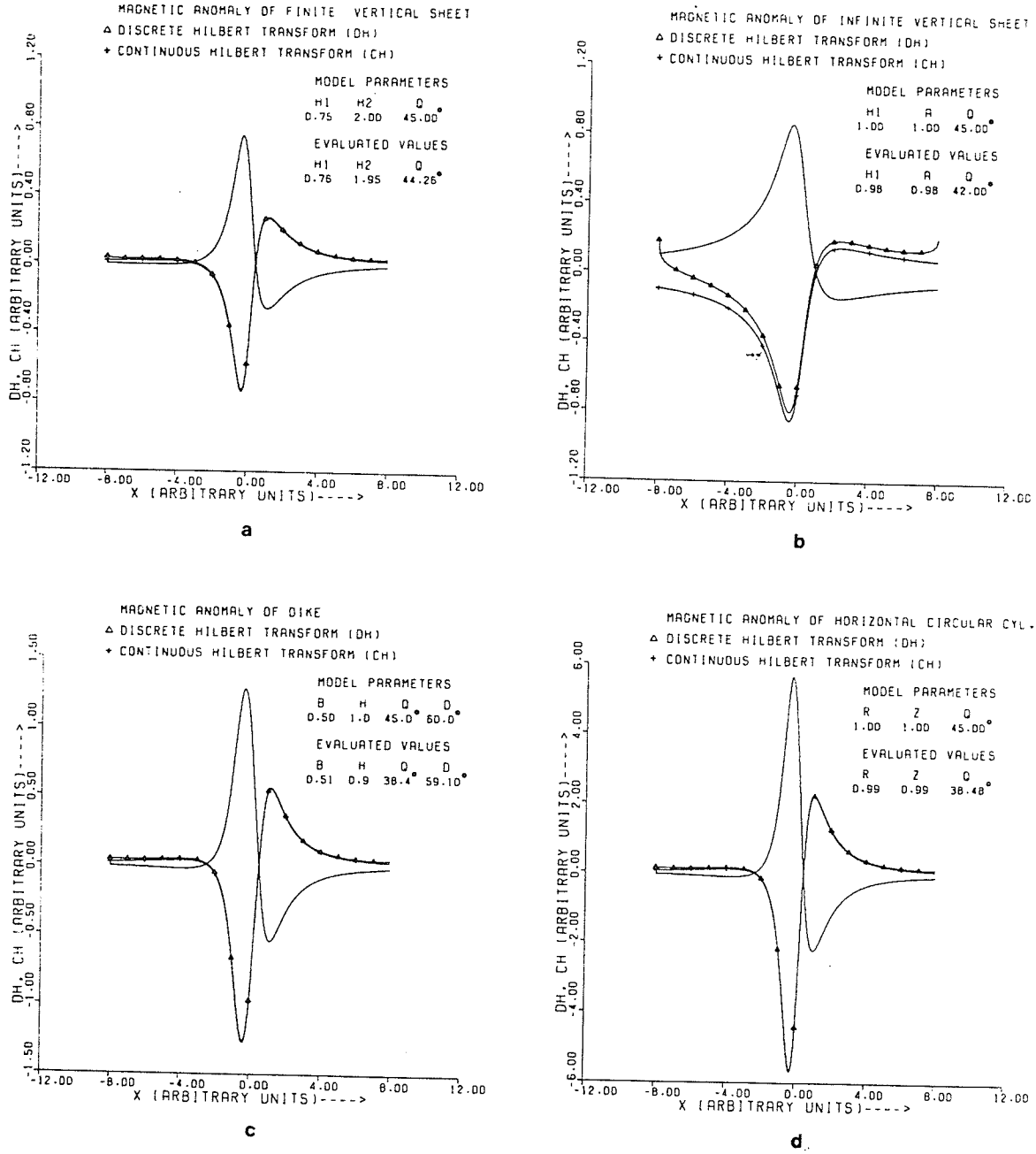


Fig. 3.3 Example of using the 1-D Hilbert transforms in quantitative interpretation of 2-D magnetic bodies, the polarization angle ( Q ) = 45°.

(a) Computed vertical magnetic effect of the vertical sheet ( finite depth extent ) and the Hilbert transforms.

(b) Computed vertical magnetic effect of the vertical sheet ( infinite depth extent ) and the Hilbert transforms.

(c) Computed first horizontal derivative of the vertical magnetic effect of the dike and the Hilbert transforms.

(d) Computed vertical magnetic effect of the horizontal circular cylinder and the Hilbert transforms.

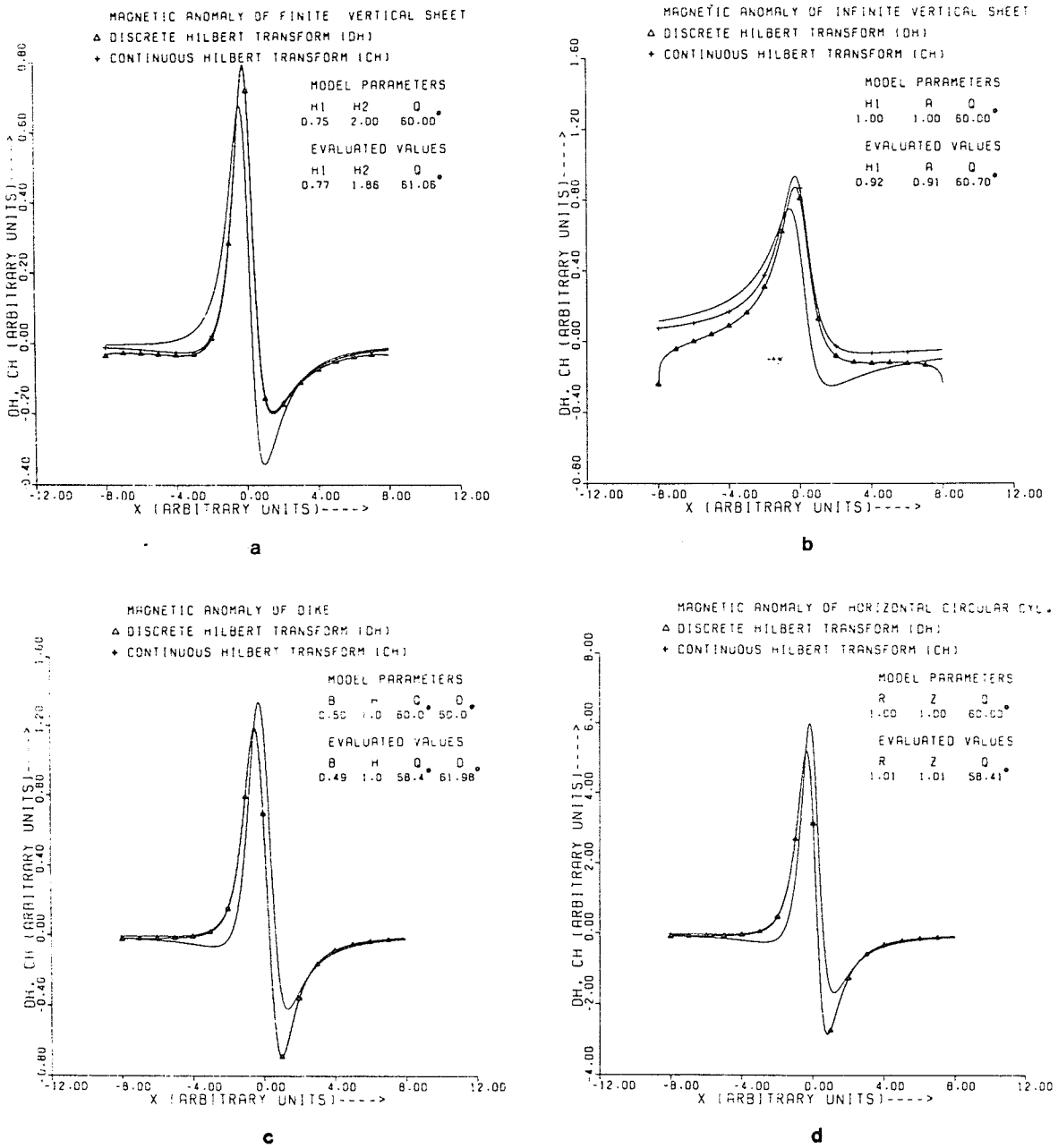


Fig. 3.4 Example of using the 1-D Hilbert transforms in quantitative interpretation of 2-D magnetic bodies, the polarization angle ( Q ) = 60°.

(a) Computed vertical magnetic effect of the vertical sheet ( finite depth extent ) and the Hilbert transforms.

(b) Computed vertical magnetic effect of the vertical sheet ( infinite depth extent ) and the Hilbert transforms.

(c) Computed first horizontal derivative of the vertical magnetic effect of the dike and the Hilbert transforms.

(d) Computed vertical magnetic effect of the horizontal circular cylinder and the Hilbert transforms.

### 3.2.6 Theory of the Method proposed by Green ( 1976 ) and Izzeldin ( 1983 )

In this method I will try to find the physical parameters of two dimensional structures ( the dipping fault, the semi-infinite dike, and the horizontal cylinder ).

#### 3.2.6a The Dipping Fault

Consider a total field anomaly $\Delta F(x)$ caused by a dipping fault structure with a susceptibility contrast K. Let the strike of the fault be Ø when measured clockwise from magnetic north and let the x-direction be measured normal to the strike ( Fig. 3.5 ). The positive Z-direction is vertically downwards. Let the depth to the top of the fault be h. The total field anomaly $\Delta F(x)$ of the dipping fault is given by Grant and West ( 1965, p.320 ) as following;

$$\Delta F(x) = KTC[\sin d \cos(d-2b) \operatorname{Log}((x - t \cot d)^2 + (h+t)^2/(x^2+h^2)) + 2 \sin d \sin(d-2b)(\arctan(x-t \cot d)/(h+t)) - \arctan(x/h)] \qquad 3.2\text{-}36$$

where

$C = ( I - \cos^2 I \cos^2 Ø )$

I = the inclination of the geomagnetic field;

$b = \tan^{-1}[\tan I/\sin Ø]$

T = the base value of the geomagnetic field

If we take the partial derivative of $\Delta F(x)$ with respect to x and h, respectively, then

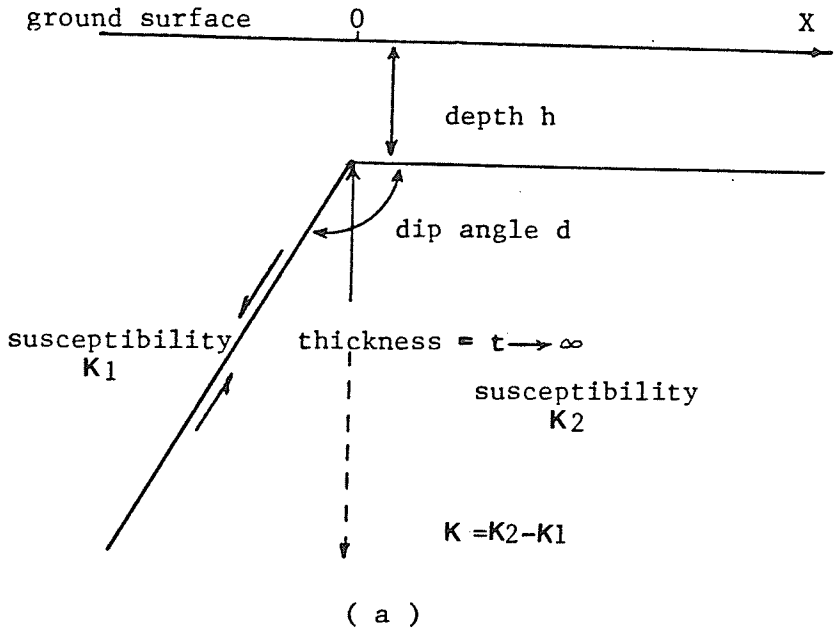


( a )

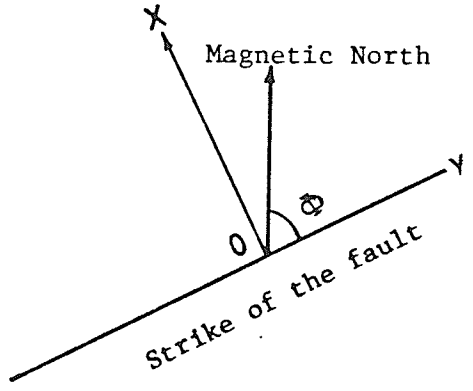


( b )

Fig. 3.5 (a) and (b) represent a sectional and a plan view of a dipping fault with coordinate system.

$$d\,\Delta F(x)/dx = 2KTC \sin d[(h \sin \lambda + x \cos \lambda)/(h^2 + x^2)] \qquad 3.2\text{-}37$$

and

$$d\,\Delta F(x)/dh = 2KTC \sin d[(-h \cos \lambda + x \sin \lambda)/(h^2 + x^2)] \qquad 3.2\text{-}38$$

where

$$\lambda = d - 2b.$$

If the angle $\theta$ is introduced such as

$$\tan \theta = x/h$$

where

$$x^2 + h^2 = r^2 ,$$

the equations ( 3.2-37 ) and ( 3.2-38 ) can be rewritten as

$$d\,\Delta F(x)/dx = -(2KTC \sin d)(\sin(\theta + \lambda))/r \qquad 3.2\text{-}39$$

and

$$d\,\Delta F(x)/dh = (2KTC \sin d) \cos(\theta + \lambda)/r \qquad 3.2\text{-}40$$

Since equation ( 3.2-40 ) turns out to be the Hilbert transform of equation ( 3.2-39 ) ( Green and Stanley, 1975 ), the amplitude function will be given as;

$$A(x) = d\,\Delta F(x)/dh - j\,d\,\Delta F(x)/dx \qquad 3.2\text{-}41$$

From equations ( 3.2-39 ) and ( 3.2-40 ) it can be shown that

$$A(x) = (2KTC \sin d)[(\exp j(\theta + \lambda))/(x + jh)]. \qquad 3.2\text{-}42$$

The analytical signal A(x) is a complex quantity whose amplitude A(x) and phase (Ph) are given by:

$$|A(x)| = (2KTC \sin d)/((x^2 + h^2))^{1/2} \qquad 3.2\text{-}43$$

$$Ph(x) = \arctan[(d\,\Delta F(x)/dx)/(d\,\Delta F(x)/dh)] \qquad 3.2\text{-}44$$

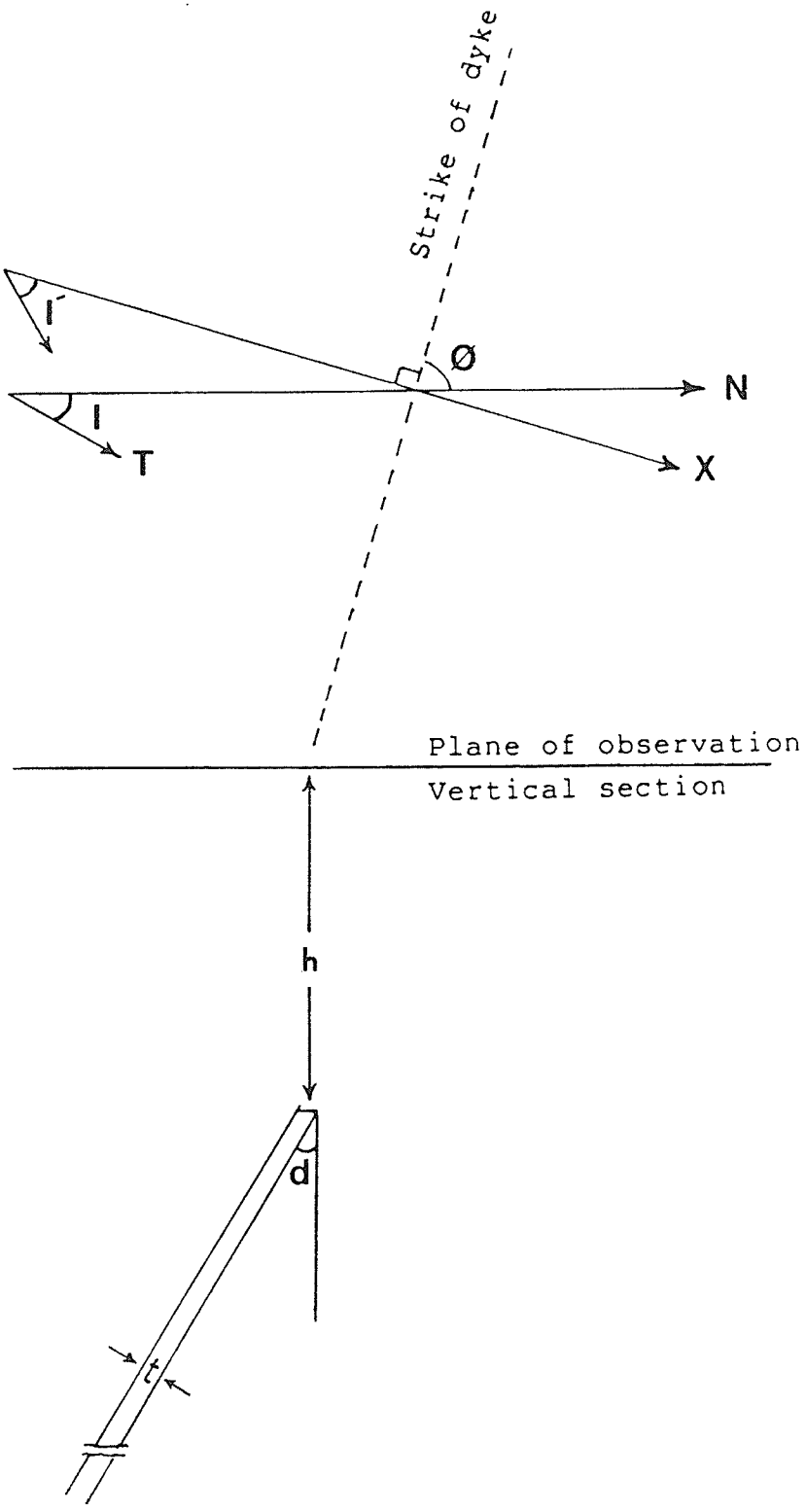


Fig. 3.6 Geometry of the thin semi-infinite dyke.

It can be shown that the amplitude, A(x) is a symmetrical, bell-shaped function and x = h at $|A(x)|/|A(0)|$ = 0.707 as we will see in Fig. 3.9.

3.2.6b The Semi-Infinite Dike

The magnetic total field anomaly ΔF, in any arbitrary direction, measured along a profile normal to the strike of a semi-infinite dike( Fig. 3.6 ) is given by the general formula ( Koefoed, 1972/unpublished notes ) as following :-

$$\Delta F = C\,[(h/R^2)\cos\alpha + (x/R^2)\sin\alpha] \qquad 3.2\text{-}45$$

Where;

$C = ( K\ T\ t \sin I \cos\beta.\eta)/( 2\ \pi \sin I' )$

$R^2 = x^2 + h^2$

$\alpha = s + i - d$

K = magnetic susceptibility contrast

T = total geomagnetic flux density ( Gammas )

t = the thickness of the dyke

I = the inclination of the normal geomagnetic Field

I′ = the angle between the projection of the geomagnetic field on the X-Z plane and the X-axis = arctan ( tan I/sin Ø)

Ø = angle between strike of dyke and the magnetic north.

s = angle between the projected direction of measurements, on the X-Z plane and the X-axis ( equals I′ )

$\beta$ = angle between direction of measurements and its projection on the X-Z plane.

$\eta = [\tan^2(I' - d) + 1/(1 + K)^2]/[\tan^2 (I' - d) + 1]$

i = angle between polarization and the horizontal plane

i′ = the projections of angle i on the X-Z plane

The partial differentiation of equation ( 3.2-45 ) yields:

$$d\Delta F/dx = (C/R^2)\sin(2\theta_1 - \alpha) \qquad 3.2\text{-}46$$

and

$$d\Delta F/dh = (C/R^2)\cos(2\theta - \alpha) \qquad 3.2\text{-}47$$

where;

$$\theta = \arctan(x/h)$$

Equation ( 3.2-47 ) turns out to be the Hilbert transform of equation ( 3.2-46 ) i.e.

$$d\Delta F/dh = ht[d\Delta F/dx] \qquad 3.2\text{-}48$$

and the phase becomes

$$Ph(x) = \arctan[(d\Delta F/dx)/(d\Delta F/dh)] = (2\theta - \alpha) \qquad 3.2\text{-}49$$

## 3.2.6c The Horizontal Cylinder

Let us use similar notations as in the previous section( semi-infinite dike), then, the total field anomaly ΔF due to a horizontal cylinder is given by:-

$$\Delta F = (C/R^2)\cos(\alpha - 2\theta) \qquad 3.2\text{-}50$$

where

$C = -(T\ K\ a \sin I \cos\beta)/(\pi(2 + K)\sin I')$ and

$\alpha = s + i'$, R and $\pi$ as in ( 3.2-47 ) and "a" is the cross sectional area of the cylinder

Now

$$ht(\Delta F) = (C/R^2)\sin(\alpha - 2\theta) \qquad 3.2\text{-}51$$

$$|A(x)| = [ht^2(\Delta F) + \Delta F^2]^{1/2} = C/R^2 \qquad 3.2\text{-}52$$

and

$$Ph(x) = \arctan [ht(\Delta F)/\Delta F] = (2\theta - \alpha) \qquad 3.2\text{-}53$$

The amplitude function A(x) has one maximum at x = 0 and half maximum at x = h i.e. both the depth and location of the horizontal cylindrical magnetic body can be determined uniquely. The phase Ph(x) has the interpretive significance that it is equal to "$-\alpha$" at the origin.

### 3.2.7 Application of the Green and Izzeldin ( 1983) Method

The amplitude function A(x) is of particular importance in the interpretation of magnetic profiles. The depth h to the top of the fault can be obtained from the width of the symmetrical peak. The phase angle Ph(x) also has important interpretive significance:

$$Ph(x) + Ph(-x) = 2\lambda = 2(2b - d) \qquad 3.2\text{-}54$$

In particular, $Ph(0) = \lambda = 2b - d$ and because Ph(x) is known, as well as $b = \arctan(\tan I/\sin \emptyset)$, the dip of the fault d is immediately obtained. Equation ( 3.2-54 ) can be used to assure accuracy in the calculated value of Ph(x).

Because x, h, and d are now known, it is obvious from equation (3.2-43) that KTC can be estimated. Hence the susceptibility K can be determined because the total field T and the constant $C(C = I - \cos^2 I \cos^2 \emptyset)$, are already known.

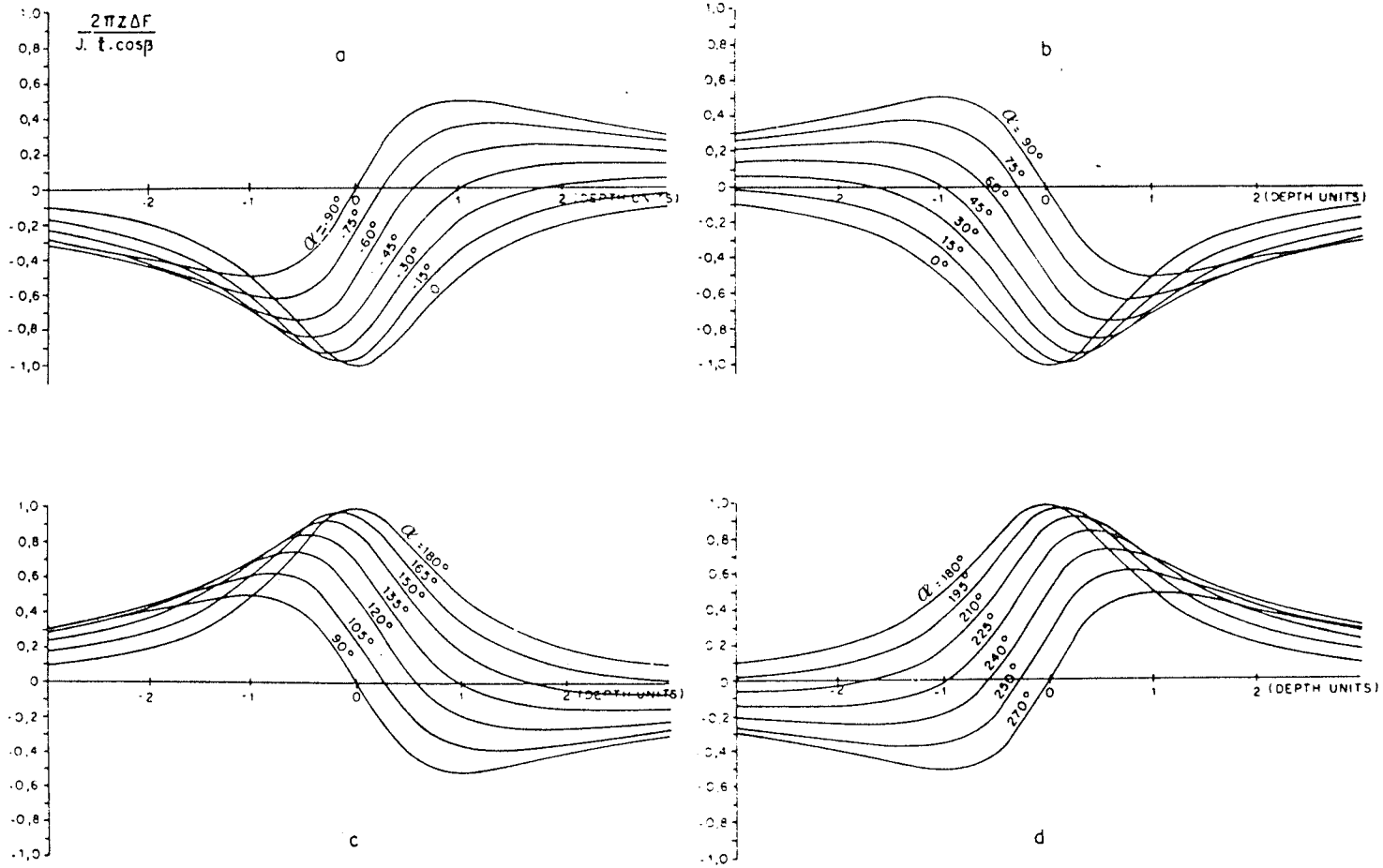


Fig. 3.7 Master curves for the semi-infinite dike: a) (s + i′ - **d**) from -90 to 0 degrees.
b) (s + i′ - **d**) from 0 to 90 degrees.
c) (s + i′ - **d**) from 90 to 180 degrees.
d) (s + i′ - **d**) from 180 to 270 degrees.
( Izzeldin, 1983 )

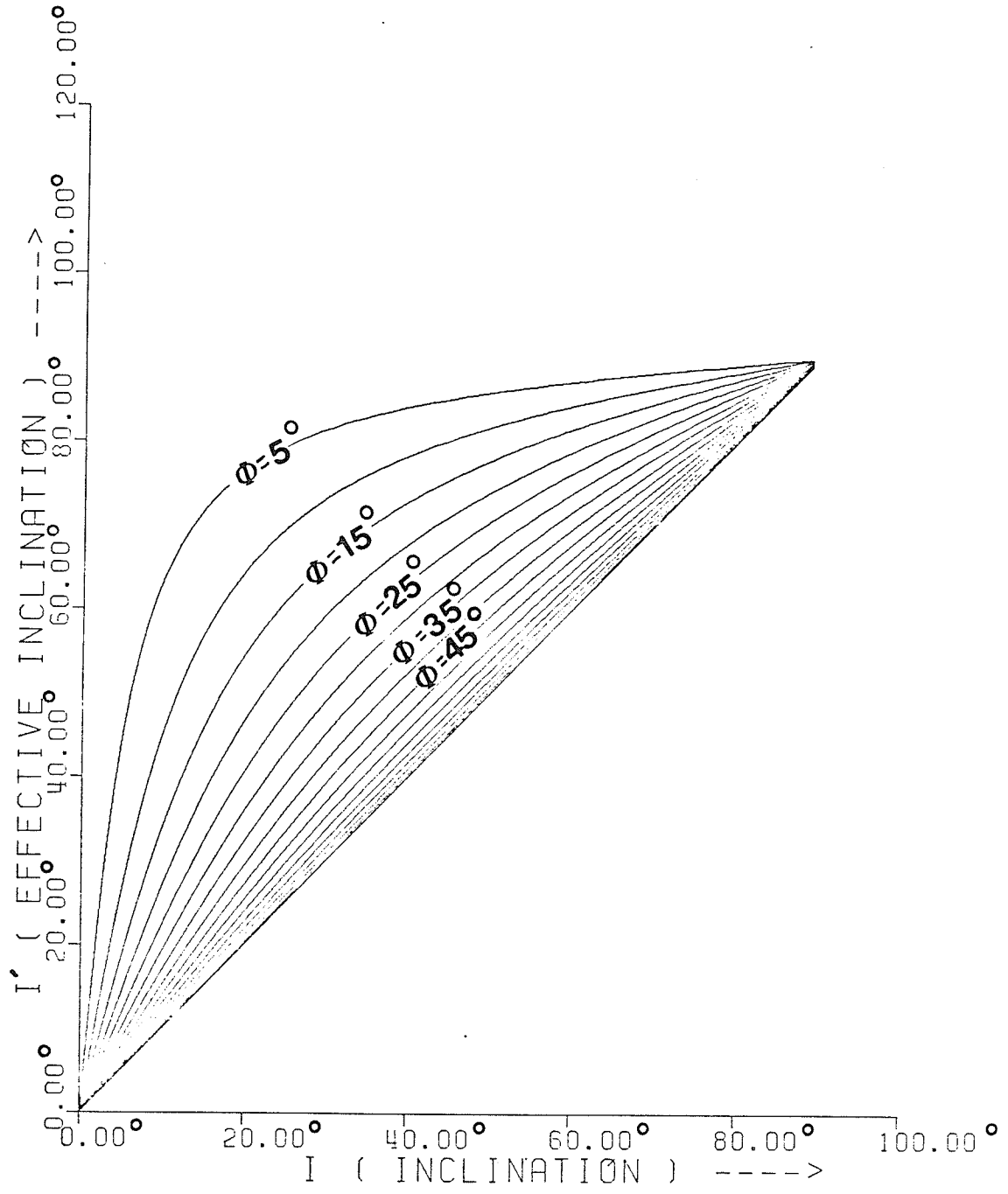


Fig. 3.8 Variation of effective inclination angle (I′) with inclination (I) and strike Ø as parameters.

The location and depth of the dike are determined from $|A(x)|$. A better estimation of depth is obtained from the average of the two values of( Xmax - $X_{1/2}$max) and location when A(x) is maximum.

The phase angle is Ph(0) = $-\alpha = -(s+i'-d)$. This can be achieved by comparing the field curve with the set of master curves ( Fig. 3.7 ). Angle "s" is equal to I', $90^0$ or $0^0$ in case of total, vertical or horizontal field data, respectively. Angle Ø is read from the flux density map as the angle between the magnetic north and the long axis of the anomaly. The inclination I is obtained from published magnetic charts. Utilizing the Fig. 3.8 with the known values of I and Ø, the angle I' can be determined. The determination of the dip angle depends on whether the susceptibility is known, whether a small value can be assumed or whether we have no idea about its magnitude. In the first case, the determination of angle d(dip) is straight forward since

$$i' - d = \arctan[(1 + K) \tan (I' - d)]$$

Furthermore from the modulus $|A(x)max| = (KTt\eta \cos \beta \sin I) /(2\pi h^2 \sin I')$, the thickness of the dike is readily determined if the susceptibility is known.

The procedure for determination of the relative location and depth of the horizontal cylinder from $|A(x)|$ is analagous to that of the infinite dike. The phase angle is Ph(0) = $-\alpha = -(s+i')$. Since "s" is always known, i' can be determined. The maximum amplitude Ph(x) is equal to

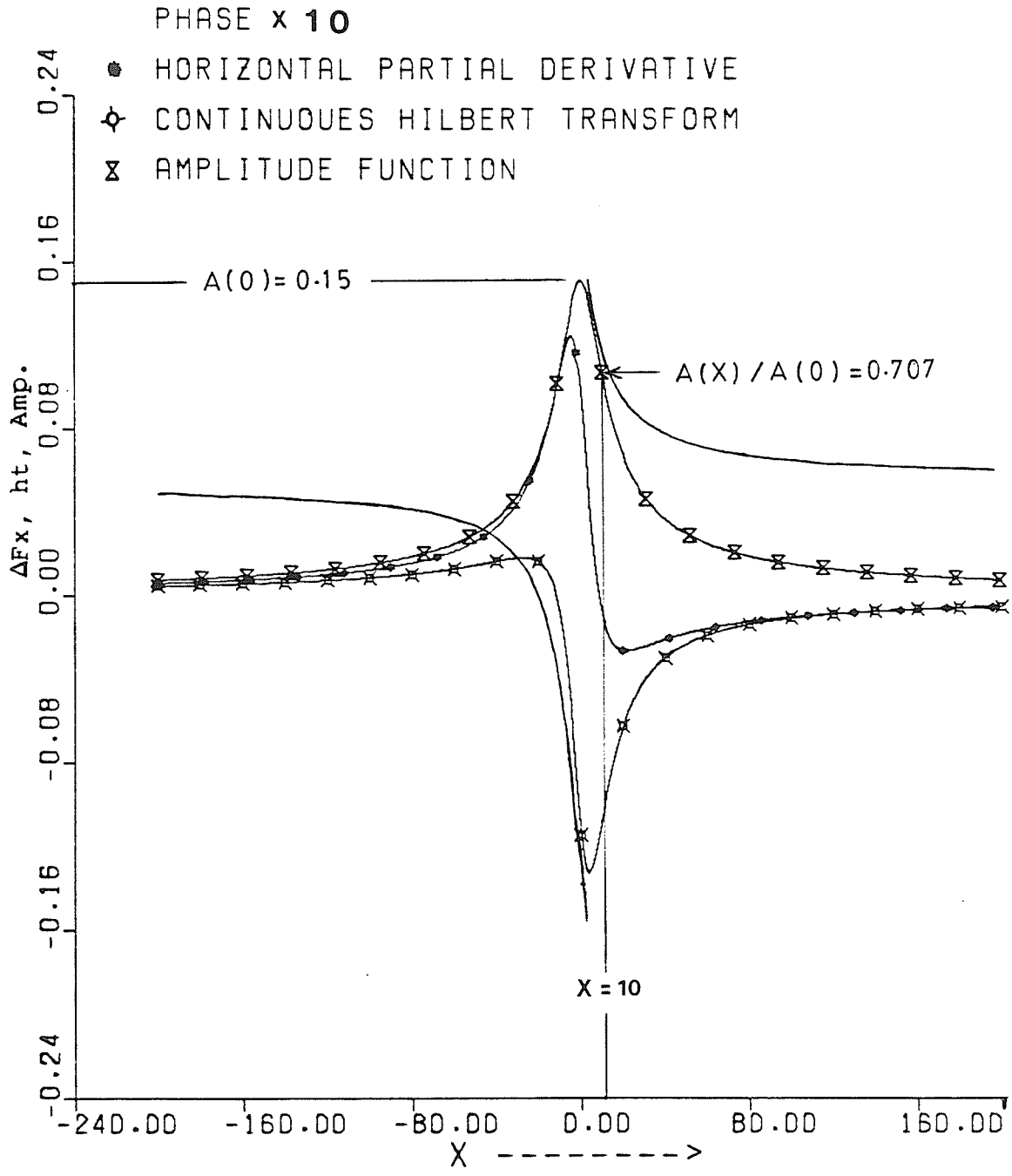


Fig. 3.9 The horizontal derivative, Hilbert transform, phase and amplitude function of the theoretical anomaly of a dipping fault.

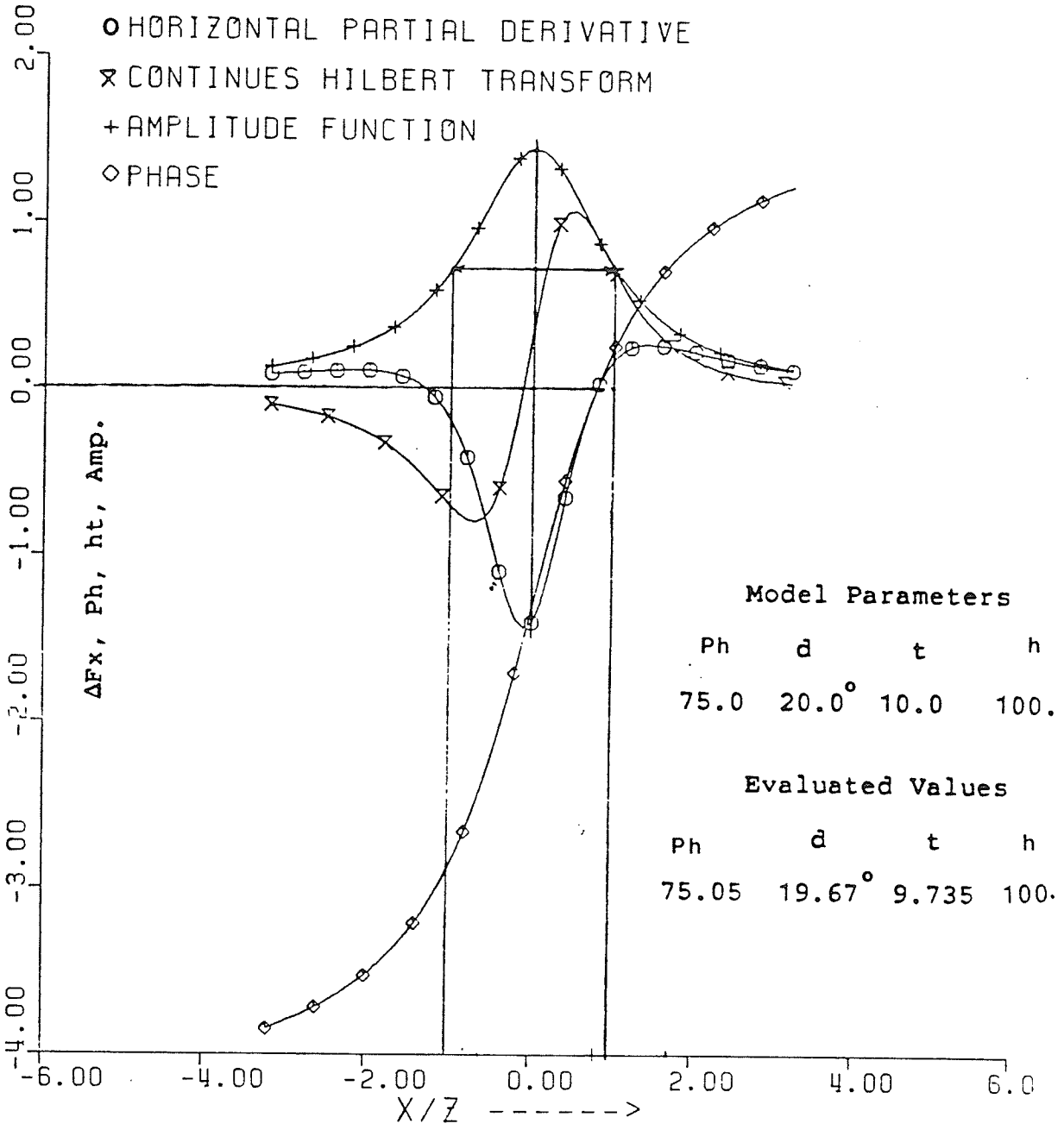


Fig. 3.10 The Hilbert transform, horizontal derivative, amplitude function and the phase of the theoretical anomaly (ΔF) of a semi-infinite dike.

$(T\ K\ t \sin I \cos \beta)/((K + 2)\pi\ h^2 \sin I')$.

In this expression, all the parameters except K and t are known. If either K or t is known or can be assumed to be known, the other can be determined.

### 3.2.8 Examples with Theoretically Computed Data

In the first example, the theoretical magnetic profile $\Delta F(x)$ over a dipping infinite fault is calculated ( Fig. 3.9 ) at $I = 62^0$, strike angle $(\emptyset) = 160^0$, dip( d ) = $70^0$, depth ( h ) = 10 ( arbitrary unit ). The computed values show, at Ph = 0, $d = 73^0$, and at $A(x)/A(0) = 0.707$, x = h = 10 ( arbitrary unit ).

Next, the total field anomaly is calculated for a semi-infinite dike with the following parameters: $T = 3500\gamma$, K = 2, $I = 30^0$, $\emptyset = 70^0$, t = 10m, h = 100m and $d = 20^0$. The computed quantities $d\Delta F/dx$, $d\Delta F/dh$, A(x) and Ph(x) of the anomaly of the dike is shown in Fig. 3.10 using cell size of 0.1 depth units.

Linear regional gradients cause a vertical shift in $d\Delta F/dx$ but have no influence on $d\Delta F/dh$, as the Hilbert transform of a constant is zero. It follows that the position of maximum and half-maximum of the function $|A(x)|$ are not affected. Depth to dike is found to be 100 m and location at x = -5m. From the known Ph(x) and Figs. 3.7, 3.8 and 3.10, it can be found that $Ph = 75.05^0$, $I' = 32.47'$ and (i'

- d) = 34.4°. Now if we know K to be 2, ( I′ - d ) will be 12.8° and thus d is 19.67° which is sufficiently accurate estimate of the true value of 20°.

In case of the horizontal cylinder, the total magnetic flux density anomaly is calculated with the following parameters: T = 35,000γ, K = 2, I = 30°, Ø = 70°, a = 314 $m^2$ and h = 100m. Fig. 3.11 shows the Hilbert transform, the amplitude function A(x) and the phase Ph(x) of the total magnetic flux density anomaly of the horizontal cylinder. From A(x), the depth is found to be 100 m and the location x = 5m. Using the plot of Ph(x), (s + i′) is found to be 75.05° and thus i′ = 30.4′. It is seen that s and i′ do not differ appreciably as expected with homogeneous magnetization due to induction.

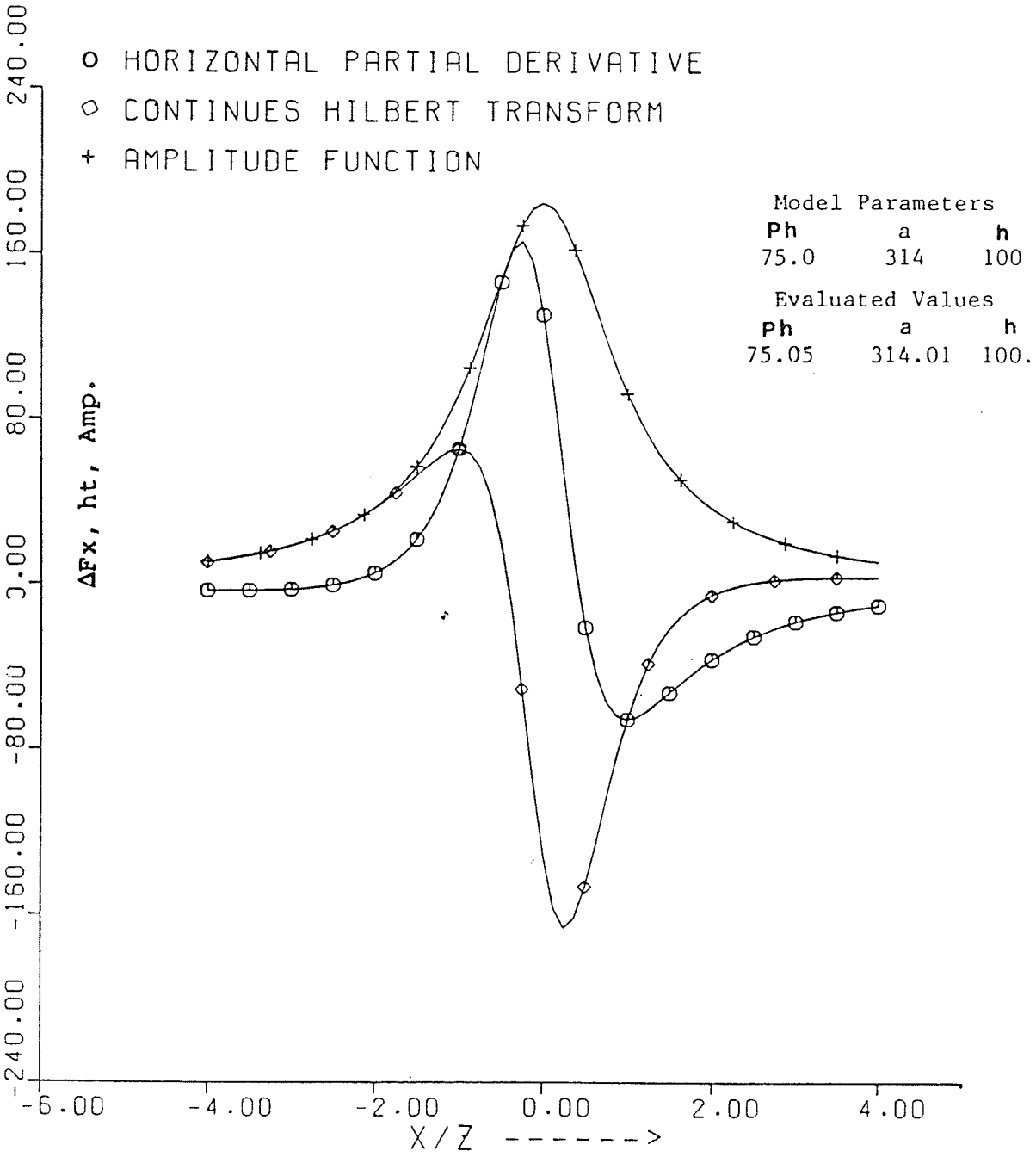


Fig. 3.11a The horizontal derivative, Hilbert transform and amplitude function of the theoretical anomaly (ΔF) of a horizontal cylinder.

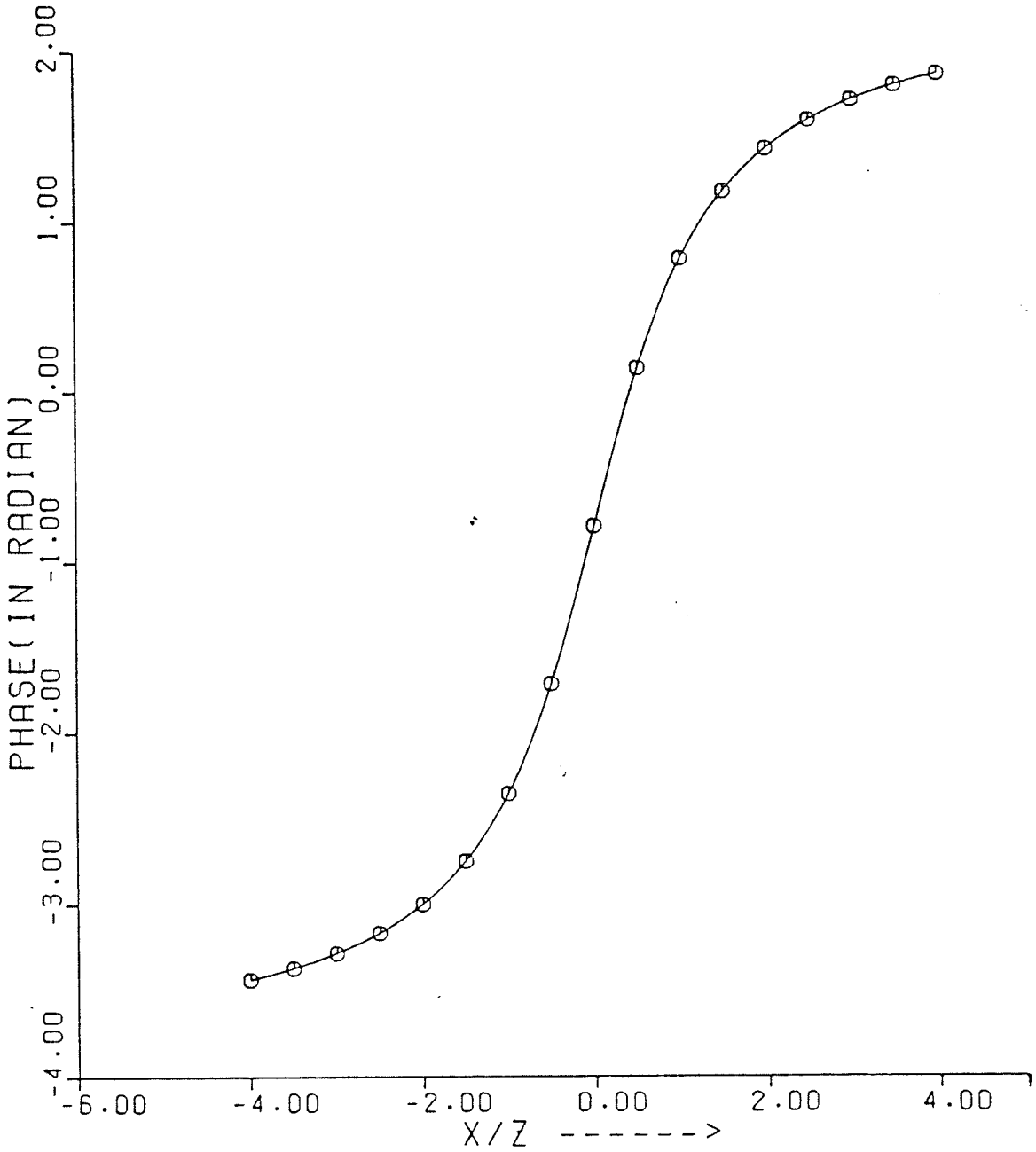


Fig. 3.11b The phase of the theoretical anomaly (ΔF) of a horizontal cylinder.

## 3.3 HILBERT TRANSFORM AND GRAVITY RELATIONS

In this section I want to discuss the application of 1-D Hilbert transform in the gravity data interpretation. I will follow the work by Mohan et al. ( 1982 ). Since a fault structure can be approximated by two semi infinite horizontal sheets; one displaced vertically from the other, or by combining a pair of the slabs to make a true fault.

### 3.3.1 Dipping Fault Model

For a semi-infinite dipping fault block of finite throw ( Fig. 3.12a ), the gravity field formula is given by (Jung 1961)

$$g(x) = 2\,G\,\rho \sin d\,[(x + h_1 \cot d)\sin d\{\sin d \ln(r_B/r_A) - \cos d(\phi_B - \phi_A)\} + (h_2\phi_B - h_1\phi_A)] \qquad 3.3\text{-}1$$

Where;

G = the gravitational constant

$\rho$ = the density contrast

d = the dip of the fault

$h_1$ = the depth to the top of the fault

$h_2$ = the depth to the bottom of the fault

By differentiating equation ( 3.3-1 ) with respect to x twice, we obtain;

$$g''(x) = 2\,G\,\rho \sin d\,[\{(h_1 \cos d - x \sin d)/r_A^2\} - \{((2h_2 - h_1)\cos d - x \sin d)/r_B^2\}] \qquad 3.3\text{-}2$$

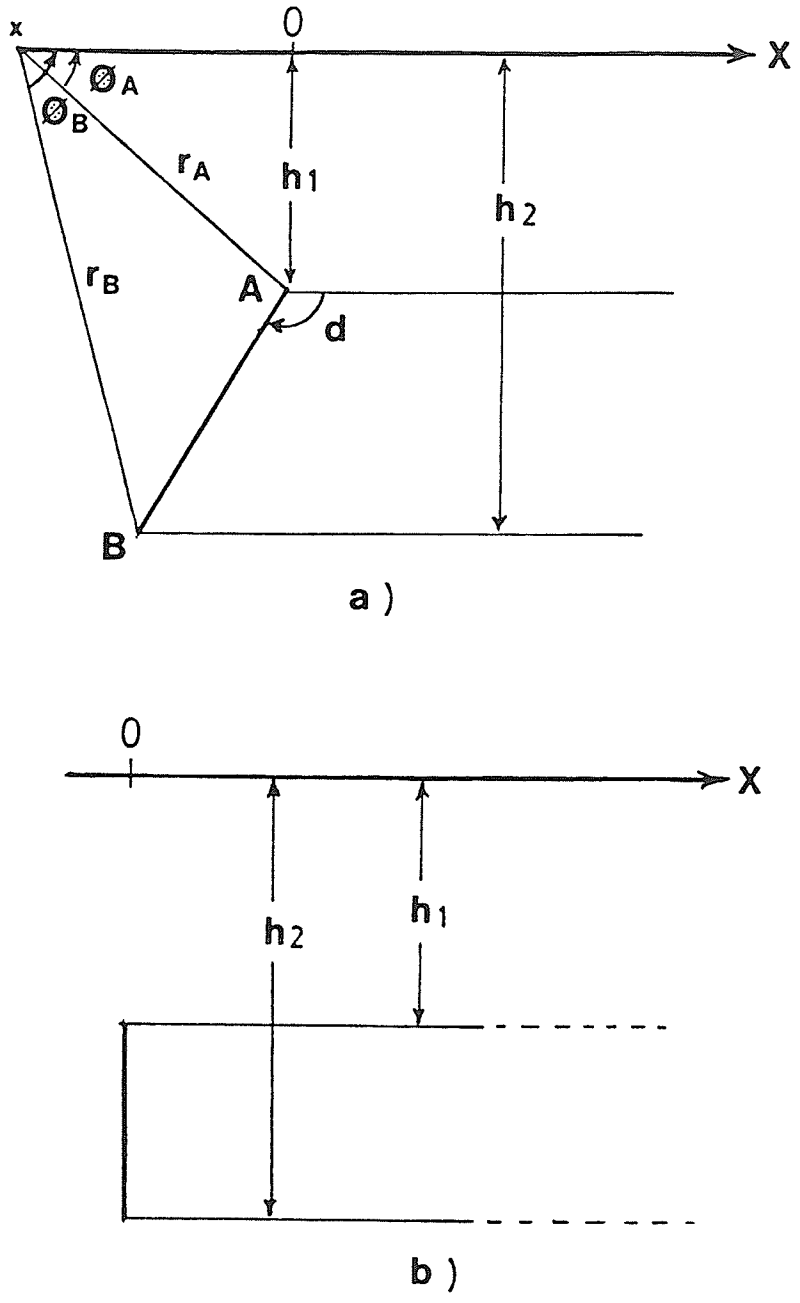


Fig. 3.12 (a) Geometry of the two-dimensional dipping fault.
(b) Geometry of the two-dimensional vertical fault

Equation ( 3.3-2 ) can be rewritten as,

$$g''(x) = 2\,G\,\rho \sin d[\{(h_1 \cos d - x \sin d)/(x^2+h_1^2)\} + \{((x-D)\sin d - h_2 \cos d)/((x-D)^2+h_2^2)\}] \qquad 3.3\text{-}3$$

where $D = (h_2 - h_1) \cot d$.

The Fourier transform of $g''(x)$ is given by;

$$F(\omega) = \int_{-\infty}^{\infty} g''(x) \exp(-j\omega x)\, dx$$

$$= \int_{-\infty}^{\infty} g''(x)[\cos \omega x - j \sin \omega x]\, dx \qquad 3.3\text{-}4$$

Substituting for $g''(x)$ from equation ( 3.3-3) in equation ( 3.3-4 ) and evaluating the integral, the real and imaginary components of the Fourier transform are obtained as:

$$Fr(\omega) = 2\,\pi\,G\,\rho \sin d\,[\exp(-\omega h_1) \cos d - \cos (d - \omega D) \exp(-\omega h_2)] \qquad 3.3\text{-}5$$

and

$$Fi(\omega) = 2\,\pi\,G\,\rho \sin d\,[\exp(-\omega h_1) \sin d - \sin (d - \omega D) \exp(-\omega h_2)] \qquad 3.3\text{-}6$$

The Hilbert transform of $g''(x)$ is then defined as

$$ht(x) = (1/\pi) \int_{-\infty}^{\infty} [Fi(\omega) \cos \omega x - Fr(\omega) \sin \omega x]\, d\omega \qquad 3.3\text{-}7$$

Substituting equations ( 3.3-5 ) and ( 3.3-6 ) in equation ( 3.3-7 ), and after integration, the Hilbert transform is obtained as,

$$ht(x) = 2\,G\,\rho \sin d\,[\{(h_1 \sin d - x \cos d)/(x^2 + h_1^2) + \{((x-D) \cos d - h_2 \sin d)/((x-D)^2+h_2^2)\}]. \qquad 3.3\text{-}8$$

Following Nabighian ( 1972 ) we determine the origin by examing the maxima of,

$$A(x) = [\ \{g''(x))\}^2 + \{ht(x)\}^2\ ]^{1/2}. \qquad 3.3\text{-}9$$

Then the approximate dip of the fault block is determined as follows

At $x = 0$, the equations ( 3.3-3 ) and ( 3.3-8 ) reduce to

$$g''(0) = 2\ G\ \rho \sin d\ [\ \cos d\{(1/h_1) - (h_2/(D^2+h_2^2))\} - \{(D \sin d\ )/(D^2+h_2^2)\}] \qquad 3.3\text{-}10$$

and

$$ht(0) = 2\ G\ \rho \sin d\ [\ \sin d\{(1/h_1) - (h_2/(D^2+h_2^2))\} - \{(D \cos d\ )/(D^2+h_2^2)\}]. \qquad 3.3\text{-}11$$

From equations ( 3.3-10 ) and ( 3.3-11 ) we have

$$[g''(0)/ht(0)] = [M \cot d - N]/[M - N \cot d] \qquad 3.3\text{-}12$$

where

$$M = [(1/h_1) - (h_2/(D^2+h_2^2))] \quad \text{and} \quad N = D/(D^2+h_2^2).$$

For large values of $h_2$, N approaches zero. So for many practical purposes the equation ( 3.3-12 ) can be approximated to be

$$\cot d = [g''(0)/ht(0)]. \qquad 3.3\text{-}13$$

For $g''(0) = 0$, d becomes $90^0$ which is the case of a vertical fault. The graphs of the second horizontal derivative of the gravity effect of an inclined fault block $g''(x)$, and its

side of the origin ( Figs. 3.13a and 3.13c ). If the abscissa of the points of intersection are $x_1$ and $x_2$ then

$$g''(x_{1,2}) = ht(x_{1,2})$$

i.e.

$$x^2_1(h_1 - h_2 - D) + x_1(D^2+h_2^2-h_1^2-2hD) = h_2\, h_1^2-h\, h_2^2-h_1^2D - h_1D^2 \qquad 3.3\text{-}14$$

and

$$x^2_2(h_1-h_2-D) + x_2(D^2+h_2^2-h_1^2-2hD) = h_2\, h_1^2-h\, h_2^2-h_1^2D-h\, D^2 \qquad 3.3\text{-}15$$

Solving equations( 3.3-14 ) and ( 3.3-15 ), the depths to the top $h_1$, and bottom $h_2$ are obtained as;

$$h_1= [\{(x^2_1+x_2) \pm ((x_1+x_2)^2+4x_1x_2(k_2+k_3))^{1/2}\}/ + 4x_1x_2(k_2+k_3))^{1/2}\}/\{2(k_2+k_3)\}] \qquad 3.3\text{-}16$$

and

$$h_2 = (k_3h_1^2 - x_1x_2)/(k_1h_1) \qquad 3.3\text{-}17$$

where;

$k_1 = ( 1 + P^2 )/( 1 - P )$

$k_2 = ( 1 +2P - P^2 )/( 1 - P )$

$k_3 = P( 1 + P )/( 1 - P)$ and $P = \cot d.$

Finally the density contrast $\rho$ is determined from

$$\rho= (1/(2G \sin d))[(\{g''(0)\}^2+\{ht(0)\}^2)/(A+B+C)]^{1/2} \qquad 3.3\text{-}18$$

where

$A = 1/h_1^2$, $B = ( D^2+h_2^2+4D\, h_2 \cos d \sin d)/(h_2^2+ D^2)^{1/2}$

$C = -2(h_2 + 2D \sin d \cos d)/(h_1(h_2^2 + D^2))$.

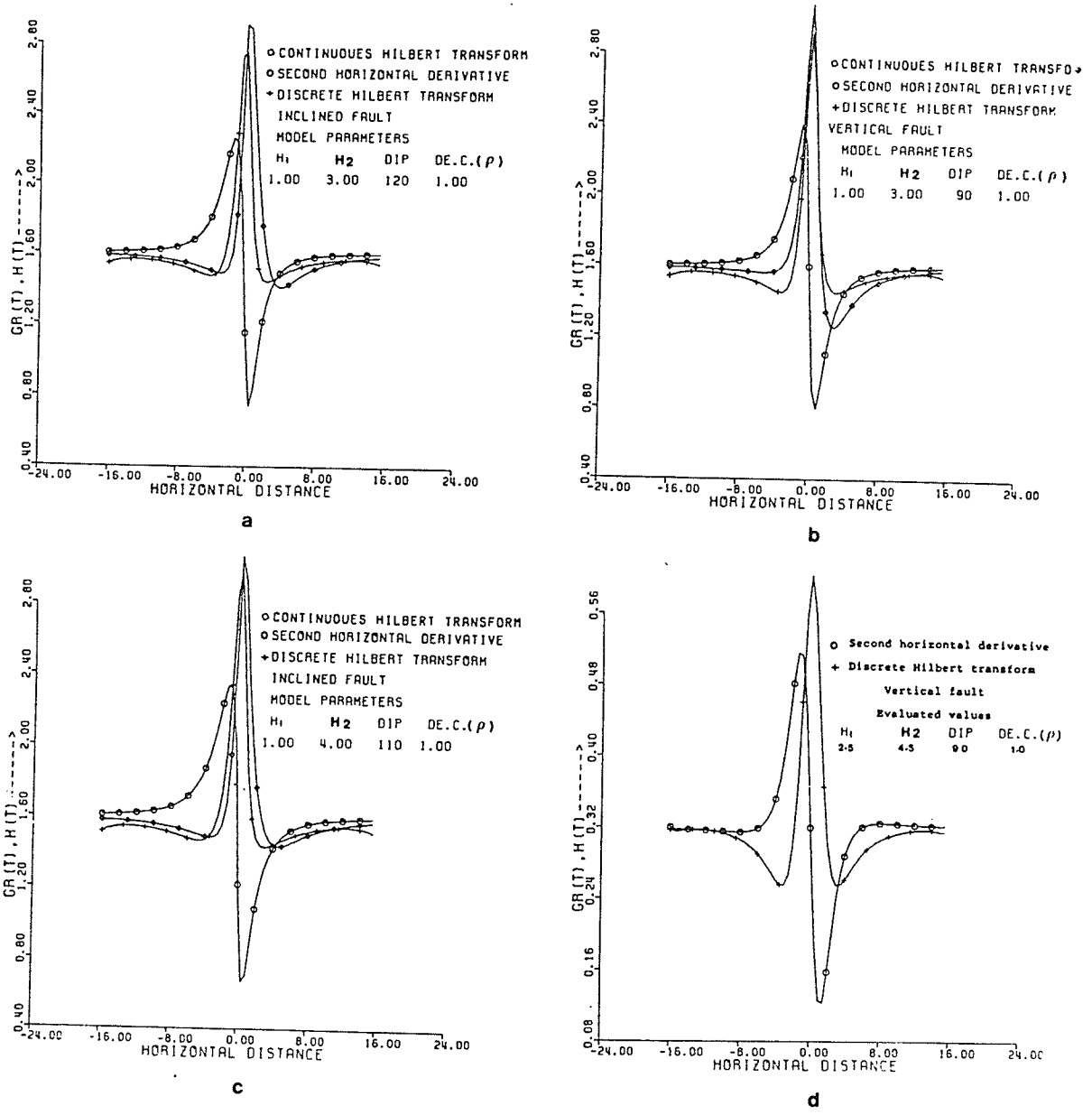


Fig. 3.13 Example of using 1-D Hilbert transform in quantitative interpretation of the gravity effect of the 2-D fault.

Thus, the above analysis facilitates the determination of all the parameters of a dipping fault.

### 3.3.2 Vertical Fault Example

The semi-infinite vertical fault block ( Fig. 3.12b ) is a special case of the dipping fault with d assuming the value of $\pi/2$. The second horizontal derivative of the vertical fault and its Hilbert transform are thus obtained by substituting $d = \pi/2$ in equations ( 3.3-3 ) and ( 3.3-8 );

$$g_1''(x) = 2\,G\,\rho[(x/(x^2+h_2^2)) - (x/(x^2+h_1^2))] \qquad 3.3\text{-}19$$

and

$$ht_1(x) = 2\,G\,\rho[\{h_1/(x^2+h_1^2)\}-\{h_2/(x^2+h_2^2)\}]. \qquad 3.3\text{-}20$$

As in the previous section, the graphs of $g_1''(x)$ and $ht_1(x)$ are found to intersect on either side of the origin ( Fig. 3.13b ). The parametric evaluation in the case of a vertical fault can be made simply by substituting $d=\pi/2$ in equations (3.3-16), (3.3-17) and (3.3-18) which yield the depths to the top and bottom and the density contrast as follows:-

$$h_1 = [(x_1+x_2) \pm\{(x_1+x_2)^2+4x_1x_2\}^{1/2}]/2 \qquad 3.3\text{-}21$$

$$h_2 = -x_1\,x_2/h \qquad 3.3\text{-}22$$

and

$$\rho = [h\,h_2\{(g''(0))^2+(ht(0))^2\}^{1/2}\}/\{2G(2-h_1)\}]. \qquad 3.3\text{-}23$$

Table 6. Theoretical Examples( In arbitrary units)

| | Parameters | d | $h_1$ | $h_2$ | $\sigma$ |
|---|---|---|---|---|---|
| Dipping fault | | | | | |
| Model I | Assumed values | 120.0 | 1.00 | 3.00 | 1.0 |
| | Evaluated values | 123.8 | 1.11 | 3.14 | 1.03 |
| Model II | Assumed values | 110.0 | 1.00 | 4.00 | 1.00 |
| | Evaluated values | 114.6 | 0.97 | 3.90 | 1.11 |
| Vertical fault | | | | | |
| Model I | Assumed values | ----- | 0.50 | 1.00 | 1.00 |
| | Evaluated values | ----- | 0.56 | 0.99 | 1.28 |
| Model II | Assumed values | ----- | 1.00 | 3.00 | 1.00 |
| | Evaluated values | ----- | 1.00 | 2.71 | 0.95 |

### 3.3.3 Test Examples with Discrete Theoretical Data sets

The theoretical derivations developed earlier can be made applicable to discrete field data sets, by introducing the Discrete Fourier Transform ( DFT ) and the Discrete Hilbert Transform .

The real and imaginary components of the DFT are given by ( Gold and Rader, 1969 ),

$$Fr(n\omega_0) = \sum_{L=0}^{N-1} g''(L.\Delta x)\cos(n\omega_0.L.\Delta x) \qquad 3.3\text{-}25$$

and

$$Fi(n\omega_0) = \sum_{L=0}^{N-1} g''(L.\Delta x)\sin(n\omega_0.L.\Delta x) \qquad 3.3\text{-}26$$

The discrete Hilbert Transform is defined as,

$$ht(L.\Delta x) = (1/\pi)\left[ \sum_{n=0}^{(N/2)-1} Fi(n\omega_0)\cos(n\omega_0.L\Delta x) - \sum_{n=0}^{(N/2)-1} Fr(n\omega_0)\sin(n\omega_0.L\Delta x)\right] \qquad 3.3\text{-}27$$

where $\omega_0 = 2\pi /N.\Delta x$ ( radians per unit length ) is the fundamental frequency, $\Delta x$ is the station spacing and N is the total number of observed values.

### 3.3.3a Dipping Fault

Two theoretical models ( Table 6 ) are analysed to examine the validity of the earlier procedure, with the help of equations (3.3-3) and (3.3-8). The second horizontal deriva-

tive of the gravity effect and its Hilbert transform are computed in each case and shown in Fig. 3.13a and 3.13c. The Discrete Hilbert Transform, Dht(L.$\Delta$X), is also computed in each case and shown in Fig. 3.13a and 3.13c. The length of profile ( X ) is 32 ( arbitrary units ) which is digitized to 64 equal parts and the station spacing is 0.5. Using the equations (3.3-13), (3.3-16), (3.3-17) and (3.3-18) the parameters namely the dip d, the depth to the top $h_1$, the depth to the bottom $h_2$ and the density contrast $\rho$ are evaluated and presented in Table 6.

### 3.3.3b Vertical Fault

In the case of a vertical fault, two theoretical models are studied, using the corresponding equations ( 3.3-19 ) to ( 3.3-23 ), and one of these models ( Model II ) is shown in the Fig. 3.13b. The parameters, namely the depth to the top $h_1$, the depth to the bottom $h_2$ and the density contrast $\rho$ are evaluated and presented in the Table 6.

### 3.3.4 Quantitative Interpretation of Gravity Field Data

As I have shown, the application of Hilbert transform in evaluating theoretical data can be extended to evaluate the parameters for the field data. The second horizontal derivative of the anomaly can be computed numerically, and smoothed by using Least squares curve-fitting, Cubic spline method and FFT algorithm. The Least squares and Cubic spline are discussed below in more detail.

### 3.3.4a Least-Squares Curve-Fitting

Since the real data collected in the field represent a discrete sequence and contain irregularities in comparision with theoretical data. For this reason one tries to obtain the best fit of the field data by using a Least-squares polynomial which approximately represents the data( field data) set.

Suppose we have a field data set representing a vertical fault;

$G(x_0)$, $G(x_1)$,$G(x_2)$, .....G(xn) along profile a $x_0$, $x_1$, $x_2$, .....xn.

Then, the best fit may be obtained with $\bar{n}$-degree polynomial $g\bar{n}(X)$

$$g\bar{n}(x) = R\bar{n}x^{\bar{n}} + R\bar{n}-_1 x^{\bar{n}-_1} + .....R_1x + R_0$$

where

$0 < \bar{n} < n$. The $R\bar{n}$, $R\bar{n}_1$, ..... $R_1$ are the solution of the following equations;

$$a\bar{n}_0 R\bar{n} + a\bar{n}_{-1 0} R\bar{n}_1 + .... a_{00}R_0 = \Sigma\, G(xi)F_0(xi)$$

$$a\bar{n}_1 R\bar{n} + a\bar{n}_{-1 1} R\bar{n}_1 + ....' a_{0 1}R_0 = \Sigma\, G(xi)f_1(xi)$$

. . .

. . .

. . .

$$a\bar{n}\bar{n}R\bar{n} + a\bar{n}_{-1}\bar{n}R\bar{n}_{-1} + .... a_0\bar{n}R_0 = \Sigma\, G(xi)f\bar{n}(xi) \text{ and}$$

$$f_0(x) = 1,\ f_1(x)=x,\ ....f\bar{n}(x)=x^{\bar{n}}$$

$$akj = ajk = \sum_{i=0}^{\bar{n}} fk(xi)fj(xi)$$

where

$k = 0, 1, 2, .....\bar{n}$

$j = 0, 1, 2, .....\bar{n}.$

The second horizontal derivative of the polynomial $g\bar{n}(x)$ is

$$\ddot{g}\bar{n}(x) = \bar{n}(\bar{n}_{-1})R\bar{n}x^{\bar{n}-2} + (\bar{n}_{-1})(\bar{n}_{-2})R\bar{n}_{-1}x^{\bar{n}-3} + .....R_2$$

A computer program was written in double precision to perform this task and this program determines the optimum degree one can choose to get the best fit and one can interpolate the data by using the best fit polynomial.

In general the best fit depends on the data and the degree of the polynomial. If the degree is high one will get large deviations from a smooth curve through the data and more fluctuations. In such case, the Least-Squares approach is not appropriate.

### 3.3.4b Fitting Data with a Cubic Spline

For simplicity the numerical experiments were carried out for a vertical fault where the data are digitized into 64 equal parts along profile X with a station spacing of 0.5 ( arbitrary unit ) ( Fig. 3.13d ). By using a subroutine CUBSPL, I determined the values of S (second derivatives) for cubic splines that fit a set of x, $g(x)$-Pairs passed to the subroutine in two vectors. Since the solution of the tridiagonal matrix system is much easier and quick, the CUBSPL took advantage of this fact. The original subroutine CUSPL was taken from the Applied Numerical Analysis ( chapter 10 ) by Gerald( 1982 ).

## 3.4 GENERAL COMMENTS

In magnetics, the interpretation of vertical magnetic anomalies caused by simple Sheets ( finite and infinite depth extent ), Dikes, Horizontal circular cylinders and dipping faults can be achieved by using 1-D Hilbert transform techniques.

The differentiation of V(x) or $\Delta F(x)$ with respect to x introduces a certain amount of error, and the Hilbert transform is affected while it was evaluated using the Fourier transform and consequently its value depends upon the FFT algorithm. The sampling interval and the sampling rate used

in digitizing the potential field data and their gradients play an important role in minimizing errors.

The same Hilbert transform techniques used in magnetics can be easily extended in gravity, and the physical parameters of the dipping fault can be obtained. It may be mentioned here that if the differentiation is carried out effectively and more accurately in the frequency domain, the errors will be reduced sufficiently to obtain a reliable second derivative profile( Mohan, 1982 ).

It should also be pointed that the error in the evaluation of parameters depends on the measurement and the quality of the gravity field data as much as the computation of derivatives.

# CHAPTER 4

# APPLICATION OF 1-D HILBERT TRANSFORM IN SEISMIC SIGNAL ANALYSIS AND FILTERING

## 4.1 INTRODUCTION

In recent years the discrete Hilbert transform has found more and more applications in theory and practice of digital signal processing. The representation of a signal as the real part of a complex function in time is a useful device in many areas of signal analysis.

In seismic application, the conventional seismic signal can be viewed as the real component of a complex signal which can be uniquely calculated under usual conditions. In this chapter I will demonstrate a significant improvement of a real seismic signal in the form of the complex envelope ( amplitude and phase ) which may be obtained by using the discrete Hilbert transform techniques. The pulse I shall study is in a form of the Berlage function often used to simulate seismic signals ( Kulanek and Klima, 1970 ).

In addition, I am going to discuss the application of Hilbert transform on the spectral factorization which is related to the minimum phase and inverse filters. Also the discussion will be extend to the ideal filtering processes

which can be directly expressed in terms of Hilbert transforms. I will also consider such filters as Lowpass and Bandpass filters.

## 4.2 HILBERT TRANSFORM IN SEISMIC SIGNAL ANALYSIS

Application of the Hilbert transform (1-D) in seismic signal analysis has been very useful, especially when we represent the signal as the real part of a complex function in time. In general terms, the advantages of the complex envelope stem from the natural separation of amplitude information from angle information. In a real signal, these are blended in such a way which can be confusing to visual analysis. In this section we will see how the complex envelope of a seismic wavelet can be calculated.

Let us start our discussion by assuming a signal, P(t), which can represent a seismic trace of finite duration that has been digitized for computer processing. Thus, the time variable t assumes only integer values, t = 0, 1, 2, .....N-1, where the duration of P(t) is N samples. We try to represent this signal as the real part of a complex envelope, $\bar{P}(t)$ ( the bar over each symbol indicating a complex quantity),

$$P(t) = \text{Re}\ \bar{P}(t) = \text{Re}[|\bar{P}(t)|\exp\{j\ Ph(t)\}] \quad 0 \le t < N \quad 4.2\text{-}1$$

where $|\bar{P}(t)|$ is the envelope of P(t). Some times we call it E(t). The Ph(t) is the angle function or phase function.

It is the polar notation of equation (4.2-1) that will be most useful in what follows. If one can visualize the $\bar{P}(t)$ in the complex plane as a vector with length $|\bar{P}(t)|$ rotating with angle Ph(t) with respect to the real axis, the analogy with a "time-varying phasor" is clear (Bracewell, 1965). Consequently the definition of instantaneous amplitude and frequency as the length and rotational velocity, respectively, of a vector $\bar{P}(t)$ gives

$$\left( \begin{array}{l} \text{instantaneous amplitude} = |\bar{P}(t)| = E(t) \\ \text{instantaneous radian frequency} = (d/dt)Ph(t) \end{array} \right) \quad 4.2\text{-}2$$

Of course, equation (4.2-1) is insufficient for calculating $\bar{P}(t)$ from a given P(t), since the imaginary part is completely unspecified. However, the complex envelope can be derived from equation (4.2-1) by specifying that it be linear, that is, the scaling and addition of real signals correspond to a similar scaling and addition of their complex envelopes, and that (4.2-1) reduces to a phasor representation in the special case where P(t) is a pure sinusoid with an integer number of periods in time interval t = (0,N).

It is important for us here to note that the complex envelope so derived is a complex signal which lends to equation ( 4.2-2), an interpretation which is intuitively meaningful. That is the instantaneous amplitude and frequency agree with amplitudes measured at signal peaks and frequencies calculated from zero crossings.

The Hilbert transformed signal is variously known as the quadrature signal ( Gabor, 1946 ) or the allied signal ( Jeffreys and Lapwood, 1957 ), while the complex envelope is also known as the analytiç signal belonging to P(t) ( Gabor, 1946 ) since the real part of P(t) is given by equation (4.2-1). The envelope E(t) and phase Ph(t) of a function, P(t), can be obtained by using the discrete Hilbert transform as

$$E(t) = [\, P^2(t) + P_H^2 ]^{1/2} = ( Pc Pc^{*} )^{1/2} \qquad 4.2\text{-}3$$

and $$Ph(t) = \arctan[P / P(t)] \qquad 4.2\text{-}4$$

where

$P_H$ = Hilbert transform of P(t), $Pc^{*}$ = Conjugate of Pc

Pc = Complex discrete function of P(t)

## 4.3 BERLAGE FUNCTION

Let us look first at an artificial pulse whose characteristics we can control. The pulse we shall study is a form of the Berlage function often used to simulate seismic signals ( Kulhanek and Klima, 1970). The definition of the Berlage function is given in equation ( 2.5-2 ). This pulse is shown in the Fig. 4.1a. In this example the sine factor makes the pulse oscillate with 0.5 sec between zero-crossings, while the $t^2$ and exp factor give rise to a defined onset at t = 0 and an exponentially decaying tail. The complex representation for the given pulse is found by replacing the sine term by a complex exponential as is done with phasors. That is,

$$P(t) = \mathrm{Re}\; t^2 \exp(2 - 2t) \exp[j(2\pi t - \pi/2)]. \qquad 4.3\text{-}1$$

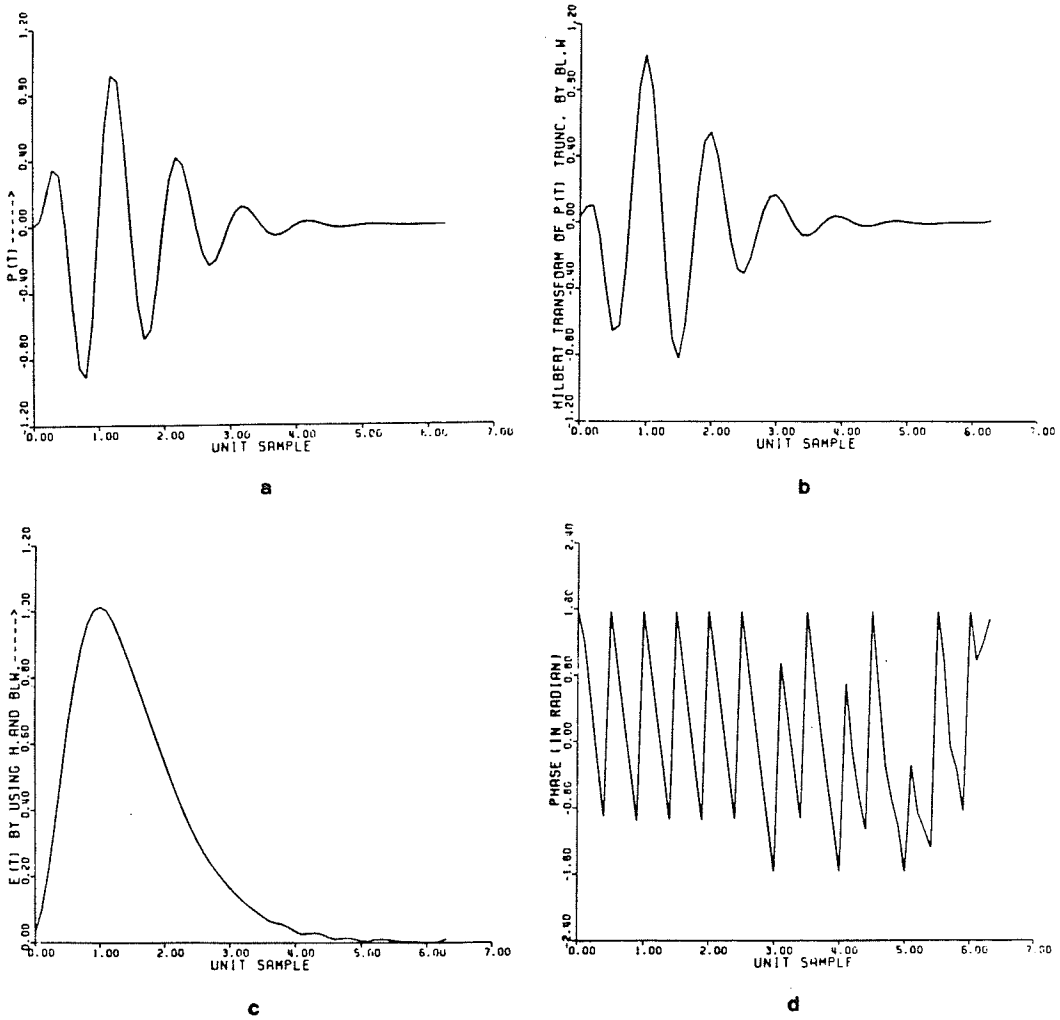


Fig. 4.1 An artifical pulse and its Hilbert transform and complex envelope: (a) Real pulse P(t), (b) Hilbert transform of P(t), (c) and (d) envelope and angle function, respectively, obtained by using eqs. 2.3-1 and 2.3-2.

While this is a good representation and provides instantaneous amplitude and angle functions directly, it is not very useful in studying seismic records. A seismic record can never be specified mathematically in a form such as Berlage function, and because of the irregularities in a signal, the simple replacement of a sinusoid by a complex exponential function which led to equation (4.3-1) is often inappropriate for seismic signals. On the other hand, a method that can calculate the complex envelope of a given recorded signal is an acceptable approach as shown in previous section.

The result of this work is demonstrated in the Fig. 4.1b-d. A detailed comparison of the computed values shows that the complex envelope is equivalent to equation (4.3-1) to very good approximation. That is,

$$\left.\begin{aligned} \bar{P}(t) &= t^2\exp(2 - 2t)\exp(j(2\pi t - \pi/2), \\ |\bar{P}(t)| &= t^2\exp(2 - 2t) \\ Ph(t) &= 2\pi t - \pi/2. \end{aligned}\right| \qquad 4.3\text{-}2$$

The errors are most noticeable in the angle function before t = 0 sec and beyond t = 5 sec. They occur at times when the given pulse is very weak or not defined, since the angle of a very small complex vector is ill-defined in a practical sense. It can be shown that, the errors in equation (4.3-2) are due to spectral truncation effects beyond computer roundoff error which we need not consider in further detail here because they are not important for real seismic signals. These relationships between the envelope and instantaneous

amplitude and frequency and the original pulse series will however be important in what follows.

## 4.4 SIMULATION OF ARTIFICIAL SIGNAL

Since the Berlage function is a simple pulse which has the most basic properties of seismic signals such as oscillatory nature and the definite onset, the coda of the first onset can be realistically simulated by adding attenuated copies of the basic pulse , if necessary delayed in the wake of the initial onset.

That is, if "tn" and "an" represent the delay and scale factor of the nth pulse added into the coda, the synthetic signal has the form

$$S(t) = P(t) + \sum_{n} an\ P(t - tn) \qquad 4.4\text{-}1$$

where tn is the positive delay to preserve the initial onset of S(t) at t = 0.

The equation (4.4-1) has a very attractive physical interpretation. If the inital pulse P(t) represents the main arrival at the recording station, then the delayed pulses may represent minor wavelets arriving subsequently. These may be reverberations from inhomogeneities beneath the station or pulses from multiple paths in the layered transmission medium. The positive and negative values of "an" correspond to positive and negative reflections of the main wavelet or the primary event.

Table 7. Delays( tn ) and scale factors( an ) of an artifical pulse ( Fig.4.2a ).

| n | Delay tn, sec. | Scale factor an |
|---|---|---|
| 1 | 1.6 | 0.29 |
| 2 | 2.3 | -0.24 |
| 3 | 3.9 | 0.36 |
| 4 | 5.5 | -0.37 |
| 5 | 8.5 | 0.20 |
| 6 | 9.8 | 0.25 |
| 7 | 11.3 | 0.15 |

From the standpoint of physical interpretation of equation (4.4-1), the real justification lies in how realistically it can simulates real seismic records. The Fig. 4.2a shows a synthetic signal constructed in this way. Here, seven secondary pulses follow the initial one, with delays and scale factors as listed in Table 7. The onset times for each of the secondary pulses are shown in the Fig. 4.2a.

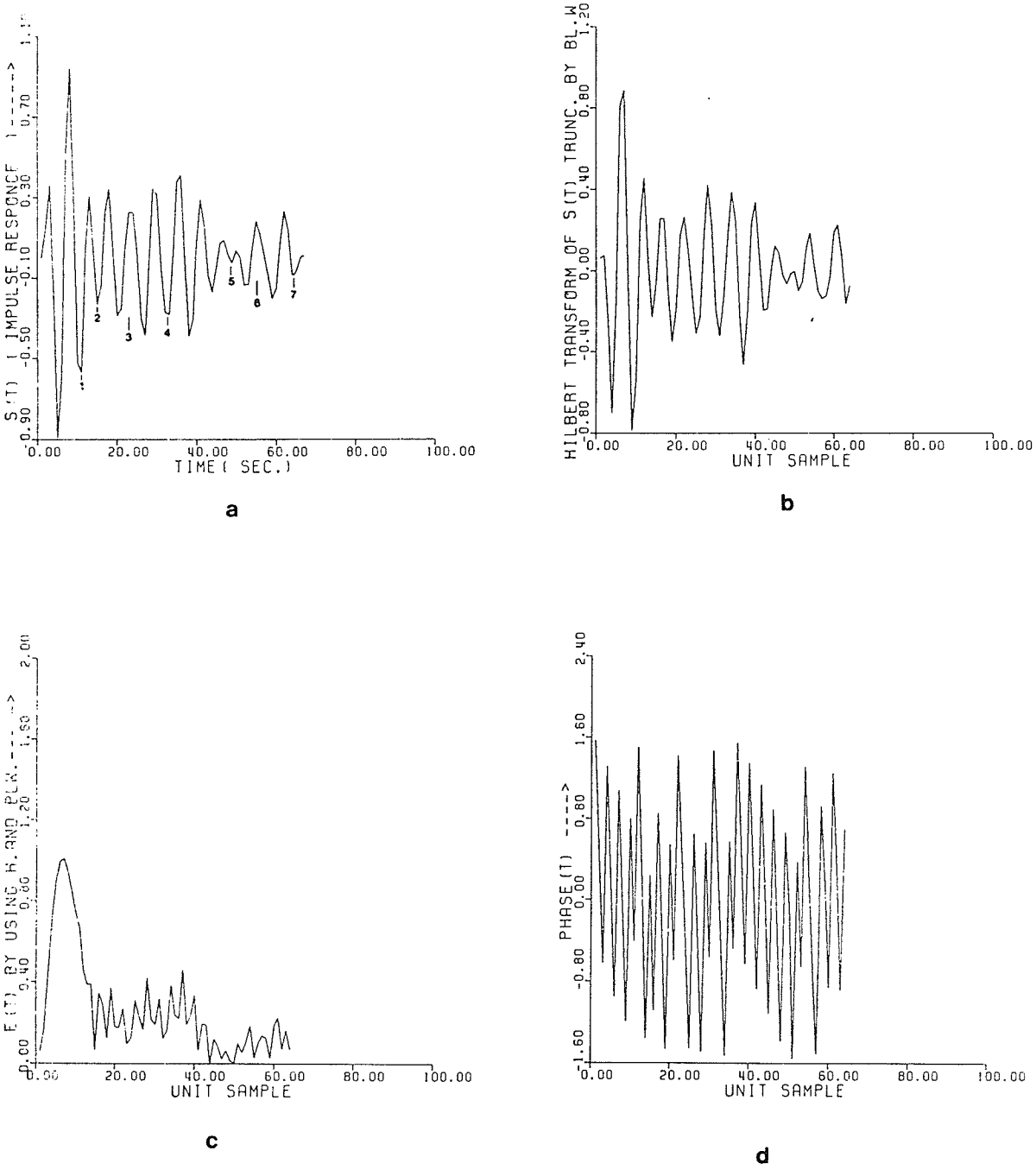


Fig. 4.2 An artifical pulse and its Hilbert transform and complex envelope: (a) Real pulse S(t), (b) Hilbert transform of S(t), (c) and (d) complex envelope as envelope and angle function, respectively.

## 4.5 HILBERT TRANSFORM AND SYNTHETIC OR ARTIFICIAL SIGNAL

The artificial signal of the Fig. 4.2a simulates a real seismic record. Therefore, the Hilbert transform yields the imaginary part of the artificial signal as we know ( from chapter II ), and, we can calculate the envelope and phase functions by using equations (4.2-3 ) and ( 4.2-4), resulting in the envelope and phase as shown in the Fig.4.2c-d.

From an alternative viewpoint, we can also express S(t) in terms of P(t), the complex envelope of the basic pulse. Owing to the linearity of the complex envelope, it follows from equation ( 4.4-1 ) that;

$$S(t) = P(t) + \sum_{n} an\ P(t - tn). \qquad 4.5\text{-}1$$

Equation (4.5-1) can be generalized to allow imaginary values of "an". These correspond to transmission along paths which pass through internal caustics ( Jeffreys and Lapwood, 1957 ). Therefore, the complex envelope of the synthetic signal is a summation of basic complex envelopes just as the artifical signal ( equation 4.4-1 ) is a summation of basic pulses. The effects of this summation are clearly indicated in the envelope ( Fig. 4.2c ) with the exception of pulses 1 and 7, each of which gives rise to a local peak as shown in the Fig. 4.2c with the onset time fairly accurately preserved.

We must be careful to note, however, that equation (4.5-1) indicates an addition of complex quantities, while

the envelope represents complex magnitude of the result. Thus there exists possibility of constructive and destructive interference among the component pulses. For example, the envelope shows no clear indication of pulse 1, and pulse 7 is greatly distorted by interference with preceeding pulses.

The effects of the summation equation (4.5-1) are also indicated in the angle function of Fig. 4.2d although not in such a direct way. If we consider the basic complex envelope P(t) as a vector rotating in the complex plane, interference between two pulses corresponds to their vector addition. In general , these vectors will not have the same angle because of their relative time shift, and the resultant angle function will have the angle of the sum vector with respect to the real axis. Thus, as one vector decreases in magnitude and the other increases, the resultant vector must speed up or slow down its rotation in order to align itself more closely with the vector of increasing magnitude.

While the arrival of a very strong pulse produces a very noticeable effect in the envelope, phase differences between the vectors corresponding to two interfering pulses are limited to $\pm\pi$ radians. Also, depending upon the relative angle between the oncoming pulse and the signal preceding it, the arrival of a very strong pulse may not produce any noticeable angular effect at all. This type of very different different behavior of the envelope and angle function is one

example of how the two bear very different types of information about the same signal.

## 4.6 SPECTRAL FACTORIZATION

Spectral factorization is a method of estimating the one time function which is also minimum phase. The minimum-phase function has many applications in exploration seismology. It, and it alone, may also be used for feedback filtering. It will arise frequently in wave propagation problems. It arises in the theory of prediction and regulation for the given spectrum. It determines the minimum amount of dispersion in viscous wave propagation which is implied by causality. And it also finds application in two-dimensional potential theory where a vector field magnitude is observed and the components are to be inferred.

There are four methods of doing spectral factorization. The methods are Root method, the Toeplitz method, Whittle's exp-log method and the Kolmogoroff method. I will discuss only one of these which is related to Hilbert transform. The readers may refer to Fundamentals of Geophysical Data Processing with Application to Petroleum Prospecting by Claerbout ( 1976 ) for the first three methods.

## 4.6.1 The Kolmogoroff Method

Let us consider $x_0$, $x_1$, $x_2$,.....as a time domain coefficients of a polynomial X(Z) and $X(\omega_0)$, $X(\omega_1)$,.....$X(\omega n)$ as a frequency-domain representation of the polynomial X(Z). The following spectral factorization method is explained in detail by Claerbout ( 1976 ). If we start with a time function or Z transform $X(Z) = x_0 + x_1 Z$ where Xk is the Fourier transform of the time function, that is, X(Z) evaluated at numerous( k = 0, 1, ..... n ) places on the unit circle ( Claerbout, 1976 ).

Given the following identities

$$Rk = \bar{X}k\, Xk = \exp[\ln(Rk)] = \exp(Uk), \qquad 4.6\text{-}1$$

the addition and subtraction of arbitrary function $j\phi k$ to the exponential term in equation 4.6-1 gives

$$Rk = \exp[(1/2)(Uk - j\,\phi k)]\exp[(1/2)(Uk + j\,\phi k)]$$
$$= \bar{B}k\, Bk \qquad 4.6\text{-}2$$

Now the question is what $\phi k$ should be used to guarantee that B transforms to a minimum-phase, one-sided time function ?. By looking at Whittle's method, we note that the only significant properties of $U^+(Z)$ are that it is finite and that the time function U(t) vanishes prior to t = 0. Thus we expect that $\phi k$ should be chosen so that, when $Uk + j\phi k$ is transformed into the time domain, the resulting time function $U^+(t)$ should vanish for negative time.

To estimate $\not\delta k$, we take Uk into the time domain getting Ut. Then we multiply by the real step function in time obtaining $U^{+}(t) = U_0, U_1, \ldots$ . This implies that in the frequency domain Uk has been convolved with $\delta k = 0 + j$ ($90^0$ phase shifter ). Thus, $\not\delta$ has been generated. To get $U^{+}(Z)$ we have to drop all of the negative powers of Z in U(Z). For simplicity, consider a case when the U(t) is real; then

$$U(Z) = \ldots + U_1 Z^{-1} + U_0 + U_1 Z + U_2 Z^2 + \ldots \quad 4.6\text{-}3$$

$$U = U_0(\cos 0) + 2U_1 \cos \omega + 2U_2 \cos 2\omega + \ldots \quad 4.6\text{-}4$$

If we consider $\not\phi$ as new function i.e. by replacing cosine by sine in the above expression

$$\not\phi = 2U_1 \sin \omega + 2U_2 \sin 2\omega + \ldots \quad 4.6\text{-}5$$

by combining U with $j\not\phi$ we find

$$(1/2)(U + j\not\phi) = 1/2\ U_0 + U_1 Z + U_2 Z^2 + \ldots$$

$$= U^{+}(Z). \quad 4.6\text{-}6$$

The operation of changing cos(t) to sin(t) would be called $90^0$ phase shift filtering ( Hilbert transform ). Here we have changed $\cos(\omega)$ to $\sin(\omega)$ with the result that $U^{+}(Z)$ has only positive coefficients of Z.

The Kolmogoroff method of spectral factorization is very fast in a computer because fast Fourier transforms may be used. Its principle disadvantage is that summation around the unit circle is always slightly different than integration about the circle. A simple program to perform spectral factorization by means of fast Fourier transform and Hilbert

transform is written for this research. Complex arithmetic is mandatory. However, the results are approximate since integration around the unit circle has to be approximated by summation over four points.

## 4.7 INVERSE FILTERS

If we assume Y is the known output of a filter B and X is an unknown input, then we have a problem that one often has with a transducer/recorder system.

For example, the output of a seismometer is a wiggly line from which the seismologist may wish to determine the displacement velocity or acceleration of the ground. To undo the filtering operation of the filter B(Z), I will try to find another filter A(Z) where B(Z)A(Z) = 1, that means A(Z) is inverse of B(Z).

Let's take an example, if B(Z) = 1 - Z/2, then, by Taylor's power series formula, we have

$$A(Z) = 1/(1-Z/2) = 1+Z/2+Z^2/4+Z^3/8+Z^4/16 +..... . \quad 4.7\text{-}1$$

We can represent this polynomial in a computer since the filter coefficients will drop off rapidly in magnitude. But if B(Z) = 1 - 2Z, then

$$A(Z) = 1/(1 - 2Z) = 1 + 2Z + 4Z^2+ 8Z^3+ 16Z^4+..... \quad 4.7\text{-}2$$

Here the coefficients of the series increase without bound which in fact will produce a serious problem. A more mathe-

matical description of the state of affairs results from solving for the zeros of B(Z). This is equivalent to find a value of $Z_0$ for which $B(Z_0) = 0$. For example for $B(Z) = 1 - Z/2$ we find $Z = 1/2$. The general case for wavelets with complex coefficients is that, if the solution value $Z_0$ of $B(Z_0) = 0$ lies inside the unit circle in the complex plane, then 1/B(Z) will have coefficients which blow up; and if the root lies outside the unit circle, then the inverse 1/B(Z) will be bounded.

### 4.7.1 1-D Minimum-Phase

The minimum-phase function has further applications in geophysics such as the feedback filtering or inverse filters, Homomorphic filtering or Homomorphic deconvolution, Zero-lag inverse filter, Minimum entropy deconvolution, etc. It determines the minimum amount of dispersion in viscous wave propagation which is implied by causality. In this section I will discuss one of these uses which is related to seismic exploration.

The Homomorphic system is a nonlinear system which obeys a generalized principle of superposition ( Oppenheim, 1975 ), that is used to separate the wavelet ( seismic source ) and the impulse response of the transmission path from a seismic record. If the wavelet or the impulse response of the transmission channel is minimum-phase, a seismic record is often represented as the convolution of a wavelet with the

impulse response of the transmission path. Since the wavelet or the impulse response of the transmission path obeys the minimum-phase assumption, the seismic record will be a minimum-phase, in which case, the Homomorphic filter works nicely, but a problem will arise when the seismic record is a mixed-phase i.e. both of the wavelet and the impulse response of the transmission are not minimum-phase, in which case the Homomorphic system fails. To solve this problem we have to change the seismic record which is mixed-phase to minimum-phase and this may be achieved by application of Hilbert transform or the other appropriate methods mentioned in the section 4.6. The procedure of transforming the mixed-phase to the minimum-phase function by Hilbert transform was given in chapter 2. Fig. 4.3a-b is an example of a mixed-phase and its corresponding minimum-phase function obtained using Hilbert transform technique.

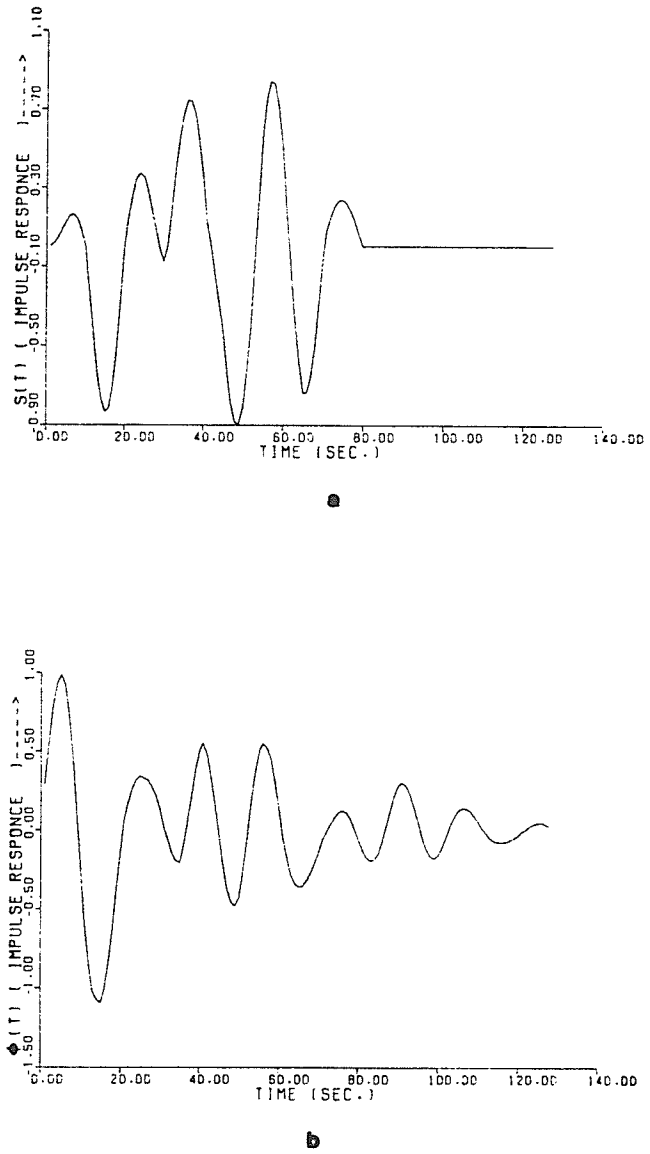


Fig. 4.3 (a)- A mixed phase signal S(T). (b)- a minimum phase of signal S(T) obtained by using 1-D Hilbert transform.

## 4.8 HILBERT TRANSFORM AND LINEAR FILTERING RELATIONS

The Hilbert transform has become important adjunct to the more familiar integral transforms, such as Laplace and Fourier transforms, in analysing signals and systems. It can be shown that many ideal filtering processes can be expressed in terms of Hilbert transforms ( Fig. 4.4a ).

### 4.8.1 Lowpass Filtering

If the function $X_1(t)$ has spectral content within the frequency interval $(-f_c, f_c)$, then it is said to be the lowpass portion of the input X(t). A real-valued, band limited ( 0.0 - 2.5 Hz ) function S(t), ( Fig. 4.4b ) may be used in defining a double-sideband suppressed-carrier signal

$$X(t) = 2\, S(t) \cos(2\pi f_c t) \; . \qquad 4.8\text{-}1$$

The lowpass signal is also given as;

$$X_1(t) = S(t) \cos(2\pi f_c t) + ht[S(t)] \sin(2\pi f_c t) \qquad 4.8\text{-}2$$

where the ht[S(t)] is the Hilbert transform of S(t), the $X_1(t)$ is the lowpass signal and the $X_1(\omega)$ is the magnitude spectrum of the $X_1(t)$ ( Fig.4.4c-d ).

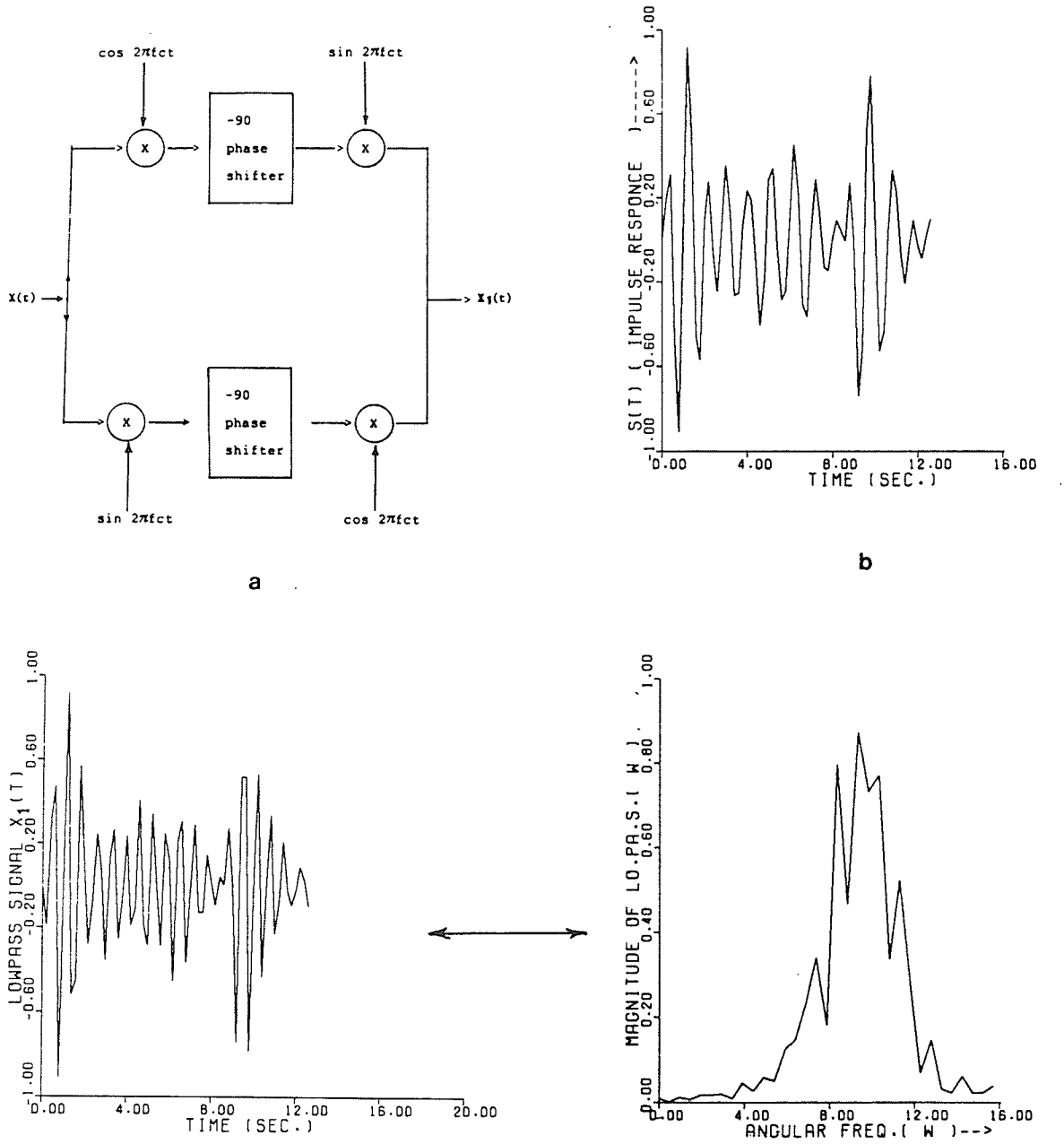


Fig. 4.4 (a) Lowpass filtering via Hilbert transform filtering. (b) The real signal S(t). (c) The lowpass signal $X_1(t)$. (d) The magnitude of amplitude spectrum of the lowpass signal $X_1(t)$.

### 4.8.2 Bandpass Signals

Many of the data processing applications of analytic signals concern narrow-band communication signals. In such applications it is sometimes convenient to represent a bandpass signal in terms of lowpass signal. To see how this can be done, consider a complex lowpass signal;

$$X(n) = Xr(n) + j\ Xi(n) \qquad 4.8\text{-}3$$

where Xi(n) is the Hilbert transform of Xr(n), then the bandpass signals can be expressed in terms of lowpass signals as following:-

$$Br(n) = Xr(n) \cos \omega cn - Xi(n) \sin \omega cn \qquad 4.8\text{-}4a$$

$$= A(n) \cos(\omega cn + Ph(n)) \qquad 4.8\text{-}4b$$

$$Bi(n) = Xr(n) \sin \omega cn + Xi(n) \cos \omega cn \qquad 4.8\text{-}5a$$

$$= A(n) \sin(\omega cn + Ph(n)) \qquad 4.8\text{-}5b$$

Equations (4.8-4a) and (4.8.5a) are the desired representations of bandpass signals in terms of lowpass signals. We note that equations (4.8-4b) and (4.8-5b) are in the form of a sinusoid modulated in both amplitude and phase.

## 4.9 GENERAL COMMENTS

By studying artificially constructed signals and proceeding to seismic records, it can be seen that the complex envelope which is obtained by 1-D Hilbert transform is more amenable to visual interpretation than the real signal itself. This is attributed to the natural separation of amplitude information from phase information.

Many ideal filtering processes such as lowpass and bandpass filtering can be expressed in terms of 1-D Hilbert transform, and this leads to possibility of using this transform in a Homomorphic filtering ( nonlinear system ) as a linear system. Also the 1-D minimum-phase which has many applications in geophysics is easily obtained by using 1-D Hilbert transform.

The amount of error introduced in computation depends on the FFT algorithm, sampling rate and discrete Hilbert transform.

# CHAPTER 5

# TWO-DIMENSIONAL(2-D) HILBERT TRANSFORM

## 5.1 INTRODUCTION

Since Read and Treitel ( 1973 ) conceived the idea on the stabilization of 2-D recursive filters via the discrete Hilbert transform by using the 2-D signum and bdy functions, Bose and Prabhu (1979 ) extended the idea of 1-D discrete Hilbert transform to 2-D using several forms such as, cotangent, sine, and complex exponential forms. Nabighian ( 1983 ) derived yet another expression of the 2-D case by using the 2-D signum function, later to apply them in the potential field data analysis.

In a 2-D space, the Hilbert transform is composed of two parts, one part acting on the X component and the other on the Y component. One of the applications of using 2-D Hilbert transform is based on the fact that the horizontal and vertical derivatives of a 3-D potential function are the Hilbert transform of each other (Nabighian, 1983).

In this chapter we are going to review some of the relations which are related to 2-D Hilbert transform. For example, the 2-D Fourier transform and the convolution in 2-D signals are considered as the key points in deriving the 2-D Hilbert transform in several forms. Also we will try to ex-

tend the idea of 1-D Hilbert transform to 2-D case in integral form.

In addition, we are going to discuss some other relations such as the 2-D discrete Hilbert transform and the minimum phase which is related to the 2-D recursive filters and associated stability problems, and the relationships between the vertical and horizontal derivatives of a 3-D potential function.

## 5.2 2-D FOURIER TRANSFORMS

In the 2-D Hilbert transform, the 2-D Fourier transform plays key role in each step of the processes as in 1-D case. However, I am not going to deal with this topic itself in more detail, but I will try to derive some more useful relations which will be very useful in deriving 2-D Hilbert transform.

The Fourier transform of 2-D signals can be derived from 1-D Fourier transform as follow. The transform of f(x,y) with respect to x is

$$B(k,y) = \int_{-\infty}^{\infty} f(x,y)\ \exp(jkx)\ dx \qquad 5.2\text{-}1$$

and the transform of B(k,l) with respect to y is;

$$F(k,l) = \int_{-\infty}^{\infty} B(k,y)\ \exp(jly)\ dy. \qquad 5.2\text{-}2$$

Thus f(x,y) <—> B(k,y) <—> F(k,l)

Therefore, the Fourier transform of 2-D signals is

$$F(k,l) = \int_{-\infty}^{\infty}\int f(x,y)\ \exp[-j(kx+ly)]\ \ dx\ dy. \qquad 5.2\text{-}3$$

From 1-D inversion formula we have

$$f(x,y) = (1/2\pi) \int_{-\infty}^{\infty} B(k,y)\ \exp(jkx)\ \ dk, \qquad 5.2\text{-}4$$

and

$$B(k,y) = (1/2\pi) \int_{-\infty}^{\infty} F(k,l)\ \exp(jly)\ \ dl. \qquad 5.2\text{-}5$$

These equations (5.2-4 and 5.2-5) yield the following result of the inversion formula;

$$f(x,y) = (1/4\pi^2) \int_{-\infty}^{\infty}\int F(k,l)\ \exp[j(kx+ly)]\ \ dk\ dl \qquad 5.2\text{-}6$$

## 5.3 THE CONVOLUTION OF 2-D SIGNALS

In previous chapters, it has been shown that the 1-D Hilbert transform convolved with a given function in time domain has yielded the Hilbert transform of the given function. Similarly, we would like to define the convolution of a given function in 2-D ,to represent the 2-D Hilbert transform relations.

Given two functions f(x,y) and h(x,y), we define their convolution g(x,y) by:-

$$g(x,y) = \int_{-\infty}^{\infty}\int f(t_1,t_2)\ h(x-t_1,y-t_1)\ dt_1\ dt_2$$

$$= \int_{-\infty}^{\infty}\int h(t_1,t_2)\ f(x - t_1, y - t_2)\quad dt_1\ dt_2 \qquad 5.3\text{-}1$$

This operation may also be written in the form

$$g(x,y) = f(x,y)**h(x,y)$$

and in Fourier transform domain

$$f(x,y)**f(x,y) \longleftrightarrow F(k,l)\ F(k,l).$$

## 5.4 THE 2-D HILBERT TRANSFORM EQUATIONS

In this section I am going to derive the 2-D Hilbert equation in integral form as an extension of 1-D case. From the previous section the 2-D Fourier transform of a function f(x,y) is F(k,l) ( equation 5.2-3 ) and the inverse of F(k,l) is f(x,y) ( equation 5.2-6 ).

The forward 2-D Fourier transform ( equation 5.2-3 ) can be written as

$$F(k,l) = \int_{-\infty}^{\infty}\int f(x,y)\ \cos(kx + ly)\ dx\ dy$$
$$- j \int_{-\infty}^{\infty}\int f(x,y)\ \sin(kx + ly)\ dx\ dy \qquad 5.4\text{-}1$$

i.e,

$$F(k,l) = Fr(k,l) - j\ Fi(k,l)$$

where Fr(k,l) and Fi(k,l) are the real and imaginary parts of the forward transform, equation (5.4-1). Then we obviously have

$$Fr(k,l) = \int_{-\infty}^{\infty}\int f(x,y)\ \cos\ (kx + ly)\ dx\ dy \quad \text{and}$$

$$Fi(k,l) = \int_{-\infty}^{\infty}\int f(x,y)\ \sin(kx + ly)\ dx\ dy \qquad 5.4\text{-}2$$

It also follows that,

$$F(-k,-l) = Fr(k,l) + j\,Fi(k,l), \qquad 5.4\text{-}3$$

because

$$\left.\begin{aligned} Fr(-k,-l) &= Fr(k,l) \quad (\text{ even function }) \\ \text{and}\quad Fi(-k,-l) &= -Fi(k,l) \quad (\text{ odd function }) \end{aligned}\right| \qquad 5.4\text{-}4$$

Therefore

$$\left.\begin{aligned} Fr(k,l) &= [F(k,l) + F(-k,-l)]/2 \\ Fi(k,l) &= j\ [F(k,l) - F(-k,-l)]/2 \end{aligned}\right) \qquad 5.4\text{-}5$$

From the equation (5.2-6), the inverse Fourier transform may be divided into regions of positive and negative frequency, i.e.,

$$\begin{aligned} f(x,y) &= (1/4\pi^2) \int_{-\infty}^{0}\int F(k,l)\ \exp[j(kx + ly)]\ dk\ dl \\ &\quad + (1/4\pi^2) \int_{0}^{\infty}\int F(k,l)\ \exp[j(kx + ly)]\ dk\ dl \\ &= (1/4\pi^2) \int_{0}^{\infty}\int F(-k,-l)\ \exp[-j(kx + ly)]\ dk\ dl \\ &\quad + (1/4\pi^2) \int_{0}^{\infty}\int F(k,l)\ \exp[j(kx+ly)]\ dk\ dl \end{aligned} \qquad 5.4\text{-}6$$

upon substituting the equation (5.3-5) we have an equation with positive frequency only.

$$f(x,y) = (1/2\pi^2) \int_0^{\infty}\int Fr \cos(kx+ly)\, dk\, dl$$

$$+ (1/2\pi^2) \int_0^{\infty}\int Fi \sin(kx+ly)\, dk\, dl \qquad 5.4\text{-}7$$

Next a complex function may be defined as

$$fc = f(x,y,\sigma) - j\, f(x,y,\sigma) \qquad 5.4\text{-}8$$

This complex function is made up of the original real part, $f(x,y)$, and a part called the quadrature function, $f_H(x,y)$ which is nothing other than the Hilbert transform of $f(x,y)$. The quadrature is defined so that it introduces a $90^0$ phase shift. Therefore, for examples, sines are converted to cosines and cosines are converted to negative sines in equation (5.4-7)

$$f_H(x,y,0) = (1/2\pi^2) \int_0^{\infty}\int [Fi \cos(kx+ly)$$

$$- Fr \sin(kx+ly)]\, dk\, dl \qquad 5.4\text{-}9$$

and

$$fc(x,y,\sigma) = (1/2\pi^2) \int_0^{\infty}\int [Fr(k,l) - j\, Fi(k,l)].$$

$$\exp(j(kx+ly) \exp(-\sigma(kx+ly))\, dk\, dl. \qquad 5.4\text{-}10$$

Substituting Fr and Fi from equation (5.4-2) into equation (5.4-9) one can relate $f_H$ and f more clearly.

$$f_H(x,y) = (1/2\pi^2) \int_{-\infty}^{\infty}\int_{-\infty}^{\infty}[f(X,Y)\ \sin(kX+lY)\ \sin(kx+ly)$$

$$-f(X,Y)\ \cos(kX+lY)\ \sin(kx+ly)]\ dX\ dY\ dk\ dl$$

$$= \lim_{(k',l')\to\infty} (1/2\pi^2) \int_{0}^{k'}\int_{-\infty}^{l'} \int_{-\infty}^{\infty} f(X,Y)\ \sin[k(X-x)$$

$$+l(Y-y)]\ dx\ dy\ dk\ dl \qquad 5.4\text{-}11$$

Integrating first with respect to dk dl we obtain;

$$f_H(x,y) = \lim_{(l',k')\to\infty} (1/2\pi^2)\ \mathbb{P}^2 \int_{-\infty}^{\infty}\int f(X,Y)[(1$$

$$-\cos\{k'(X-x)+l'(Y-y)\}/(X-x,Y-y)]\ dX\ dY \qquad 5.4\text{-}12$$

where, $\mathbb{P}$ indicates the Cauchy principle value.

It can be shown that

$$\lim_{(k',l')\to\infty} (1/2\pi^2)\ \mathbb{P}^2 \int_{-\infty}^{\infty}\int f(X,Y)[\cos(k'(X-x)$$

$$+ l'(Y-y))]/(X-x,Y-y)\quad dX\ dY = 0 \qquad 5.4\text{-}13$$

Using the Riemann-Lebesque Lemma, we have, then,

$$f_H(x,y) = -(1/2\pi^2)\ \mathbb{P}^2 \int_{-\infty}^{\infty}\int [f(X,Y)/(x-X,y-Y)]\ dx\ dy \qquad 5.4\text{-}14$$

Equation (5.4-14) is known as the 2-D Hilbert transform in integral form.

## 5.5 2-D HILBERT TRANSFORM AND DOUBLE CONVOLUTION

In this section I will discuss and derive the 2-D Hilbert transform in the respective "cotangent" and "sine" form ( Bose and Brabhu, 1979 ). By assuming a 2-D complex discrete pulse $P(i_1,i_2)$ which is defined by its real and imaginary

components $PR(i_1,i_2)$ and $PI(i_1,i_2)$, respectively, where $i_1$ and $i_2$ are integer numbers. The following relations are straightforward, but tedious in calculations.

When $i_1$ is even, and $i_2$ is even

$$PI(i_1,i_2) = (2/N_1N_2) \sum_{k_1=1,3,\ldots}^{N_1-1} \sum_{k_2=1,3,\ldots}^{N_2-1} PR(k_1,k_2) \cdot [\cot \pi(i_1-k_2)/N_1 + \cot \pi(i_2-k_2)/N_2 \qquad 5.5\text{-}1a$$

When $i_1$ is even, and $i_2$ is odd

$$PI(i_1,i_2) = (2/N_1N_2) \sum_{k_1=1,3,\ldots}^{N_1-1} \sum_{k_2=0,2,\ldots}^{N_2-1} PR(k_1,k_2) \cdot [\cot \pi(i_1-k_2)/N_1 + \cot \pi(i_2-k_2)/N_2 \qquad 5.5\text{-}1b$$

When $i_1$ is odd, and $i_2$ is even

$$PI(i_1,i_2) = (2/N_1N_2) \sum_{k_1=0,2,\ldots}^{N_1-1} \sum_{k_2=1,3,\ldots}^{N_2-1} PR(k_1,k_2) \cdot [\cot \pi(i_1-k_2)/N_1 + \cot \pi(i_2-k_2)/N_2 \qquad 5.5\text{-}1c$$

Finally, when $i_1$ is odd, and $i_2$ is odd

$$PI(i_1,i_2) = (2/N_1N_2) \sum_{k_1=0,2,\ldots}^{N_1-1} \sum_{k_2=0,2,\ldots}^{N_2-1} PR(k_1,k_2) \cdot [\cot \pi(i_1-k_2)/N_1 + \cot \pi(i_2-k_2)/N_2 \qquad 5.5\text{-}1d$$

Note that when $i_1$ or $i_2$ is even (odd), the dummy variable in the summation assumes only odd (even) positive integer values, and the Kernel within the double summation contains a function expressible in sum-separable form. The sine form of the 2-D discrete Hilbert transform( Dht ), also derivable by a routine, but with tedious calculations, is written below in equation (5.5-2) for the sake of completeness.

$$PI(i_1,i_2) = (1/N_1N_2) \sum_{k_1=0}^{N_1-1} \sum_{k_2=0}^{N_2-1} PR(k_1,k_2)[$$

$$\sum_{m_1=1}^{(N_1/2)-1} \sin 2\pi m_1(i_1 - k_2)\{1 - (-1)^{i_2-k_2}\}/N_1$$

$$+ \sum_{m_2=1}^{(N_2/2)-1} \sin 2\pi m_2(i_2 - k_2)\{1 - (-1)^{i_1-k_1}\}/N_2] \quad 5.5\text{-}2$$

It should be observed that the 2-D Dht is expressible as a double convolution.

$$PI(i_1,i_2) = \sum_{k_1=0}^{N_1-1} \sum_{k_2=0}^{N_2-1} PR(k_1,k_2)\, Dht(i_1 - k_1, i_2 - k_2) \quad 5.5\text{-}3$$

for $i_1 = 0, 1, 2, \ldots, N_1-1$, and $i_2 = 0, 1, 2, \ldots, N_2-1$

Where in the case of sine form representation,

$$Dht(i_1-k_1,i_2-k_2) = (1/N_1N_2)[\sum_{m_1=1}^{(N_1/2)-1} \sin 2\pi m_1(i_1-k_1)[1-(-1)^{i_2-k_2}]/N_1$$

$$+ \sum_{m_2=0}^{(N_2/2)-1} \sin 2\pi m_2(i_2-k_2)\{1-(-1)^{i_1-k_1}\}/N_2]. \quad 5.5\text{-}4$$

As a convolution of arrays with a sum-separable Kernel a result of general interest will be derived which will be useful in the computation of the 2-D Dht. Consider the convolution of a spatially truncated data array $X(k_1,k_2)$ for $k_1 = 0, 1, 2, \ldots\ldots\ldots, N_1-1$, and $k_2 = 0, 1, 2, \ldots\ldots\ldots\ldots, N_2-1$ with a spatial truncated sum-separable impulse response operator

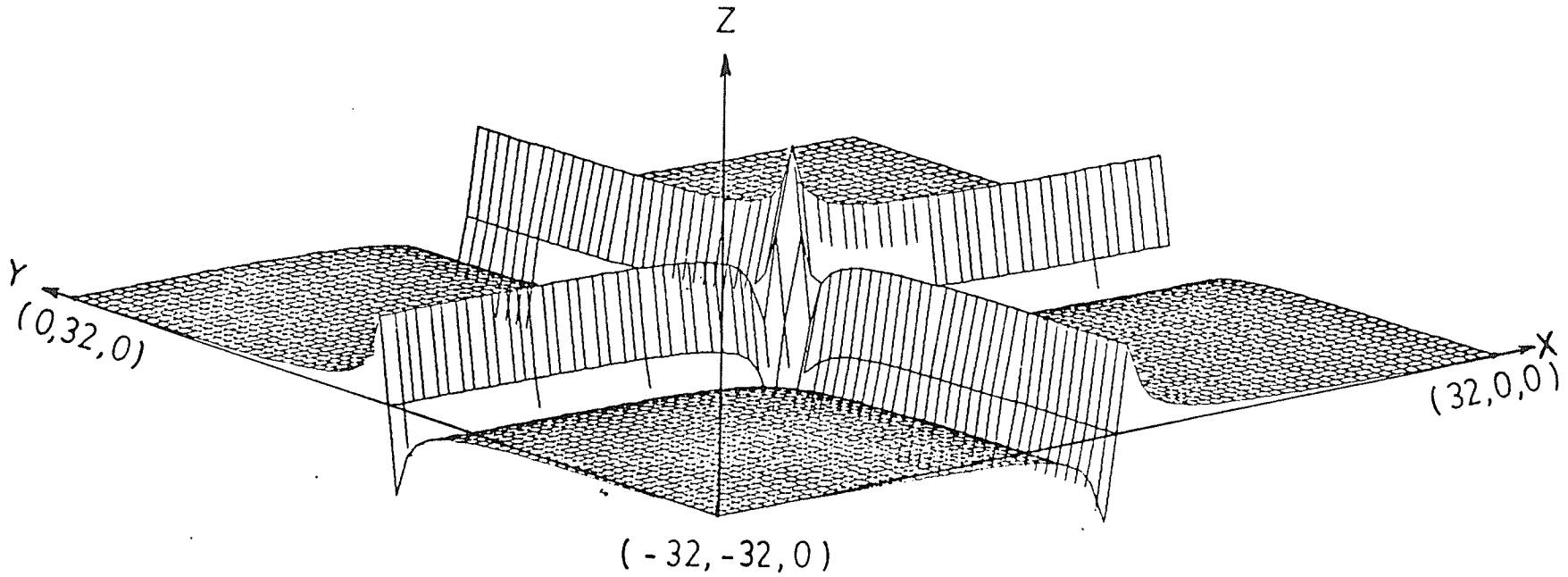


Fig. 5.1 Two dimensional Hilbert transform is obtained by using the cotangent form.

$$Dht(i,j) = Dht_1(i) + Dht_2(j), \qquad 5.5\text{-}5$$

and suppose that the output array of interest is $Y(i,j)$ in (5.5-6) for $i = 0, 1, \ldots N_1-1$, $j = 0, 1, \ldots N_2-1$.

$$Y(i,j) = \sum_{k_2=0}^{N_2-1} \sum_{k_1=0}^{N_1-1} X(k_1,k_2)[Dht_1(i - k_1) + Dht_2(j - k_2)] \qquad 5.5\text{-}6$$

The results of that section will be extended to the case when the impulse response operator in equation (5.5-5) takes the particular form in form in equation ( 5.5-7 ) as a consequence of the obtained representaion of the Hilbert transformer in equation (5.5-1). For each part in equation (5.5-1) with corresponding range for(i,j)

$$Dht(i,j) = [\cot(\pi i/N_1) + \cot(\pi j/N_2)]\{2/(N_1N_2)\}. \qquad 5.5\text{-}7$$

Equation (5.5.7) defines the 2-D Hilbert transform operator in cotangent form ( Fig. 5.1 ) and may take matrix form also.

## 5.6 2-D DISCRETE HILBERT TRANSFORM RELATIONS

In this section I extend the idea of 1-D case to derive the 2-D discrete Hilbert transform, since this transform relates the real and imaginary parts of the discrete Fourier transform of a finite discrete causal pulse as given in equation ( 2.5-16b ). Therefore, in the 2-D case, a finite discrete pulse is causal if,

$$P(i_1,i_2) = 0 \quad \text{for } i_1 \geq N1/2 \quad \text{or } i_2 \geq N2/2 \qquad 5.6\text{-}1$$

where;

$$i_1 = 0,\ 1,\ 2,\ldots\ldots\ldots\ldots,N_1-1$$

and

$$i_2 = 0,\ 1,\ 2,\ldots\ldots\ldots\ldots,N_2-1.$$

With the same procedures as given in 1-D case, we define the even and odd parts of a pulse in 2-D as follow

$$Pe(i_1,i_2) = 1/2[P(i_1,i_2) + P(N_1 - i_1,N_2 - i_2)] \qquad 5.6\text{-}2a$$

and

$$Po(i_1,i_2) = 1/2[P(i_1,i_2) - P(N_1 - i_1,N_2 - i_2)]. \qquad 5.6\text{-}2b$$

The odd ( Po ) and even ( Pe ) parts of a 2-D causal pulse( P ) are related by

$$Po(i_1,i_2) = [sgn(i_1,i_2) + bdy(i_1,i_2)]Pe(i_1,i_2) \qquad 5.6\text{-}3$$

where the sgn function is a finite 2-D version of the 1-D signum function. It is given by

$$sgn(i_1,i_2) = \begin{pmatrix} 1 & 0 < i_1 < N_1/2 \text{ and } 0 < i_2 < N_2/2 \\ -1 & N_1/2 < i_1 < N_1 \text{ and } N_2/2 < i_2 < N_2 \\ 0 & \text{elsewhere} \end{pmatrix} \qquad 5.6\text{-}4$$

The bdy function makes boundary adjustments. This function constitutes an extension of the modulo N Kronecker delta introduced in equation ( 2.5-8 ). It is defined by;

$$bdy(i_1,i_2) = \left\{ \begin{array}{ll} 1 & i_2 = 0 \text{ and } 0 < i_1 < N_1/2 \\ -1 & i_2 = 0 \text{ and } N_1/2 < i_1 < N_1 \\ 1 & i_1 = 0 \text{ and } 0 < i_2 < N_2/2 \\ -1 & i_1 = 0 \text{ and } N_2/2 < i_2 < N_2 \\ 0 & \text{elsewhere} \end{array} \right\} \qquad 5.6\text{-}5$$

By proceeding as in the derivation of equations ( 2.5-16a-b ), we can derive the relations between the real and imaginary parts of the discrete Fourier transform of a causal two-dimensional pulse. The properties in Table 2. apply directly to the 2-D case if we define even and odd functions as those for which

$$Pe(i_1,i_2) = Pe(N_1-i_1,N_2-i_2) \qquad 5.6\text{-}6a$$

and

$$Po(i_1,i_2) = -Po(N_1-i_1,N_2-i_2) \qquad 5.6\text{-}6b$$

respectively.

The real and imaginary parts of the 2-D discrete Fourier transform ( DFT ) of a pulse $P(i_1,i_2)$ will be denoted by $PR(i_1,i_2)$ and $PI(i_1,i_2)$, respectively. The pulse $P(i_1,i_2)$ is the sum of its even and odd parts

$$P(i_1,i_2) = Pe(i_1,i_2) + Po(i_1,i_2). \qquad 5.6\text{-}7$$

The 2-D discrete Fourier transform of a pulse $P(i_1,i_2)$ is defined by

$$DFT(P(i_1,i_2)) = \sum_{k_1=0}^{N_1-1} \sum_{k_2=0}^{N_2-1} W_1^{K_1 i_1} . W_2^{k_2 i_2} . P(k_1,k_2) \qquad 5.6\text{-}8$$

where;

$$W_1 = \exp(j2\pi/N_1) \quad \text{and} \quad W_2 = \exp(j2\pi/N_2).$$

Therefore, the Fourier transformation of both sides of equation (5.6-7) yields

$$DFT\ P(i_1,i_2) = DFT\ Pe(i_1,i_2) + DFT\ Po(i_1,i_2) \qquad 5.6\text{-}9$$

From Table 2.( see Chapter 2 ) we see that the DFT of a real and even function is real and even. and that the transform of a real and odd function is odd and imaginary. Thus

$$PR(i_1,i_2) = DFT\ Pe(i_1,i_2) \qquad 5.6\text{-}10a$$

and

$$PI(i_1,i_2) = -j\ DFT\ Po(i_1,i_2). \qquad 5.6\text{-}10b$$

By taking the inverse discrete Fourier transform ( IDFT ) of both sides of equation (5.6-10a), and substitution into equation (5.6-3) and equation (5.6-10b), yields the following relation

$$PI(i_1,i_2) = -j\ DFT(\ sgn(i_1,i_2) + bdy(i_1,i_2)\ IDFT(PR(i_1,i_2) \qquad 5.6\text{-}11$$

where

$$IDFT(PR(i_1,i_2)) = [1/(N_1N_2)] \sum_{k_1=0}^{N_1-1} \sum_{k_2=0}^{N_2-1} W_1^{-k_1i_1} W_2^{-k_2i_2} PR(k_1,k_2)$$

Equation (5.6-11) defines the 2-D discrete Hilbert transform, and represents a generalization of the 1-D discrete Hilbert transform given by equation ( 2.5-16b ).

## 5.7 2-D RECURSIVE FILTERS AND STABILITY PROBLEMS

Since the two-dimensional discrete Hilbert transform can be applied to obtain the two-dimensional minimum phase, which related to the two-dimensional recursive filters, therefore, the theory developed thus far has an important bearing on the two-dimensional recursive filter design prob-

lem. Two-dimensional recursive filters have been described by Shanks ( 1972 ), and their transfer functions can be written as the ratio of two polynomials in the complex variables $Z_1$ and $Z_2$

$$F(Z_1,Z_2) = [A(Z_1,Z_2)/B(Z_1,Z_2)] \ , \qquad 5.7\text{-}1$$

that is, as a ratio of two-dimensional z-transforms. These filters are stable in the bounded input-bounded output sense if and only if the polynomials $B(Z_1,Z_2) \neq 0$ for $|Z_1| \leq 1$ and $|Z_2| \leq 1$ simultaneously.

Procedures of synthesising a Recursive digital filter usually do not constrain the coefficients of the denominator polynomial to satisfy the stability conditions mentioned above. This is particularly true for time domain design procedures ( Shanks, 1967; Burrus and Parks, 1970 ). One approach of resolving this stability problem is to use a double-least-squares inverse procedure described by Shanks, Treitel, and Justice ( 1972 ). However, this procedure can adversely affect the amplitude spectrum of the stabilized filter.

In the next section I will show how to use the discrete Hilbert transform procedure to obtain a minimum-phase version of a two-dimensional array. The z-transform of such an array could be the denominator polynomial in equation (5.8-1). Application of this scheme leads to a rational filter $F(Z_1,Z_2)$ with very nearly the same amplitude spectrum as the original unstable filter F(Z1,Z2).

## 5.8 2-D MINIMUM PHASE POLYNOMIALS

A 2-D polynomial $B(Z_1,Z_2)$ is said to be minimum-phase if $B(Z_1,Z_2) \neq 0$ for $|Z_1| \leq 1$ and $|Z_2| \leq 1$ simultaneously. Note that the filter $F(Z_1,Z_2)$, in equation (5.7-1) is stable if this condition is satisfied. The 2-D discrete Hilbert transform can be applied in the same way as in the 1-D case to obtain the minimum-phase version of a given array. Thus, given a 2-D amplitude spectrum $A(i_1,i_2)$ of a causal pulse, the minimum-phase spectrum $\phi(i_1,i_2)$ is calculated by the equation;

$$\phi(i_1,i_2) = -j\ \mathrm{DFT}[\{\mathrm{sgn}(i_1,i_2) + \mathrm{bdy}(i_1,i_2)\}.\mathrm{IDFT}\{\mathrm{Log}\ A(i_1,i_2)\}] \quad 5.8\text{-}1$$

Therefore, a summary of computing the minimum-phase version of a mixed or maximum phase array may be given in the following five steps

1 - Given a finite discrete two-dimensional array, augment the coefficient array with zeros to satisfy the causality condition, and find the spectrum of this array by using 2-D fast Fourier transform

2 - Calculate the natural logarithm of the amplitude spectrum of the augmented two-dimensional array

3 - Apply the two-dimensional discrete Hilbert transform to the two-dimensional log magnitude array. Thus the log magnitude is treated as the real part and the discrete Hilbert transform then yields the imaginary part


Fig. 5.2 a) Two dimensional input sample ( in arbitrary unit ). b) The two dimensional minimum phase array of the input sample array.

4 - Use the imaginary part as the phase spectrum corresponding to the given amplitude spectrum. These two spectral characteristics completely describe the transform of the minimum-phase array

5 - After conversion from amplitude and phase to real and imaginary parts ( i.e, from polar to Cartesian representation of the complex spectrum ). Inverse transform and truncate to obtain the same dimensions as the original array. This yields the minimum-phase version of the original array ( Fig. 5.2a-b )

## 5.9 THEORY OF HORIZONTAL AND VERTICAL DERIVATIVES OF POTENTIAL FUNCTION AND 2-D HILBERT TRANSFORM

In previous sections we have investigated 1-D and 2-D Fourier transforms, horizontal derivatives of a potential function( chapter III ) and its Hilbert transform.

In the case of 2-D potential field, the vertical and horizontal derivatives of a potential function are the Hilbert transforms of each other i.e.,

$$dM/dz = H\,[dM/dx], \qquad 5.9\text{-}1$$

$$\mathcal{F}[dM/dz] = -j\,\mathrm{sgn}(\omega)\,\mathcal{F}[dM/dx] \qquad 5.9\text{-}2$$

and $$\mathcal{F}[dM/dx + j(dM/dz)] = [1 + \mathrm{sgn}(\omega)]\,\mathcal{F}[dM/dx]\ . \qquad 5.9\text{-}3$$

In the case of 3-D field, it is better to start with the following identities

$$g(p,q) = \mathcal{F}[f(x,y)], \qquad f(x,y) = \mathcal{F}^{-1}[g(p,q)] \qquad 5.9\text{-}4$$

$$\mathcal{F}[dM/dx] = jp\,\mathcal{F}(M), \quad \mathcal{F}[dM/dy] = jq\,\mathcal{F}[M]$$

and $$\mathcal{F}[dM/dz] = (p^2 + q^2)^{1/2}\,\mathcal{F}(M) \qquad 5.9\text{-}5$$

where

M is the 3-D potential function

$\mathcal{F}$ is the 2-D Fourier transform

The generalization of the 3-D problem can be accomplished in several ways, one of which is using the following identity

$$(p^2+q^2)^{1/2} = jp[-jp/(p^2+q^2)^{1/2}] + jq[-jq/(p^2+q^2)^{1/2}] \qquad 5.9\text{-}6$$

Multiplying equation (5.9-6) by F(M) and using equation (5.9-5)

$$\mathcal{F}[dM/dz] = [-jp/(p^2+q^2)^{1/2}]\,\mathcal{F}[dM/dx] + [-jq/(p^2 + q^2)^{1/2}]\,\mathcal{F}[dM/dy] \qquad 5.9\text{-}7$$

For q = 0 (2-D case), the equation ( 5.9-7 ) reduces to

$$\mathcal{F}[dM/dz] = -j(p/|p|)\,\mathcal{F}[dM/dx] = -j\,\mathrm{sgn}(p)\,\mathcal{F}[dM/dx]$$

This, with equation (5.9-2) above, represents the 2-D Hilbert transform relation between the vertical and horizontal derivatives of a potential function.

Let us introduce a generalized signum function defined as a unit vector in the (p,q) plane ( Fig. 5.3 ) whose p and q components are given by

$p/(p^2+q^2)^{1/2}$ and $q/(p^2+q^2)^{1/2}$ , i.e.

$$\mathrm{sgn}(p,q) = (p/(p^2+q^2)^{1/2})\hat{e}_x + (q/(p^2+q^2)^{1/2})\hat{e}_y \qquad 5.9\text{-}8$$

where $\hat{e}_x$ and $\hat{e}_y$ are the unit vectors in the x and y directions, respectively.

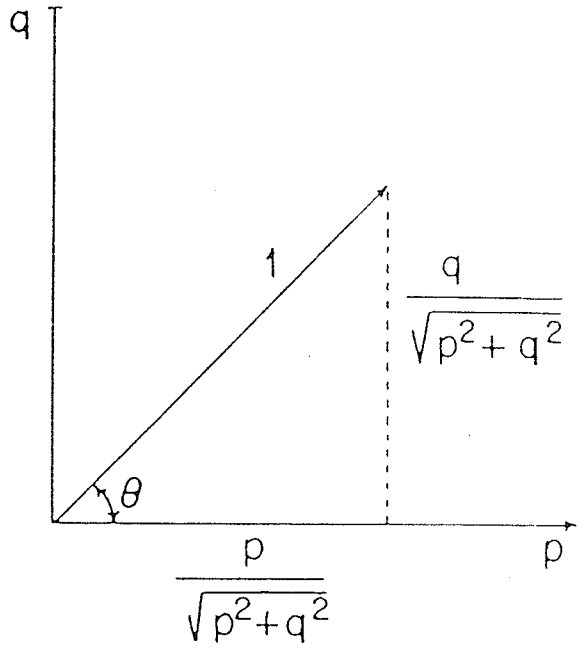


Fig. 5.3 A generalized 2-D signum function defined as a unit vector in the (p,q) plane.

The generalization of 3-D transform operator can now be written as,

$$H = -j\ \mathrm{sgn}(p,q) = H_1\hat{e}x + H_2\hat{e}y \qquad 5.9\text{-}9$$

where

$$H_1 = -jp/(p^2+q^2)^{1/2} \text{ and } H_2 = -jq/(p^2+q^2)^{1/2}$$

Letting

$$\nabla_h = (d/dx)\ \hat{e}x + (d/dy)\ \hat{e}y$$

be the horizontal gradient operator of a function, one can write equation (5.9-7) as the dot product between two vectors

$$F[dM/dz] = H.F[\nabla_h M], \qquad 5.9\text{-}10$$

or, in longhand

$$F[dM/dz] = H_1F[dM/dx] + H_2F[dM/dy] \qquad 5.9\text{-}11$$

It is worth mentioning that the computations outlined in equation (5.9-11) are very stable since both $H_1$ and $H_2$ are well behaved operators with values not exceeding ±1. This becomes especially useful if the horizontal gradients are measured directly, as is currently done in some airborne systems.

By inspection and making use of relations (5.9-5), one can invert expression (5.9-7) to obtain

$$\left( \begin{array}{l} F[dM/dx] = -H_1F[dM/dz], \\ F[dM/dy] = -H_2F[dM/dz] \end{array} \right) \qquad 5.9\text{-}12$$

By inspection, also

$$H_1F[dM/dy] = H_2F[dM/dx] \qquad 5.9\text{-}13$$

The operators H, $H_1$, and $H_2$ satisfy the following relations:

a) 2-D case($q = 0$, $H_1 = H$, $H_2 = 0$)

From equations (5.9-11) and (5.9-12) one can write in succession

$$F(dM/dz) = H\,F(dM/dx),$$

and

$$H\,F(dM/dz) = H\,H\,F(dM/dx) = -F(dM/dx),$$

which immediately implies

$$H\,H = -1. \qquad 5.9\text{-}14a$$

b) 3-D case

From equations (5.9-11), (5.9-12) and (5.9-13), one can write in succession

$$F(dM/dz) = H_1F(dM/dx) + H_2F(dM/dy),$$

and

$$H_1F(dM/dz) = H_1\,H_1F(dM/dx) + H_2H_1F(dM/dy)$$
$$= (H_1\,H_1 + H_2\,H_2)\,F(dM/dx) = -F(dM/dx),$$

which immediately implies

$$H_1\,H_1 + H_2\,H_2 = -1 \qquad 5.9\text{-}14b$$

It is evident that equation (5.9-14b) represents the 3-D extension of relation (5.9-14a). Finally, relation (5.9-3) which led to the development of the analytic signal concept in 2-D can be generalized to 3-D as

$$F[(dM/dx)+(dM/dy)+j(dM/dz)] = [1+p/(p^2+q^2)^{1/2}]\,F(dM/dx)$$
$$+ [1+q/(p^2+q^2)^{1/2}]\,F(dM/dy) \qquad 5.9\text{-}15$$

The simplicity of expression (5.9-15) as well as the obvious significance of the generalized signum function is indeed remarkable.

Since expressions (5.9-11) and (5.9-12) are multiplications in the frequency domain, their space-domain counterparts are convolution integrals. To accomplish this, equation (5.2-6) is used to invert the following transforms ( Nabihian, 1983 ):

$$\mathcal{F}^{-1}\,[-jp/(p^2+q^2)^{1/2}] = (1/2\pi)[x/(x^2+y^2)^{3/2}]$$

and

$$\mathcal{F}^{-1}\,[-jq/(p^2+q^2)^{1/2}] = (1/2\pi)[y/(x^2+y^2)^{3/2}]$$

The space-domain equivalent of expressions (5.9-11) and (5.9-12) will represent the extension to 3-D of the 2-D Hilbert transform relations for potential field data. Thus

$$dM/dz = (1/2\pi) \int_{-\infty}^{\infty}\int [(x-\xi)dM/d\xi+(y-\eta)dM/d\eta]/R^3 \; d\xi \; d\eta$$

$$dM/dx = -(1/2\pi) \int_{-\infty}^{\infty}\int [(x-\xi)dM/dz]/R^3 \; d\xi \; d\eta \qquad 5.9\text{-}16$$

and

$$dM/dy = -(1/2\pi) \int_{-\infty}^{\infty}\int [(y-\eta)dM/dz]/R^3 \; d\xi \; d\eta$$

where $(\xi,\eta)$ is the integration point in the x,y plane and

$$R^2 = (x-\xi)^2 + (y-\eta)^2$$

Up to this point, all the relations have been written in parallel to the previously developed 2-D case, and one will

recognize the terms in brackets as the Fourier transform of the x and y components of the Hilbert transform of M.

# CHAPTER 6

# REVIEW OF 3-D POTENTIAL FIELD DUE TO PRISMATIC BODIES

## 6.1 INTRODUCTION

There have been a considerable number of papers puplished on the analytical expression for magnetic field components and gravity effects due to bodies of simple geometrical shapes.

In this chapter I am going to review and simplify the mathematical expressions for magnetic total field and gravity effects and their vertical derivatives due to prismatic bodies. The discussion is also extended to multiprismatic bodies.

In gravity, a numerical expression for gravity effect due to a prismatic body was derived by Nagy ( 1966a,b ) and later modified by Goodacre ( 1972 ). In magnetics, a similar expression due to prismatic and multiprismatic bodies was derived by Bhattacharyya ( 1964, 1980 ).

The first and second vertical derivatives of potential field formula can be estimated directly or by using the fact that the horizontal and vertical derivatives of a 3-D potential function are the Hilbert transforms of each other, as stated in Chapter 5.

## 6.2 FUNDAMENTAL RELATIONS FOR MAGNETIC PRISMATIC BODIES

Consider a prism-shaped body at a depth h below the level of observation the upper surface of which is a horizontal plane and the vertical sides extend infinitely ( Fig. 6.1 ).

The polarization vector ( dF ) is taken to be at an angle $\theta$ with the direction of the earth's main field. In the case when a total field measurement will be made, the direction of measurement will, therefore, be the same as the earth's field vector which is defined by the direction cosines, l, m, and n ( Bhattacharyya, 1964 ).

Let A, B, and $\bar{J}$ be the coordinates of the volume element dA dB dJ in the prism ( Fig. 6.1 ). Let the polarization vector be characterized by the direction cosines L, M, and N. Then the field produced by the volume element dA dB $d\bar{J}$ is given by;

$$dF = I_p \, [d(1/R)/d\ell \; df_t] \; dA \; dB \; d\bar{J} \qquad 6.2\text{-}1$$

where $I_p$ is the polarization, $d\ell$ is an element of length in the direction of the polarization vector, and $df_t$ is an element in the direction of the total field of the earth. Let (x,y,z) be the coordinates of the point of the observation. Then,

$$d/df_t = l(d/dx) + m(d/dy) + n(d/dz) \qquad 6.2\text{-}2$$

$$d/d\ell = L(d/dx) + M(d/dy) + N(d/dz) \qquad 6.2\text{-}3$$

and

$$R^2 = (A - x)^2 + (B - y)^2 + (J - z)^2 \qquad 6.2\text{-}4$$

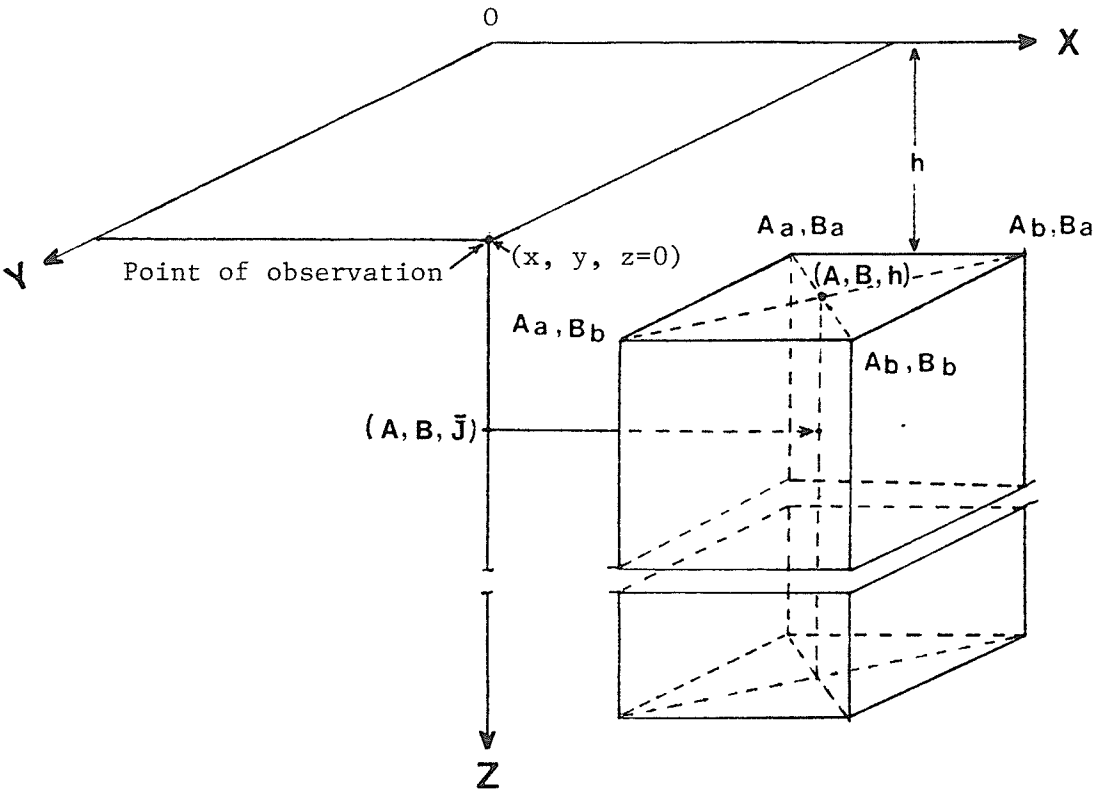


Fig. 6.1 An elementary volume of the prism and the coordinate system.

By substituting equations ( 6.2-2 ) upto ( 6.2-4 ) in equation ( 6.2-1 ) we obtain

$$dF = I_p\ [-(1/R^3)\cos\theta + (3/R^5)[lL(A - x)^2 + mM(B - y)^2 + nN(\bar{J} - z)^2 + A_{12}(A - x)(B - y) + A_{13}(A - x)(\bar{J} - z) + A_{23}(B - y)(\bar{J} - z)]]dA\ dB\ d\bar{J} \qquad 6.2\text{-}5$$

If I, and D are the inclination and declination, respectively, of the Earth's field, and $I_0$, $D_0$ the inclination and declination of the polarization vector, then $A_{12}$, $A_{13}$, and $A_{23}$ are related with direction cosines of both vectors by

$$A_{12} = Lm + Ml, \quad A_{13} = Ln + Nl \quad \text{and} \quad A_{23} = Mn + Nm \qquad 6.2\text{-}6$$

where L, M, N, l, m, and n are given as follow

$$\begin{pmatrix} L = \cos I \cos D & l = \cos I_0 \cos D_0 \\ M = \cos I \sin D & m = \cos I_0 \sin D_0 \\ N = \sin I & n = \sin I_0 \end{pmatrix} \qquad 6.2\text{-}7$$

Equation ( 6.2-5 ) may now be integrated with respect to $\bar{J}$ and the volume integral reduces to a surface integral:

$$F(x,y,z) = I_p \iint [-(\cos\theta/a^2)[1 - (h - z)/R_0] + (Nn/a^2)[1-(h-z)^3/R_0^3] + (A_{13}A_1 + A_{23}B_1)/R_0^3 + (3/a^4)[lLA_1^2 + mMB_1^2 + A_{12}A_1B_1][(2/3) - ((h - z)/R_0) + ((h - z)^3/3R_0^3]]\ dA_1\ dB_1 \qquad 6.2\text{-}8$$

where

$$\cos\theta = lL + mM + nN$$

$$A_1 = A - x, \quad B_1 = B - y, \quad a^2 = A_1^2 + B_1^2$$

$$R_0^2 = A_1^2 + B_1^2 + (h - z)^2$$

Integrate equation (6.2-8) with respect to $A_1$ and take the plane of observation to be at z = 0, then

$$F(x,y,0) = I_P \int f(B_1)\, dB_1 \qquad 6.2\text{-}9$$

where

$$f(B_1) = (A_{23}A_1B_1/P^2R_0)-(A_{13}/R_0)-(A_{12}B_1/a^2)[1 - h/R_0] + mMA_1[(1/a^2) - (h/R_0)[(1/a^2) + 1/P^2]] + NnA_1h/P^2R_0 \qquad 6.2\text{-}10$$

and

$$P^2 = h + B_1^2 \text{ and } R_0^2 = P^2 + A_1^2$$

After the integration of equation (6.2-9) with respect to $B_1$, the expression of the total anomalous field ( Bhattacharyya, 1964 ) may finally be written as

$$\Delta F(X,Y,0)/I_P = [(A_{23}/2)\, Log\{(R_0-A_1)/(R_0+A_1)\} + (A_{13}/2)log\{(R_0-B_1)/(R_0+B_1)\} - A_{12}\, Log(R_0+h) - lL \arctan (A_1B_1/(A_1^2+R_0h+h^2)) - mM \arctan (A_1B_1/(R_0^2+R_0h-A_1^2)) + nN \arctan (A_1B_1/R_0h)]_{Al}^{Au}\,{}_{Bl}^{Bu} \qquad 6.2\text{-}11a$$

Where Au, Bu are the upper limits and Al, Bl the lower limits of $A_1$ and $B_1$, respectively. L, M, and N are the direction cosines of the polarization vector. l, m, and n are the direction cosines of the Earth's magnetic field vector, and $I_P$ is the polarization magnitude.

If (A,B,h) defines the center of the upper surface of the prism( Fig. 6.1 ) which extends from Aa to Ab in the X-direction, and from Ba to Bb in Y-direction, then, Al, Au, Bl and Bu are defined as follow

$$Al = Aa - x,\ Au = Ab - x,\ Bl = Ba - y,\ Bu = Ba - y \qquad 6.2\text{-}12$$

Let us simplify equation (6.2-11a) to make it easy for numerical computation or even for a pocket calculator

$$R_0^2 = A_1^2 + B_1^2 + (h-z)^2 \Big|_{Al}^{Au}\Big|_{Bl}^{Bu} = R_1^2 + R_2^2 + R_3^2 + R_4^2$$

where

$$R_1^2 = Au^2 + Bu^2 + (h-z)^2$$

$$R_2^2 = Al^2 + Bu^2 + (h-z)^2$$

$$R_3^2 = Au^2 + Bl^2 + (h-z)^2$$

$$R_4^2 = Al^2 + Bl^2 + (h-z)^2$$

$$TERM1 = \frac{A_{23}}{2} \operatorname{Log} \frac{R_0 - A_1}{R_0 + A_1} \Big|_{Al}^{Au}\Big|_{Bl}^{Bu} = \frac{A_{23}}{2}\left[ \operatorname{Log} \frac{R_1 - Au}{R_1 + Au} - \operatorname{Log} \frac{R_2 - Al}{R_2 + Al} - \operatorname{Log} \frac{R_3 - Au}{R_3 + Au} + \operatorname{Log} \frac{R_4 - Al}{R_4 + Al} \right]$$

$$TERM2 = \frac{A_{13}}{2} \operatorname{Log} \frac{R_0 - Bl}{R_0 + B_1} \Big|_{Al}^{Au}\Big|_{Bl}^{Bu} = \frac{A_{13}}{2}\left[ \operatorname{Log} \frac{R_1 - Bu}{R_1 + Bu} - \operatorname{Log} \frac{R_2 - Bu}{R_2 + Bu} - \operatorname{Log} \frac{R_3 - Bl}{R_3 + Bl} + \operatorname{Log} \frac{R_4 - Bl}{R_4 + Bl} \right]$$

$$TERM3 = - A_{12}\, Log(R_0+h) \Big|_{Al}^{Au}\Big|_{Bl}^{Bu} = - A_{12}[\, Log(R_1+h) - Log(R_2+h) - LOG(R_3+h) + Log(R_4+h)]$$

$$TERM4 = 1L\, \tan^{-1} \frac{AlBl}{A_1{}^2+R_0h+h^2} \Big|_{Al}^{Au}\Big|_{Bl}^{Bu} = -1L\left[\tan^{-1} \frac{AuBu}{Au^2+R_1h+h^2} - \tan^{-1} \frac{AlBu}{Al^2+R_2h+h^2} - \tan^{-1} \frac{AuBl}{Au^2+R_3h+h^2} + \tan^{-1} \frac{Al\ Bl}{Al^2+R_4h+h^2}\right]$$

$$TERM5 = -mM\, \tan^{-1} \frac{A_1B_1}{R_0{}^2+R_0h-A_1{}^2} \Big|_{Al}^{Au}\Big|_{Bl}^{Bu} = -mM\left[\tan^{-1} \frac{AuBu}{R_1{}^2+R_1h-Au^2} - \tan^{-1} \frac{AlBu}{R_2{}^2+R_2h-Al^2} - \tan^{-1} \frac{AuBl}{R_3{}^2+R_3h-Au^2} + \tan^{-1} \frac{AlBl}{R_4{}^2+R_4h-Al^2}\right]$$

$$TERM6 = Nn\, \tan^{-1} \frac{A_1B_1}{R_0h} \Big|_{Al}^{Au}\Big|_{Bl}^{Bu} = Nn\left[\tan^{-1} \frac{AuBu}{R_1h} - \tan^{-1} \frac{AlBu}{R_2h} - \tan^{-1} \frac{AuBl}{R_3h} + \tan^{-1} \frac{AlBl}{R_4h}\right]$$

Then, the equation (6.2-11a) can be reduced to the following form

$$\Delta F(x,y,0)/I_P = TERM1 + TERM2 + TERM3 + TERM4 + TERM5 + TERM6 \qquad 6.2\text{-}11b$$

In equation (6.2-11a) if we substitute (h - z) for h, we obtain the the expression of the anomalous field $\Delta F(x,y,z)$. Since

$$d/dz = -d/d(h - z) \ ,$$

and

$$d^2/dz^2 = d^2/d(h - z)^2$$

the first and second vertical derivatives of the anomalous field at (x,y,0) are given by Bhattacharyya (1964) as follow

$$\frac{d}{dz}\frac{\Delta F(x,y,z)}{I} = A_{23}\frac{A_1 h}{R_0(R_0-A_1)} - A_{13}\frac{B_1 h}{R_0(R_0-B_1)} + \frac{A_{12}}{R_0}$$

$$-lL\frac{A_1B_1}{R_0(h+A_1)} - mM\frac{A_1B_1}{R_0(R_0-A_1)} + Nn\frac{A1B1(R_0+h)}{R_0(A1B_1+R_0h)}\Bigg|_{Al}^{Au}\Bigg|_{Bl}^{Bu} \qquad 6.2\text{-}13a$$

and

$$\frac{d^2}{dz^2}\frac{\Delta F(x,y,z)}{I} = A_{23}\frac{A_1}{R_0^2(R_0^2-A_1^2)}[(a^2-2h^2)R_0^2-a^2A_1^2]$$

$$+A_{13}\frac{B_1}{R_0^3(R_0-B_1)}[(a^2-2h^2)R_0^2-a^2B_1^2]+A_{12}(h/R_0^3)$$

$$-mM\frac{A_1B_1h(3R_0^2-A_1^2)}{R_0^3(R_0^2-A_1^2)^2} - lL\frac{A_1B_1h}{R_0^3(h^2+A_1^2)^2}(A_1^2+h_1^2+2R_0^2)$$

$$+nN\frac{A_1B_1h}{R_0(A_1^2B_1^2+R_0^2h^2)}\left[2\frac{(R_0^2+h)^2}{A_1^2B_1^2+R_0^2h^2} + \frac{h^2}{R_0^2} - 3\right]_{Al}^{Au}\Bigg|_{Bl}^{Bu} \qquad 6.2\text{-}14$$

Similarly, equation ( 6.2-13a ) can be simplified as follows

$$TERM1 = - A_{23} \frac{A_1 h}{R_0(R_0^2 - A_1^2)} \Bigg|_{Al}^{Au}\Bigg|_{Bl}^{Bu} = - A_{23}\left[ \frac{Auh}{R_1(R_1^2 - Au^2)} - \frac{Alh}{R_2(R_2^2 - Al^2)} - \frac{Auh}{R_3(R_3^2 - Au^2)} + \frac{Alh}{R_4(R_4^2 - Al^2)} \right]$$

$$TERM2 = - A_{13} \frac{B_1 h}{R_0(R_0^2 - B_1^2)} \Bigg|_{Al}^{Au}\Bigg|_{Bl}^{Bu} = - A_{13}\left[ \frac{Buh}{R_1(R_1^2 - Bu^2)} - \frac{Buh}{R_2(R_2^2 - Bu^2)} - \frac{Blh}{R_3(R_3^2 - Bl^2)} + \frac{Blh}{R_4(R_4^2 - Bl^2)} \right]$$

$$TERM3 = A_{12}/R_0 \Big|_{Al}^{Au}\Big|_{Bl}^{Bu} = A_{12}[\ 1/R_1 + 1/R_2 + 1/R_3 + 1/R_4\ ]$$

$$TERM4 = - lL \frac{A_1 B_1}{R_0(h^2 + A_1^2)} \Bigg|_{Al}^{Au}\Bigg|_{Bl}^{Bu} = - lL\left[ \frac{AuBu}{R_1(h^2 + Au^2)} - \frac{AlBu}{R_2(h^2 + Al^2)} - \frac{AuBl}{R_3(h^2 + Au^2)} + \frac{AlBl}{R_4(h^2 + Al^2)} \right]$$

$$TERM5 = -mM \frac{A_1 B_1}{R_0(R_0^2 - A_1^2)} \Bigg|_{Al}^{Au}\Bigg|_{Bl}^{Bu} = - mM\left[ \frac{AuBu}{R_1(R_1^2 - Au^2)} - \frac{AlBu}{R_2(R_2^2 - A_1^2)} - \frac{AuBl}{R_3(R_3^2 - Au^2)} + \frac{AlBl}{R_4(R_4^2 - Al^2)} \right]$$

$$TERM6 = Nn \frac{A_1B_1(R_0^2+h^2)}{R_0(A_1^2B_1^2+R_0^2h^2)} \Bigg|_{Al}^{Au} \Bigg|_{Bl}^{Bu} = Nn\left[ \frac{AuBu(R_1^2+h^2)}{R_1(Au^2Bu^2+R_1^2h^2)} \right.$$

$$\left. - \frac{AlBu(R_2^2+h^2)}{R_2(Al^2Bu^2+R_2^2h^2)} - \frac{AuBl(R_3^2+h^2)}{R_3(Au^2Bl^2+R_3^2h^2)} + \frac{AlBl(R_4^2+h^2)}{R_4(Al^2Bl^2+R_4^2h^2)} \right]$$

Therefore, equation (6.2-13a) can be reduced to the following form

$$d[\Delta F(x,y,z)]/dz = TERM1 + TERM2 + TERM3 + TERM4 + TERM5 + TERM6 \qquad 6.2\text{-}13b$$

Also the vertical and horizontal derivatives of the field formula, which is given in equation (6.2-11) are the Hilbert transforms of each other ( Nabighian, 1983). If we set $\Delta F(X,Y,0)=\Delta F(X,Y,0)/I_p$, then the relation becomes

$$F\{d\Delta F/dz\} = H_1\, F\{d\Delta F/dx\} + H_2\, F\{d\Delta F/dy\} \qquad 6.2\text{-}15$$

The same procedure can be extended to determine the second vertical derivative from the following relation

$$F\{d^2\Delta F/dz^2\} = H_1\, F\{d^2\Delta F/dxdz\} + H_2\, F\{d^2\Delta F/dydz\} \qquad 6.2\text{-}16$$

where $d\Delta F/dz$ is the vertical derivative of $\Delta F$, and $d^2\Delta F/dz^2$ is the second vertical derivative of $\Delta F$. By taking the inverse Fourier transforms of the equations(6.2-15) and (6.2-16) the first and second vertical derivatives can be obtained.

## 6.3 MULTIPRISMATIC MODELS IN MAGNETICS

Consider a rectangular cartesian coordinate system with x-and y-axes along the geographic north and east directions, respectively, and the z-axis pointing vertically downward. If the magnetization vector J is defined by the intensity $I_\rho$ and the direction-cosines ( L, M, N), then we can write,

$$I_\rho x = LI_\rho , \quad I_\rho y = MI_\rho , \quad \text{and} \quad I_\rho z = NI_\rho \qquad 6.3\text{-}1$$

The sides of the rectangular prism are assumed to be parallel to the x- and y-axes, respectively. The prism extends from Aa to Ab in the x direction, from Ba to Bb in the y-direction, and from h to infinity in the z direction as shown in Fig. 6.1. In this case the expression in equation (6.2-11a) can be written as;

$$\Delta F(x,y,z) = a_1 b_1 + a_2 b_2 + a_3 b_3 \qquad 6.3\text{-}2a$$

Where,

$$a_1 = I_\rho x, \quad a_2 = I_\rho y, \quad a_3 = I_\rho z$$

If we divide $a_1$, $a_2$, and $a_3$ by $I_\rho$ using equation ( 6.3-1 ), then equation ( 6.3-2a ) becomes;

$$\Delta F(x,y,z)/I_\rho = L b_1 + M b_2 + N b_3, \qquad 6.3\text{-}2b$$

where,

$$b_1 = \{(n/2)\,\mathrm{Log}((R_0-B_1)/(R_0+B_1)) - m\,\mathrm{Log}(R_0+h) - l\tan^{-1}(A_1B_1/(A_1^2+R_0h+h^2))\}\ \begin{matrix}\mathrm{Au}\ \mathrm{Bu}\\ \mathrm{Al}\ \mathrm{Bl}\end{matrix}$$

$$b_2 = \{(n/2)\,\mathrm{Log}((R_0-A_1)/(R_0+A_1)) - l\,\mathrm{Log}(R_0+h) - m\tan^{-1}(A_1B_1/(R_0^2+R_0h-A_1^2))\}\ \begin{matrix}\mathrm{Au}\ \mathrm{Bu}\\ \mathrm{Al}\ \mathrm{Bl}\end{matrix}$$

$$b_3 = \{(m/2)\ \mathrm{Log}((R_0-A_1)/(R_0+A_1)) + (1/2)\mathrm{Log}((R_0-B_1)/(R_0+B_1)) + n\ \tan^{-1}(A_1B_1/R_0h)\}\ \Big|_{Al}^{Au}\ \Big|_{Bl}^{Bu}$$

$Al = Aa - x$, $Au = Ab - x$, $Bl = Ba - y$, $Bu = Bb - y$,

and

$$R_0^2 = A_1^2 + B_1^2 + h^2$$

The discussion in the previous relations in this section was concerned with the general case of an anomalous magnetic field observed at several points on a surface of observation which is located at a height h above the prismatic body.

Let us now assume several prisms with different horizontal dimensions, and direction cosines of polarization vector, then each prism generates a unique field according to equation (6.3-2b). The expression for the total field at a point of observation, x, y and z ( Bhattacharyya, 1980 ) can be written as

$$\Delta F_t(x,y,z)/I_p = (L_1\ b_1 + M_1\ b_2 + N_1\ b_3) + (L_2\ b_4 + M_2\ b_5 + N_2\ b_6) + \ldots\ldots\ldots + (L_t\ b_n + M_t\ b_{n+1} + N_t\ b_{n+2}) \qquad 6.3\text{-}3$$

In equation (6.3-3), the terms in each bracket correspond to a particular prism, and the subscribt "t" denotes the number of the prisms which are to be included in the model.

## 6.4 GRAVITATIONAL ATTRACTION OF A PRISMATIC BODY

A numerous papers have been published on the methods of computing gravitational attraction of simple bodies such as sphere, cylinder, ellipsoid, and prism. For many of these cases, only approximate expressions have been obtained, and there are restrictions limiting the validity of the expressions near the observation point. Nagy ( 1965 ) derived a closed expression for the gravitational attraction of a prism which is valid for any point outside of or on the boundary of the prism.

Let us review the expression by Nagy ( 1966a ) below. The magnitude of the attraction of an elementary mass on a unit mass at distance r is given by:-

$$\Delta g = - G \rho (\Delta v/r^2), \qquad 6.4\text{-}1$$

where G is the gravitational constant, $\rho$ the density and $\Delta v$ the volume element.

If the angle between r and the vertical axis is denoted by $\theta$, the vertical component of the attraction of a body can be obtained by integrating $\Delta g \cos \theta$ over the volume, i.e,

$$g_z = -G\rho \int (dv/r^2) \cos \theta = - G\rho \int (z dz/r^3). \qquad 6.4\text{-}2$$

It is simple to carry out this integration for a prismatic body. Using the cartesian coordinate system shown in Fig. 6.2, equation (6.4-2 ) becomes:

$$g_z(x,y,z) = -G\rho \int_{x-u_1}^{x-u_2} \int_{y-v_1}^{y-v_2} \int_{z-w_1}^{z-w_2} (w/(u^2+v^2+w^2)^{3/2}) du\, dv\, dw \qquad 6.4\text{-}3$$

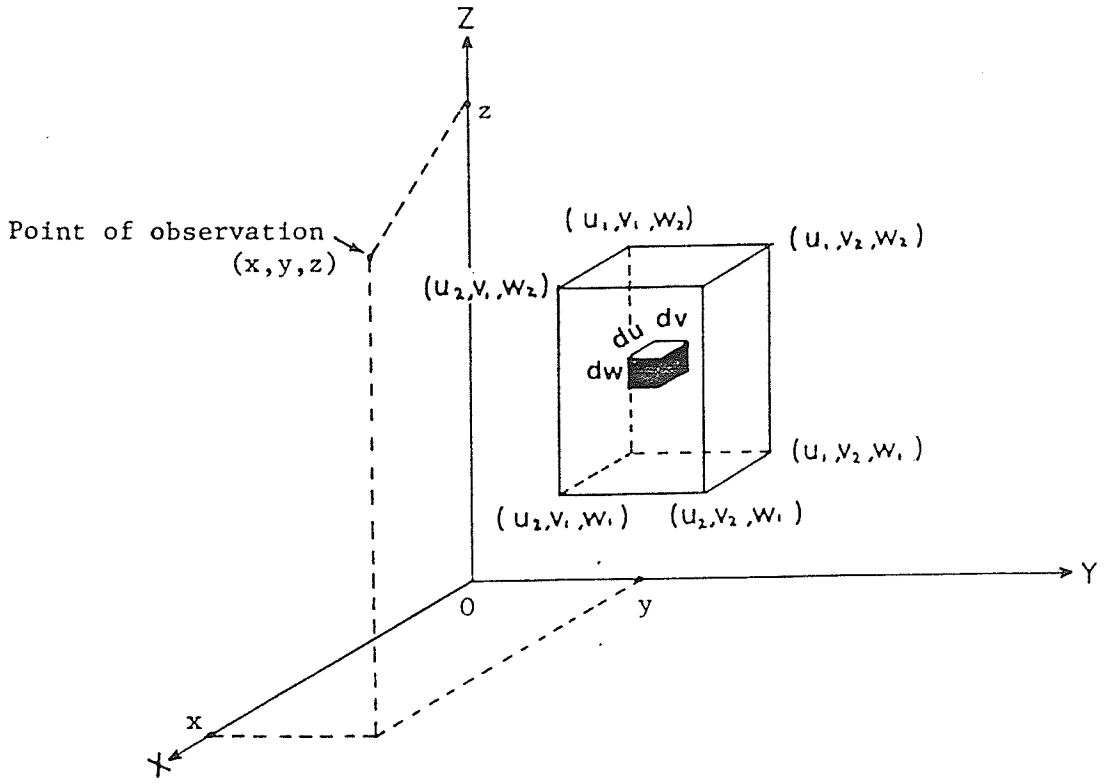


Fig. 6.2 A right rectangular prism with the volume element and its relation to the Cartesian coordinate system.

Carrying out the integration with respect to w and without substituting the limits, one finds

$$I_1 = \int (w/(u^2+v^2+w^2)^{3/2})dw = -(1/(u^2+v^2+w^2)^{1/2}) \quad 6.4\text{-}4$$

Integrating equation (6.4-4) with respect to v gives:

$$I_2 = \int I_1\, dv = \int (1/(u^2+v^2+w^2)^{1/2})\, dv$$

$$= \text{Log}\,(v+(u^2+v^2+w^2)^{1/2}) \quad 6.4\text{-}5$$

The integration of equation (6.4-5) with respect to u is slightly more complicated. One can proceed as follows

$$I_3 = \int I_2\, du = \int \text{Log}(v+(u^2+v^2+w^2)^{1/2})\, du$$

$$= u\ \text{Log}\,(v+(u^2+v^2+w^2)^{1/2})$$

$$- \int (u^2/((v+(u^2+v^2+w^2)^{1/2})(u^2+v^2+w^2)^{1/2}))du \quad 6.4\text{-}6$$

Letting $t = v+(u^2+v^2+w^2)^{1/2}$, then $u^2 = (t-v)^2 - v^2 - w^2$ one has

$$du = [(t-v)/((t-v)^2 - v^2 - w^2)^{1/2}]\, dt$$

Thus the integral in equation (6.4-6) becomes

$$\dot{I} = \int [u^2/(v+(u^2+v^2+w^2)^{1/2})(u^2+v^2+w^2)^{1/2}]\, du$$

$$= \int [(t^2 - 2tv - w^2)^{1/2}/t]\, dt$$

$$= t^2 - 2tv - w^2 - v\ \text{Log}(t - v + (t^2-2tv - w^2)^{1/2})$$

$$- w\ \arcsin[(-tv - w^2)/(t(w^2+v^2)^{1/2}]$$

Transforming back to the original variable and noting that

$$t^2 - 2tv - w^2 = [v^2+u^2+w^2+2v(u^2+v^2+w^2)^{1/2}$$

$$- 2v^2 - 2v(u^2+v^2+w^2)^{1/2} - w^2]^{1/2} = u,$$

then

$$\dot{I} = u - v\ \text{Log}\,(u+(u^2+v^2+w^2)^{1/2}) - w\ \arcsin[-(w^2+v^2$$

$$+ v(u^2+v^2+w^2)^{1/2})/[\{v+(u^2+v^2+w^2)^{1/2}\}(v^2+w^2)^{1/2}]$$

When the limits of integration are substituted, the first term in $\dot{I}$ drops out and the following general expression to calculate the vertical component of the attraction of a prism (Nagy, 1965) is obtained

$$g_z(x,y,z)=-G\rho \Big|\Big|\Big|\, u \,\mathrm{Log}(v+(u^2+v^2+w^2)^{1/2}) + v \,\mathrm{Log}(u+(u^2+v^2+w^2)^{1/2}) - w \arcsin[(w^2+v^2+v(u^2+v^2+w^2)^{1/2})/(v+(u^2+v^2+w^2)^{1/2})(v^2+w^2)^{1/2}] \Big|_{x-u_1}^{x-u_2} \Big|_{y-v_1}^{y-v_2} \Big|_{z-w_1}^{z-w_2} \quad 6.4\text{-}7$$

where

- $g_z(x,y,z)$ is the vertical attraction at a point$(x,y,z)$
- $(u_1,v_1,w_1)$, $(u_2,v_1,w_1)$, $(u_1,v_2,w_1)$ etc. define the corners of the prism.
- $\rho$ is the density of the prism
- G is the gravitational constant, and
- z is the vertical coordinate positive upwards.

As pointed out by Nagy (1966(a),(b)), another expression for $g_z(x,y,z)$ can be given as

$$g_z(x,y,z)= -G\rho \Big|\Big|\Big|\, u \,\mathrm{Log}\,[v+(u^2+v^2+w^2)^{1/2}] + v \,\mathrm{Log}[u+(u^2+v^2+w^2)^{1/2}] - w \arctan[uv/(w(u^2+v^2+w^2)^{1/2})] \Big|_{x-u_1}^{x-u_2} \Big|_{y-v_1}^{y-v_2} \Big|_{z-w_1}^{z-w_2} \quad 6.4\text{-}8a$$

This equation (6.4-8a) can also be modified ( Goodacre, 1972 ) to give

$$g_z(x,y,z) = -G\rho \left| \; \right| \; \left| \; \right| \; u \arcsin[v/(u^2+w^2)^{1/2}] + v \arcsin[u/(v^2+w^2)^{1/2}] - w \arctan([v/(w(u^2+v^2+w^2)^{1/2})] \Bigg|_{x-u_1 \; y-v_1 \; z-w_1}^{x-u_2 \; y-v_2 \; z-w_2} \quad 6.4\text{-}9a$$

It is clear that equation (6.4-9a) has the desired symmetry properties while expression (6.4-7) does not, mainly due to the form of the argument in the arcsine term.

Equation (6.4-7) is valid only when the limits $x-u_1$, $x-u_2$; $y-v1$, $y-v_2$; and $z-w_1$, $z-w_2$ are substituted. When either the x, y, or both axes are crossed, the integration must be carried out from the lower limit to the axis, then from the axis to the upper limit, the sum of these integrations giving the required effect. To describe all possible situations to evaluate equation (6.4-7), at least five pages or more will be needed to explain all the steps. For that reason, I am going to discuss equations (6.4-8a) and (6.4-9a) only, because these two equations can be used directly without any conditions.

To make equation ( 6.4-8a ) more simple, we have to substitute the limits as following;

If we set $Au = x - u_2$, $Al = x - u_1$, $Bu = y - v_2$, $B_1 = y - v_1$, and $Cu = z - w_2$, $Cl = z - w_1$, then

$$TERM1 = u\,Log[v+(u^2+v^2+w^2)^{1/2}]\Big|_{Al\ Bl\ Cl}^{Au\ Bu\ Cu} = Au\,Log[Bu+(Au^2+Bu^2+Cu^2)^{1/2}] - Al\,Log[Bu+(Al^2+Bu^2+Cu^2)^{1/2}] - Au\,Log[Bl+(Au^2+Bl^2+Cu^2)^{1/2}] + Al\,Log[Bl+(Al^2+Bl^2+Cu^2)^{1/2}] - Au\,Log(Bu+(Au^2+Bu^2+Cl^2)^{1/2}] + Al\,Log[Bu+(Al^2+Bu^2+Cl^2)^{1/2}] + Au\,Log[Bl+(Au^2+Bl^2+Cl^2)^{1/2}] - Al\,Log[Bl+(Al^2+Bl^2+Cl^2)^{1/2}]$$

$$TERM2 = v\,Log[u+(u^2+v^2+w^2)^{1/2}]\Big|_{Au\ Bu\ Cu}^{Au\ Bu\ Cu} = Bu\,Log[Au+(Au^2+Bu^2+Cu^2)^{1/2}] - Bu\,Log[Al+(Al^2+Bu^2+Cu^2)^{1/2}] - Bl\,Log[Au+(Au^2+Bl^2+Cu^2)^{1/2}] + Bl\,Log[Al+(Al^2+Bl^2+Cu^2)^{1/2}] - Bu\,Log[Au+(Au^2+Bu^2+Cl^2)^{1/2}] + Bu\,Log[Al+(Al^2+Bu^2+Cl^2)^{1/2}] + Bl\,Log[Au+(Au^2+Bl^2+Cl^2)^{1/2}] - Bl\,Log[Al+(Al+Bl^2+Cl^2)^{1/2}]$$

$$TERM3 = w\,\arctan[uv/(w(u^2+v^2+w^2)^{1/2})]\Big|_{Al\ Bl\ Cl}^{Au\ Bu\ Cu} = Cu[\arctan\{Au\ Bu/((Cu(Au^2+Bu^2+Cu^2)^{1/2}\} - \arctan\{Al\ Bu/(Cu(Al^2+Bu^2+Cu^2)^{1/2})\} - \arctan\{Au\ Bl/(cu(Au^2+bl^2+Cu^2)^{1/2})\} + \arctan\{Al\ Bl/(Cu(Al^2+Bl^2+Cu^2)^{1/2})\}] + Cl[-\arctan\{Au\ Bu/(Cl(Au^2+Bu^2+Cl^2)^{1/2})\} + \arcta\{Al\ Bu/(Cl(Al^2+Bu^2+Cu^2)^{1/2})\} + \arctan\{Au\ Bl/Cl(Au^2+Bl^2+Cl^2)^{1/2})\} - \arctan\{Al\ Bl/(Cl(Al^2+Bl^2+Cl^2)^{1/2})\}].$$

Then, equation (6.4-8a) can be written in a simple form as follow

$$g_z(x,y,z)/G\rho = -\,(\,TERM1 + TERM2 - TERM3\,) \qquad 6.4\text{-}8b$$

Note that, the last two terms of equations ( 6.4-8a ), and ( 6.4-9a ) are the same. Therefore, the first two terms in equation ( 6.4-9a ), can be simplified as follows

$$\text{TERM1} = u \arcsin\left[v/(u^2+w^2)^{1/2}\right]_{Al\ Bl\ Cl}^{Au\ Bu\ Cu} = Au \sinh^{-1}\left[ Bu/(\right.$$

$$\left. Au^2+Cu^2)^{1/2}\right] - Al \sinh^{-1}\left[ Bu/(Al^2+Cu^2)^{1/2}\right] - Au \sinh^{-1}\left[\right.$$

$$\left. Bl/(Au^2+Cu^2)^{1/2}\right] + Al \sinh^{-1}\left[ Bl/(Al^2+Cu^2)^{1/2}\right] - Au$$

$$\sinh^{-1}\left[ Bu/(Au^2+Cl^2)^{1/2}\right] + Al \sinh^{-1}\left[Bu/(Al^2+Cl^2)^{1/2}\right]$$

$$+ Au \sinh^{-1}\left[Bl/(Au^2+Cl^2)^{1/2}\right] - Al \sinh^{-1}\left[Bl/(Al^2+Cl^2)^{1/2}\right]$$

$$\text{TERM2} = v \arcsin\left[u/(v^2+w^2)^{1/2}\right]_{Al\ Bl\ Cl}^{Au\ Bu\ Cu} = Bu \sinh^{-1}\left[ Au/(\right.$$

$$\left. Bu^2+Cu^2)^{1/2}\right] - Bu \sinh^{-1}\left[Al/(Bu^2+Cu^2)^{1/2}\right] - Bl \sinh^{-1}\left[\right.$$

$$\left. Au/(Bl^2+Cu^2)^{1/2}\right] + Bl \sinh^{-1}\left[ Al/(Bl^2+Cu^2)^{1/2}\right] - Bu$$

$$\sinh^{-1}\left[Au/(Bu^2+Cl^2)^{1/2}\right] + Bu \sinh^{-1}\left[Al/(Bu^2+Cl^2)^{1/2}\right]$$

$$+ Bl \sinh^{-1}\left[Au/(Bl^2+Cl^2)^{1/2}\right] - Bl \sinh^{-1}\left[Al/(Bl^2+Cl^2)^{1/2}\right]$$

Therefore, equation ( 6.4-9a ) can be written as follow

$$g_z(x,y,z)/G\rho = -\ (\ \text{TERM1} + \text{TERM2} - \text{TERM3}\ ) \qquad 6.4\text{-}9b$$

Since the horizontal derivatives and the vertical first derivative of the field formula are the Hilbert transforms of each other, the following relations exist as in the previous section

$$F\{dgz/dz\} = H_1\ F(dgz/dx\} + H_2\ F\{dgz/dy\} \qquad 6.4\text{-}10$$

$$F\{d^2gz/dz^2\} = H_1\ F\{d^2gz/dzdx\} + H_2\ F\{d^2gz/dzdy\} \qquad 6.4\text{-}11$$

Equations (6.4-10), and (6.4-11) yield to obtain the first and second vertical derivatives, respectively.

## 6.5 SOME GENERAL COMMENTS

Equation (6.2-10) may be conveniently utilized to obtain the total magnetic field from bodies of finite vertical extent. For example, if the prismatic body under consideration has its top at a depth $h_1$ from the plane of observation and its bottom at a depth $h_2$, one has to determine fields due to two bodies of infinite vertical extent, one at a depth $h_1$ and the other $h_2$, and then subtract the latter from the former in order to evaluate the anomalous field and its first and second vertical derivatives for the given body.

In cases where none of the horizontal sides of the body are parallel to either the x- or y-axis but where the sides are perpendicular to each other, the problem can be solved by a rotation and simultaneous translation of the axes and then substituting the new values of x and y in equation (6.2-10).

# CHAPTER 7

# APPLICATION OF 2-D HILBERT TRANSFORM IN GRAVITY AND MAGNETIC DATA INTERPRETATION

## 7.1 INTRODUCTION

In this chapter I am going to investigate the application of 2-D Hilbert transform in the interpretation of magnetic and gravity anomalies as well as their derivatives.

Extensive work has been done on the derivation of analytical expression for magnetic and gravity effects due to bodies of simple geometrical shapes. In magnetic data application, this study makes use of the vertical derivative of magnetic anomaly due to a prismatic body with arbitrary polarization, as well as bodies with irregular shape. The expression used in this study, for the total field of prismatic body, was derived by Bhattacharyya ( 1964 ).

The effect of inclination, and declination of the magnetic polarization vector on the amplitude and shape of the magnetic anomaly, and its first and second vertical derivatives are tested for various different situations.

In gravitational potential field application, the 2-D Hilbert transform technique is tested again on the gravity effects of a prismatic body, as derived by Nagy(1966(a),(b)) and Goodacre( 1972 ). The same procedure of obtaining the

vertical derivatives could be easily extended to gravity examples. The application of the 2-D Hilbert transform on a real data set was tested with the digitized gravity contour map( Gupta et al., 1984 ) as well as digitized magnetic contour map of the Sudbury area (Geological Survey of Canada), Canada.

## 7.2 SOME EXAMPLES WITH MAGNETIC PRISMATIC BODIES

The total magnetic field and their derivatives of a prismatic body with infinite vertical dimension are considered. All the coordinates are measured in terms of the spacing which is taken as unity. The center of the prism is taken to be vertically below the origin of the coordinate system chosen. The vertical projection of the prism location is denoted by stars in each field intensity contour diagram.

The first and second vertical derivatives are used in quantitative interpertation to detect the location of the prism. Several examples with different parametres have been studied to develop these techniques.

The Fig. 7.1a is the contour map of the total field with $D = D_0 = 0^0$ and $I = I_0 = 60^0$ . In this figure the positive anomaly of the total field is at a maximum distance away from the center of the prism. The vertical gradient in Fig. 7.1b is obtained by taking the derivative of equation (6.2-11a) with respect to z ( down-ward direction ), while

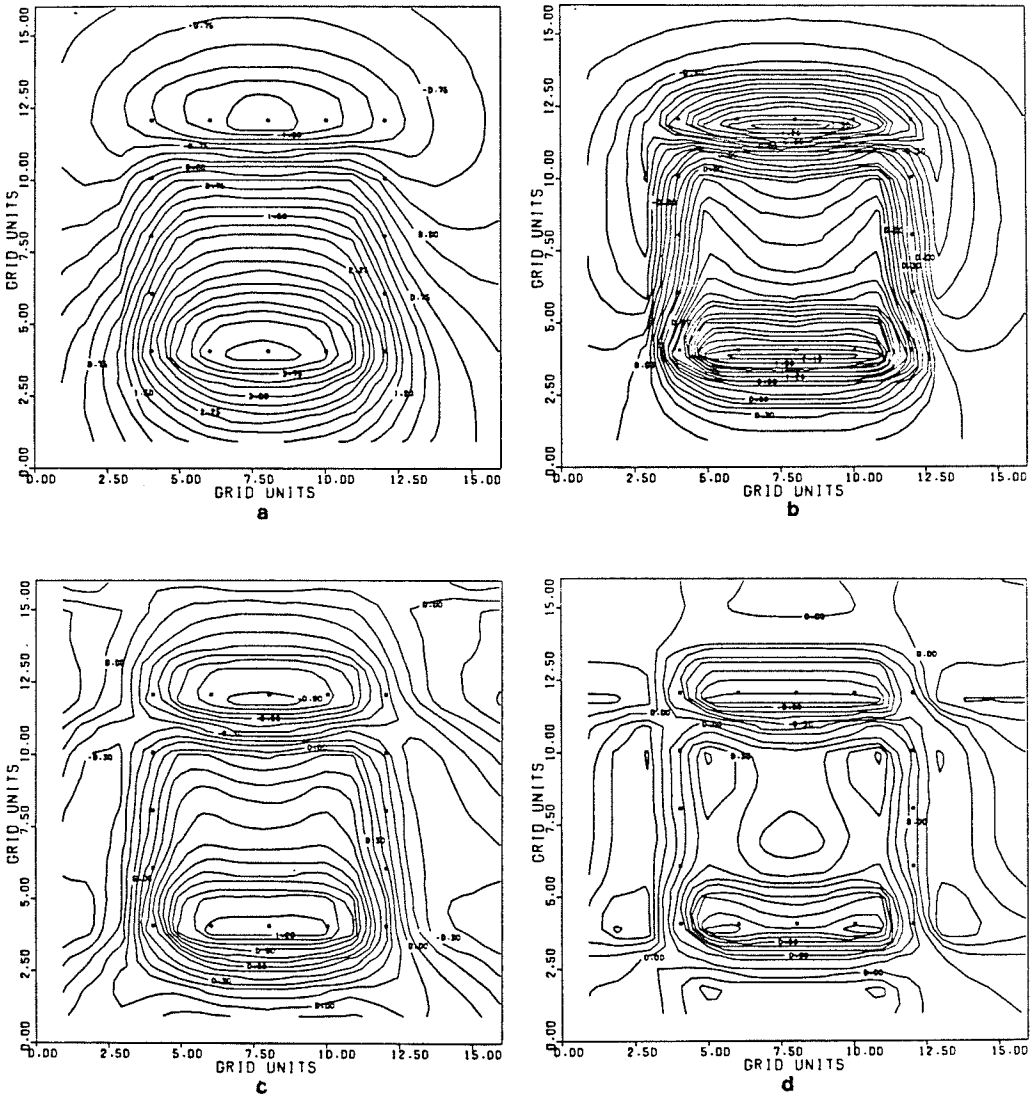


Fig. 7.1 (a) Contour diagram of the total field when $D=D_0 = 0^0$, $I=I_0= 60^0$, and h= 1 (arbitrary unit).
(b) Vertical first derivative of the total field without using 2-D Hilbert transform.
(c) Vertical first derivative of the total field obtained by using 2-D Hilbert transform.
(d) Vertical second derivative of the total field obtained by using 2-D Hilbert transform.

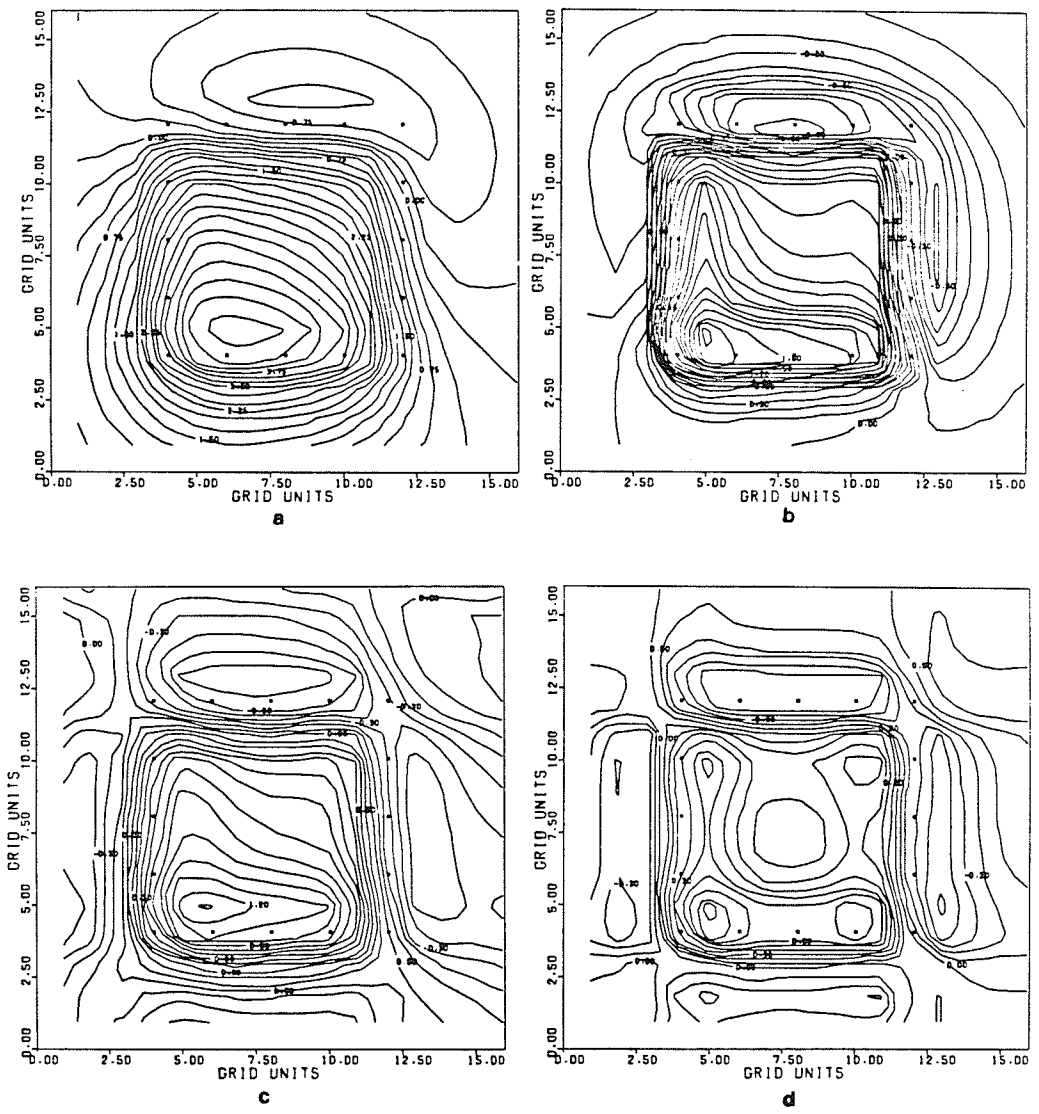


Fig. 7.2 (a) Contour diagram of the total field when D=0$^{0}$ , I=$I_0$= 60$^{0}$, D0= 45$^{0}$, and h= 1 (arbitrary unit).
(b) Vertical first derivative of the total field without using 2-D Hilbert transform.
(c) Vertical first derivative of the total field obtained by using 2-D Hilbert transform.
(d) Vertical second derivative of the total field obtained by using 2-D Hilbert transform.

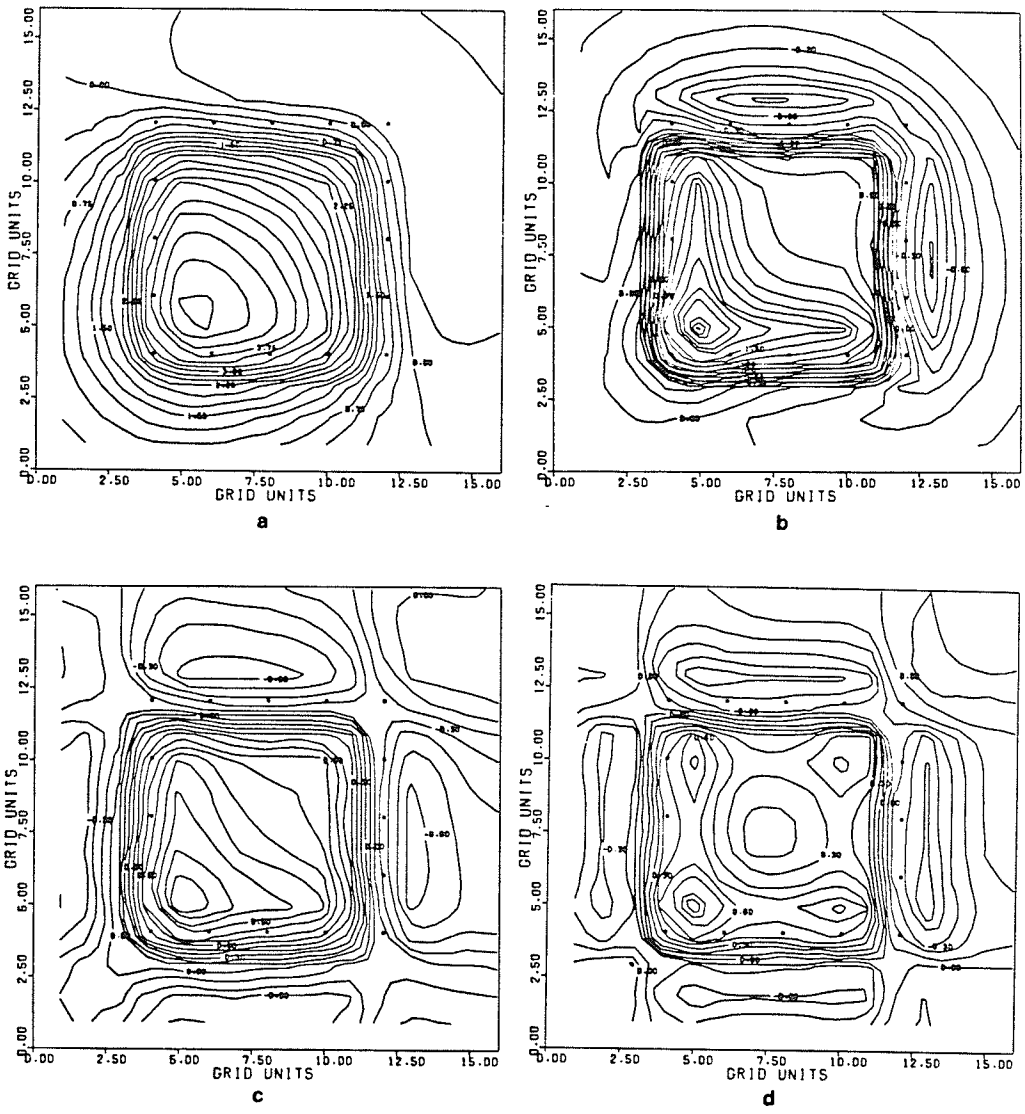


Fig. 7.3 (a) Contour diagram of the total field when D=0$^{0}$ , I=$I_0$= 60$^{0}$, D0= 90$^{0}$, and h= 1 (arbitrary unit).
(b) Vertical first derivative of the total field without using 2-D Hilbert transform.
(c) Vertical first derivative of the total field obtained by using 2-D Hilbert transform.
(d) Vertical second derivative of the total field

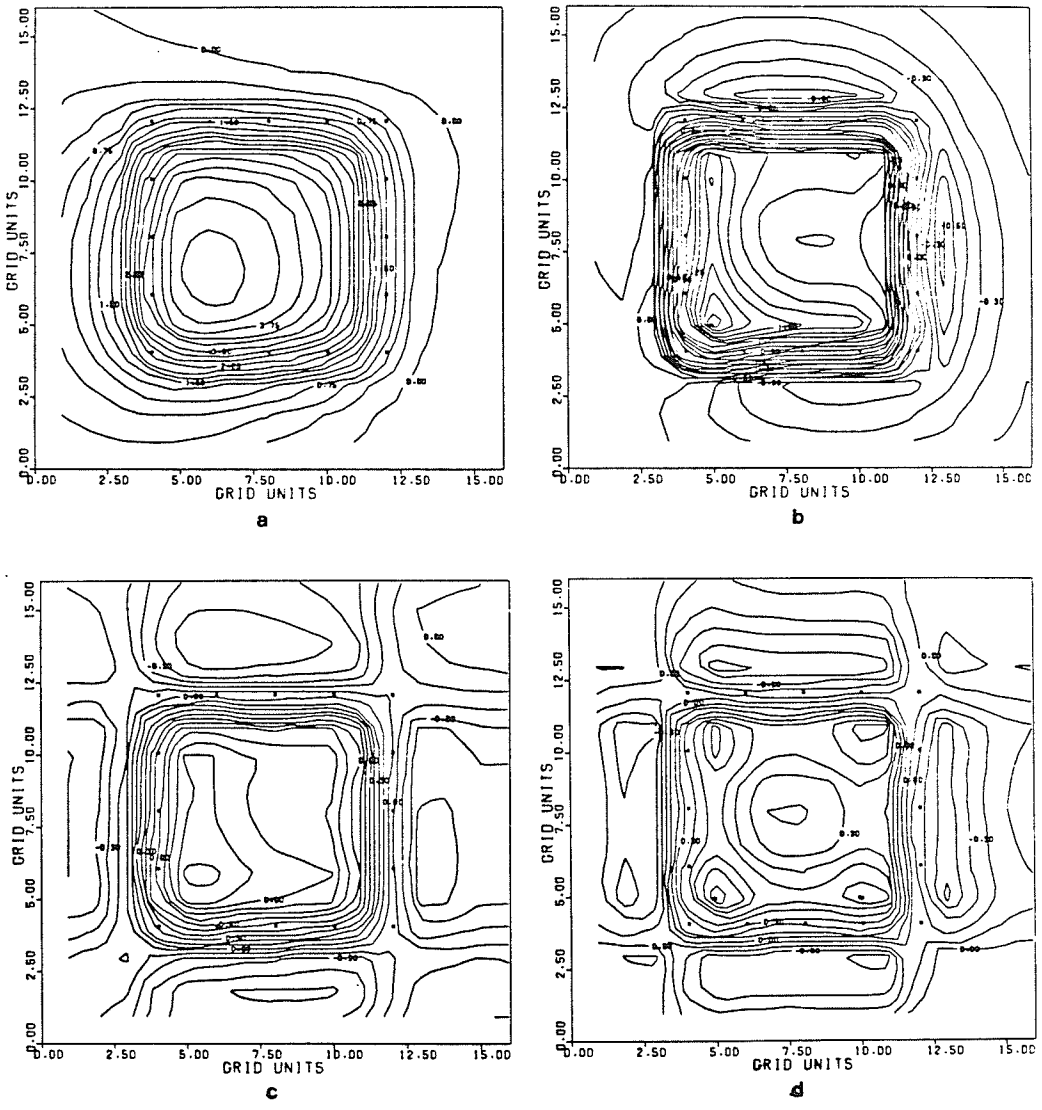


Fig. 7.4 (a) Contour diagram of the total field when $D=0^{o}$, $I=I_0=60^{o}$, $D_0=135^{o}$, and h= 1 (arbitrary unit).
(b) Vertical first derivative of the total field without using 2-D Hilbert transform.
(c) Vertical first derivative of the total field obtained by using 2-D Hilbert transform.
(d) Vertical second derivative of the total field obtained by using 2-D Hilbert transform.

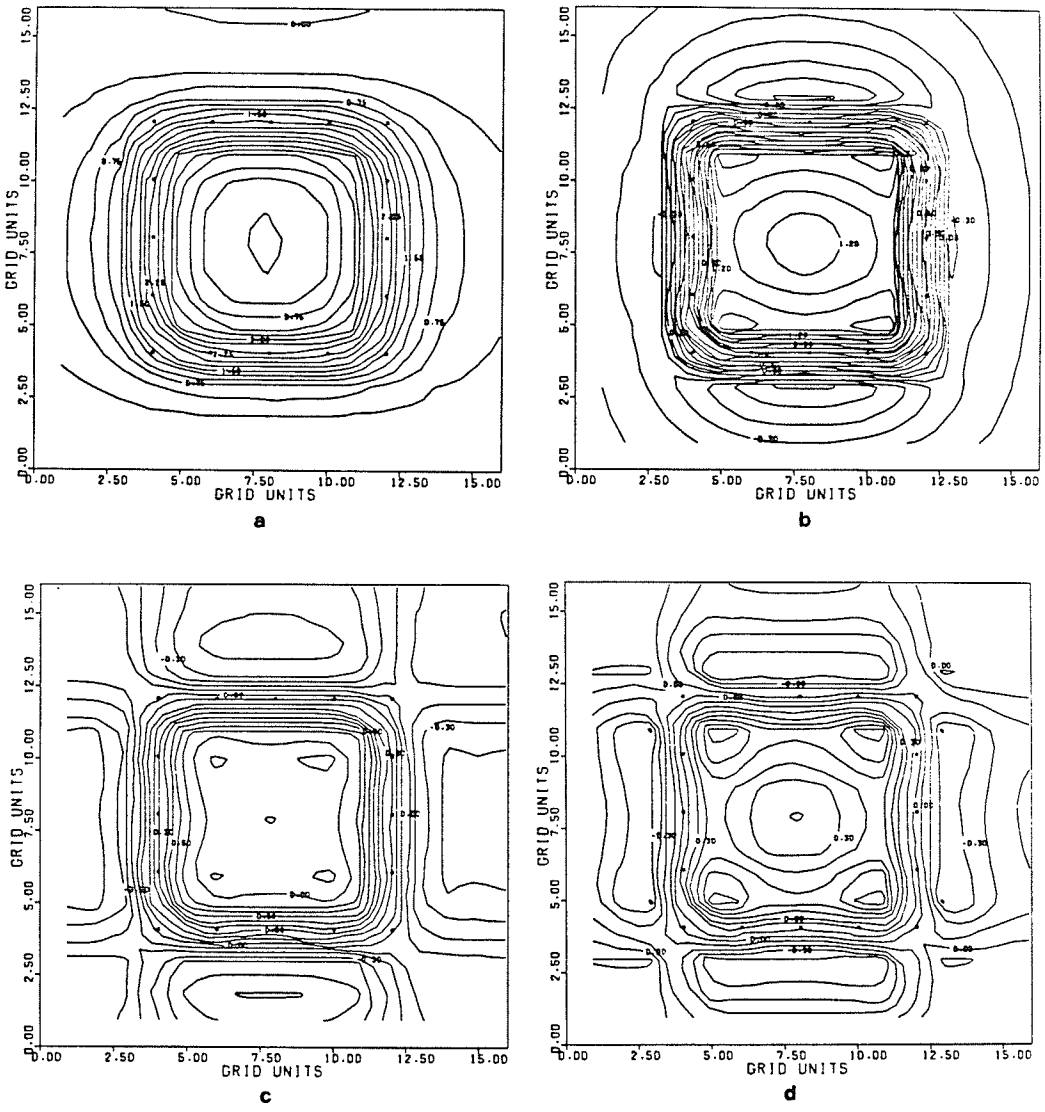


Fig. 7.5 (a) Contour diagram of the total field when $D=0^{o}$, $I=I_{o}= 60^{o}$, $D_{o}= 180^{o}$, and h= 1 (arbitrary unit).
(b) Vertical first derivative of the total field without using 2-D Hilbert transform.
(c) Vertical first derivative of the total field obtained by using 2-D Hilbert transform.
(d) Vertical second derivative of the total field obtained by using 2-D Hilbert transform.

in Fig. 7.1c the vertical gradient is obtained by taking the 2-D Hilbert transform of horizontal derivatives. The second vertical derivative in Fig. 7.1d is obtained from equation (6.2-16) by taking 2-D Hilbert transform of the horizontal derivatives of the respective first vertical derivatives.

The total field and its first and second vertical derivatives are shown in Figs. 7.2, 7.3, 7.4 and 7.5 for the cases of $D = 0^0$, $I = I_0 = 60^0$, and four values of $D_0$, e.g., $D_0 = 45^0$, $90^0$, $135^0$ and $180^0$. With the help of these diagrams it is possible to study the variation of the characteristics of the total field and its first and second vertical derivatives with the change in declination of the magnetic polarization vector with respect to that of the Earth's main field vector.

The anomaly of the total field in the Figs. 7.2, 7.3, 7.4 and 7.5 shifts toward the center and the negative anomaly away from the center as $(D_0 - D)$ increases, while, a second negative anomaly, small in magnitude , appears at the south end of the body and gradully moves toward the center with increase in $D_0$. When $D_0 = 180^0$ the contours become practicaly symmetrical with respect to the center of the prism and look as if the prism has been taken to the magnetic pole and the polarization is due to induction alone. The amplitude of the positive anomaly decreases gradually with increase in $(D_0 - D)$, reaching a minimum, and then begins to increase.

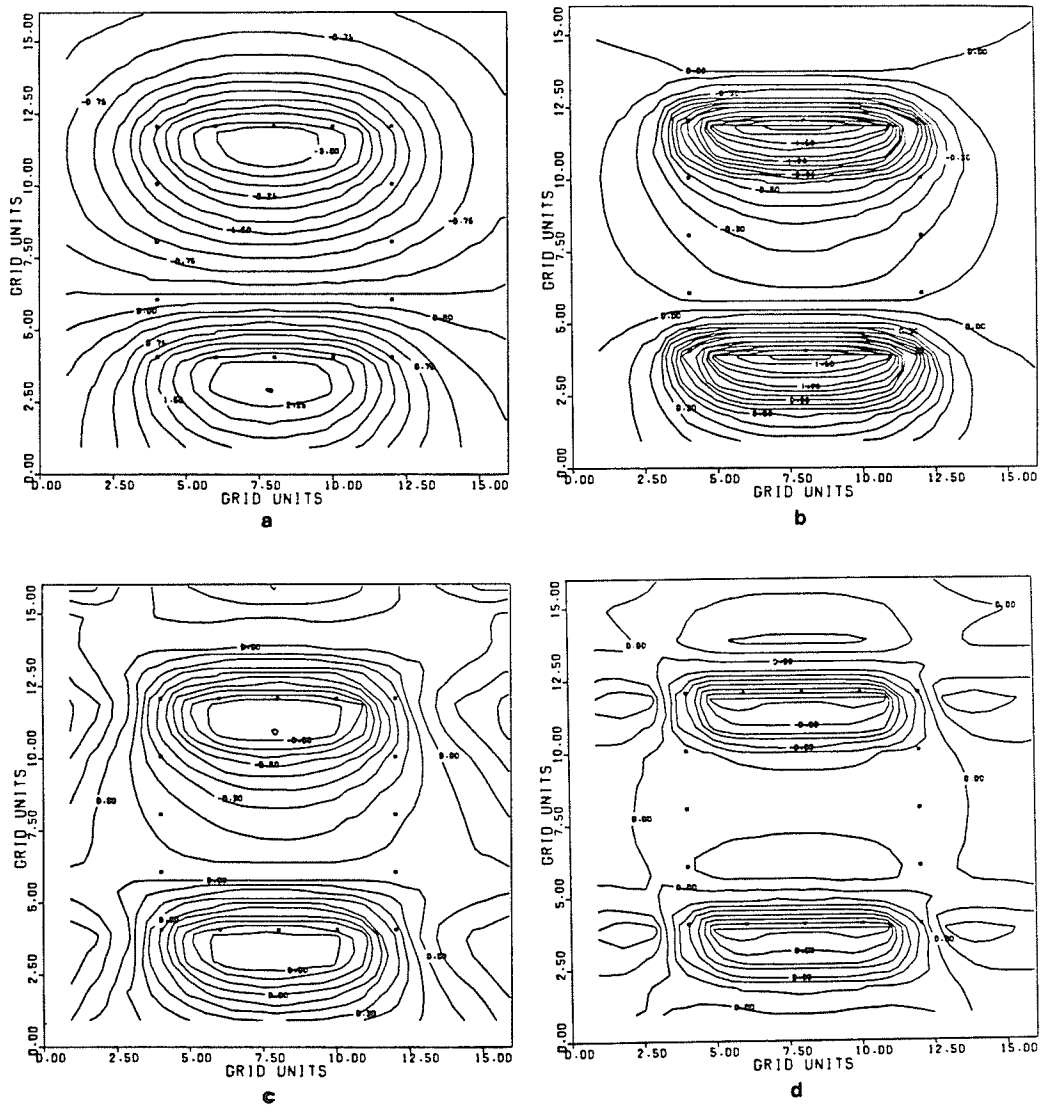


Fig. 7.6 (a) Contour diagram of the total field when $D=D_0 = 0^0$, $I= 60^0$, $I_0= 135^0$, and $h= 1$ (arbitrary unit).
(b) Vertical first derivative of the total field without using 2-D Hilbert transform.
(c) Vertical first derivative of the total field obtained by using 2-D Hilbert transform.
(d) Vertical second derivative of the total field obtained by using 2-D Hilbert transform.

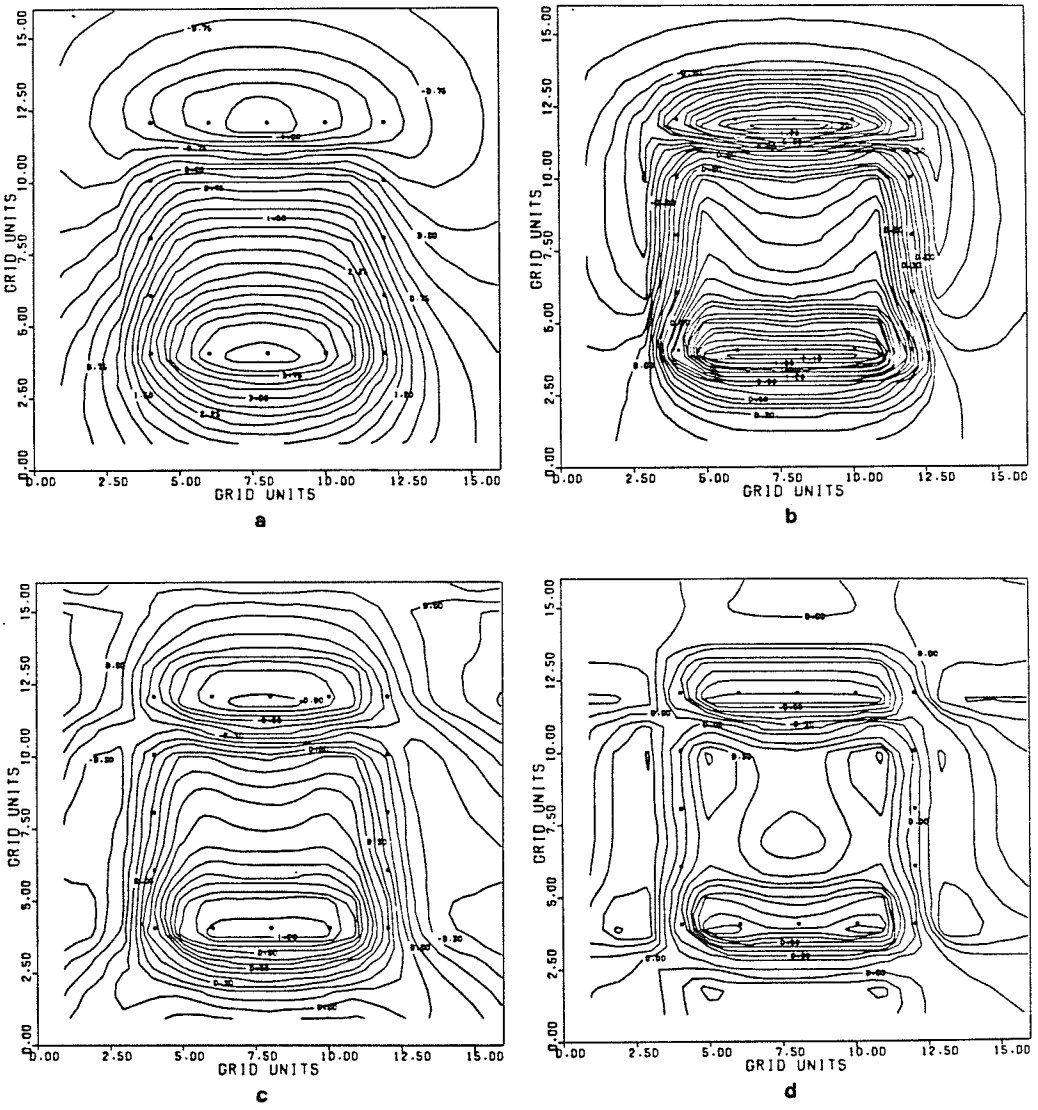


Fig. 7.7 (a) Contour diagram of the total field when $D=D_0 = 0^0$, $I= 60^0$, $I_0= 0^0$, and $h= 1$ (arbitrary unit).
(b) Vertical first derivative of the total field without using 2-D Hilbert transform.
(c) Vertical first derivative of the total field obtained by using 2-D Hilbert transform.
(d) Vertical second derivative of the total field

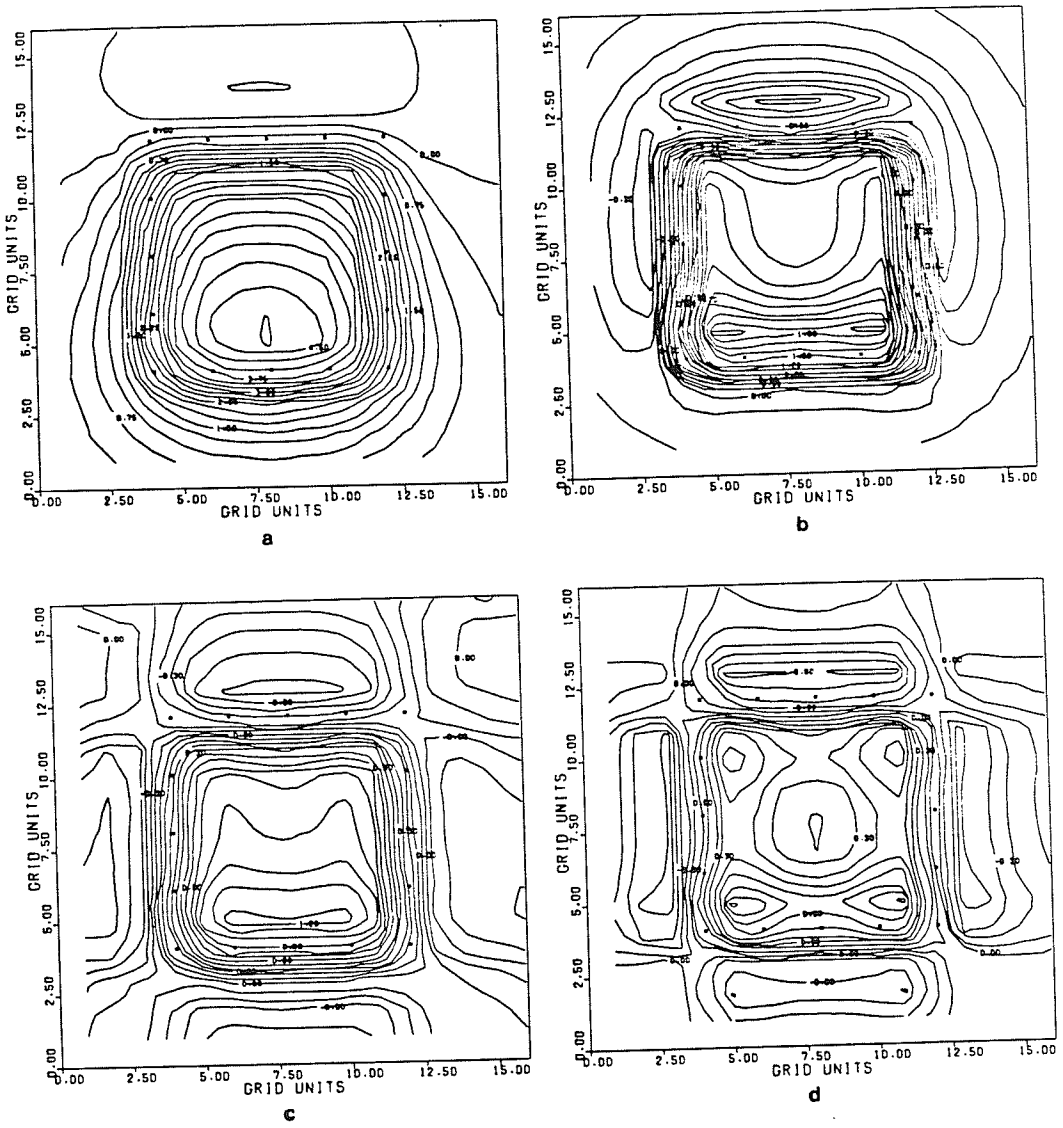


Fig. 7.8 (a) Contour diagram of the total field when $D=D_0 = 0^0$, $I= 60^0$, $I_0= 45^0$, and $h= 1$ (arbitrary unit).
(b) Vertical first derivative of the total field without using 2-D Hilbert transform.
(c) Vertical first derivative of the total field obtained by using 2-D Hilbert transform.
(d) Vertical second derivative of the total field obtained by using 2-D Hilbert transform.

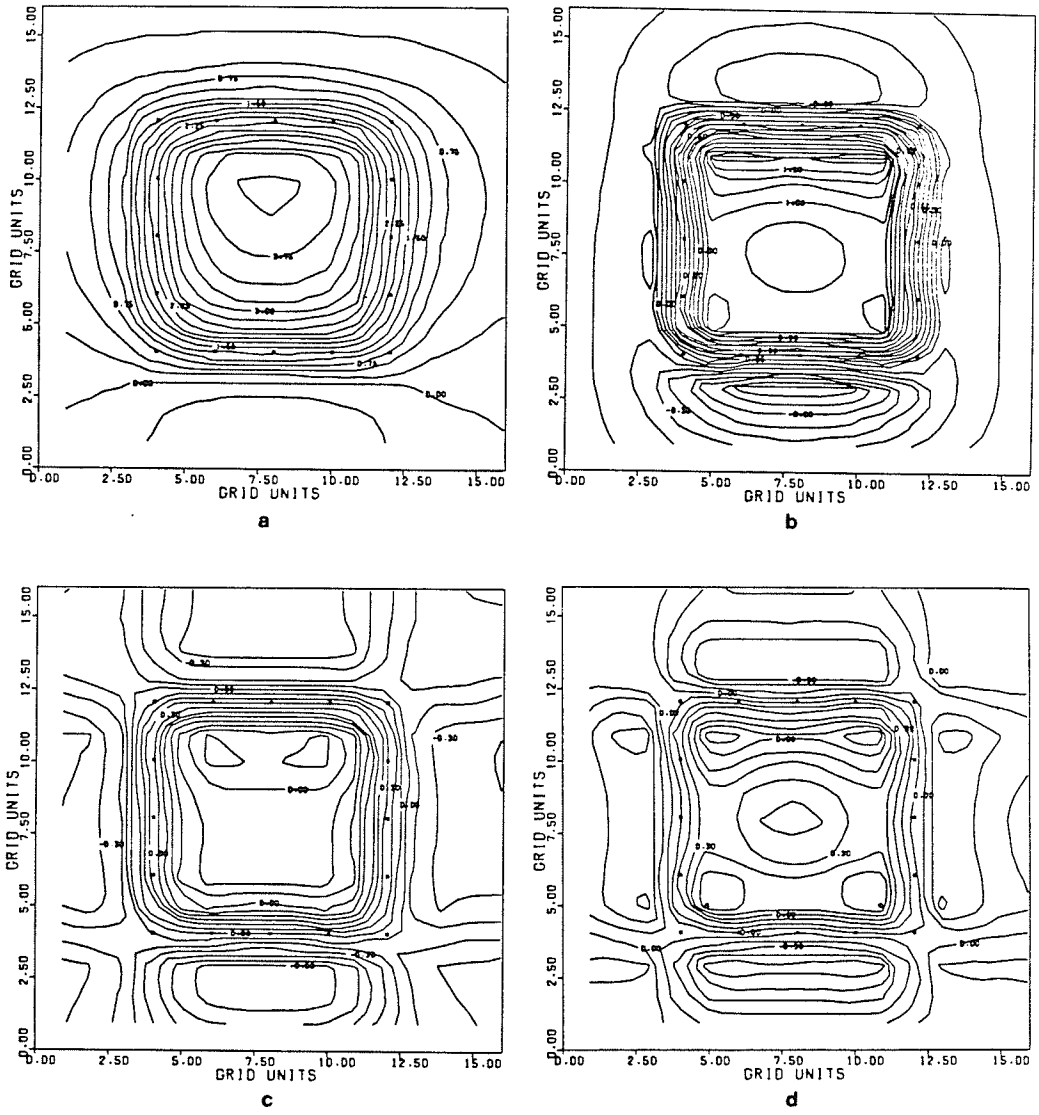


Fig. 7.9 (a) Contour diagram of the total field when $D=D_0 = 0^0$, $I= 60^0$, $I_0= 90^0$, and $h= 1$ (arbitrary unit).
(b) Vertical first derivative of the total field without using 2-DD Hilbert transform.
(c) Vertical first derivative of the total field obtained by using 2-D Hilbert transform.
(d) Vertical second derivative of the total field obtained by using 2-D Hilbert transform.

To study the variation of the characteristics of the total field and its first and second vertical derivatives with change in the inclination $I_0$ of the polarization vector, four contour maps are drawn in Figs. 7.6, 7.7, 7.8 and 7.9 by setting $I = 60^0$, $D = 0^0$ and four values of $I_0$ from $0^0$ to $135^0$ at steps of $45^0$. When $I_0 = 0^0$, i.e., the polarization vector is horizontal the negative high of the anomaly occurs at the north of the positive high, and the former is of higher amplitude than the latter. The zero contours of the vertical derivatives nowhere follow the outline of the body when $I_0 = 0^0$. As $I_0$ increases, the negative high diminishes and the positive high begins to increase, reaching a maximum, and then starts to decrease. The same applies for the vertical derivatives of the total field. All of them become more and more symmetrical with respect to the body of the prism with increase in $I_0$.

## 7.3 APPLICATIONS OF 2-D HILBERT TRANSFORM IN MULTIPRISMATIC MAGNETIC BODIES

Our study is made of magnetic anomaly and its first and second vertical derivatives due to five prismatic bodies as shown in Figs. 7.10a-c . Fig. 7.10a represents a contour diagram of the total field due to five prisms when $I=I_0=60^0$, $D=0$, $D_0=135^0$, the contour interval 0.25 ( arbitrary unit ).

The horizontal sides of the prism1 extend 14 by 14 units and its center at (32,32) grid unit, prism2 has 12 units length in x and y directions and its center at (16,16) grid unit, prism3 has 2 units less than prism2 in each horizontal dimension and its center at (48,16) grid unit, prism4 and prism5 have horizontal dimensions 8 by 8 and 6 by 6 units, and their centers at (16,16) and (48,48) grid units, respectively.

For all the prisms assume that the vertical sides are extended to infinity, and have 1 unit depth below the surface of the observation. We are not going to discuss the shape of the anomalies which are generated by these prisms, because the discussion already given in Fig. 7.5 which has the same parameters as in the case of one prism body.

Several examples ( Figs.7.10, 7.11 and 7.12 ) are tested by increasing the depth and all the prisms are assumed at the same depth except one example ( Fig. 7.12 ) the depth is assumed different for each prism in the model. For all these

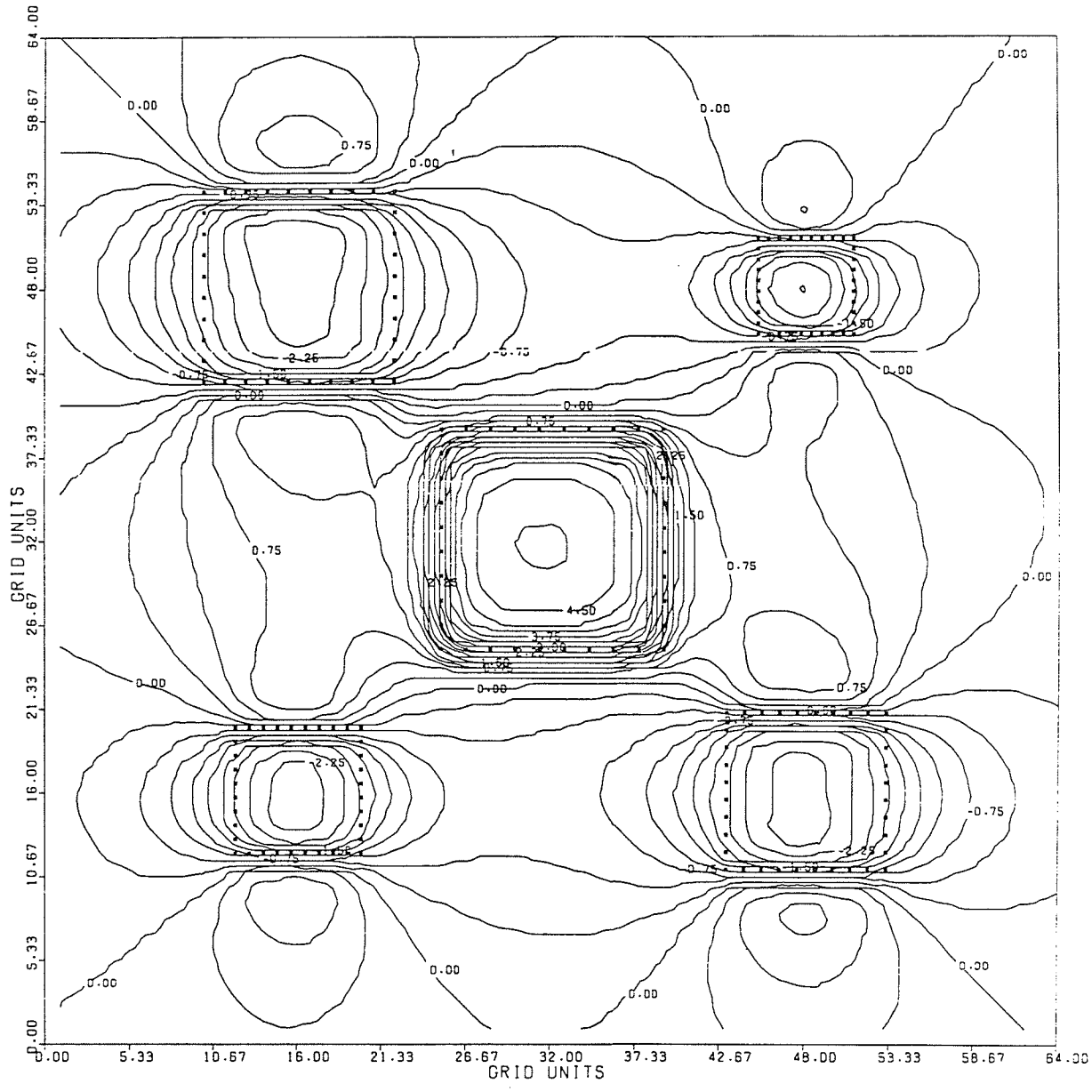


Fig. 7.10a Contour diagram of the total field due to five prismatic bodies when $I=I_0= 60^0$, $D= 0^0$, $D_0=180^0$, $h = 1$ for all the prisms ( arbitrary unit ).

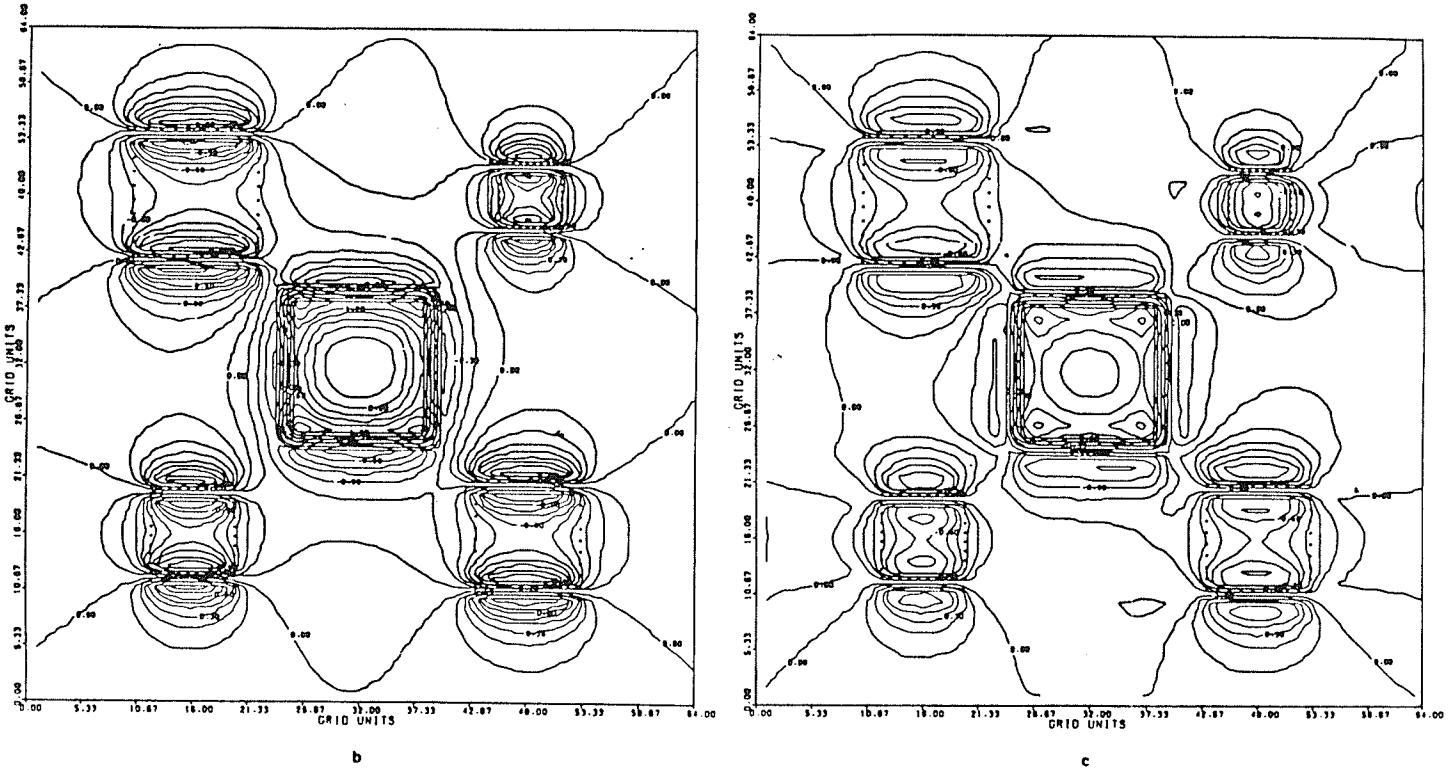


Fig. 7.10 (b) Vertical first derivative of the total field obtained by using 2-D Hilbert transform.
(c) Vertical second derivative of the total field obtained by using 2-D Hilbert transform

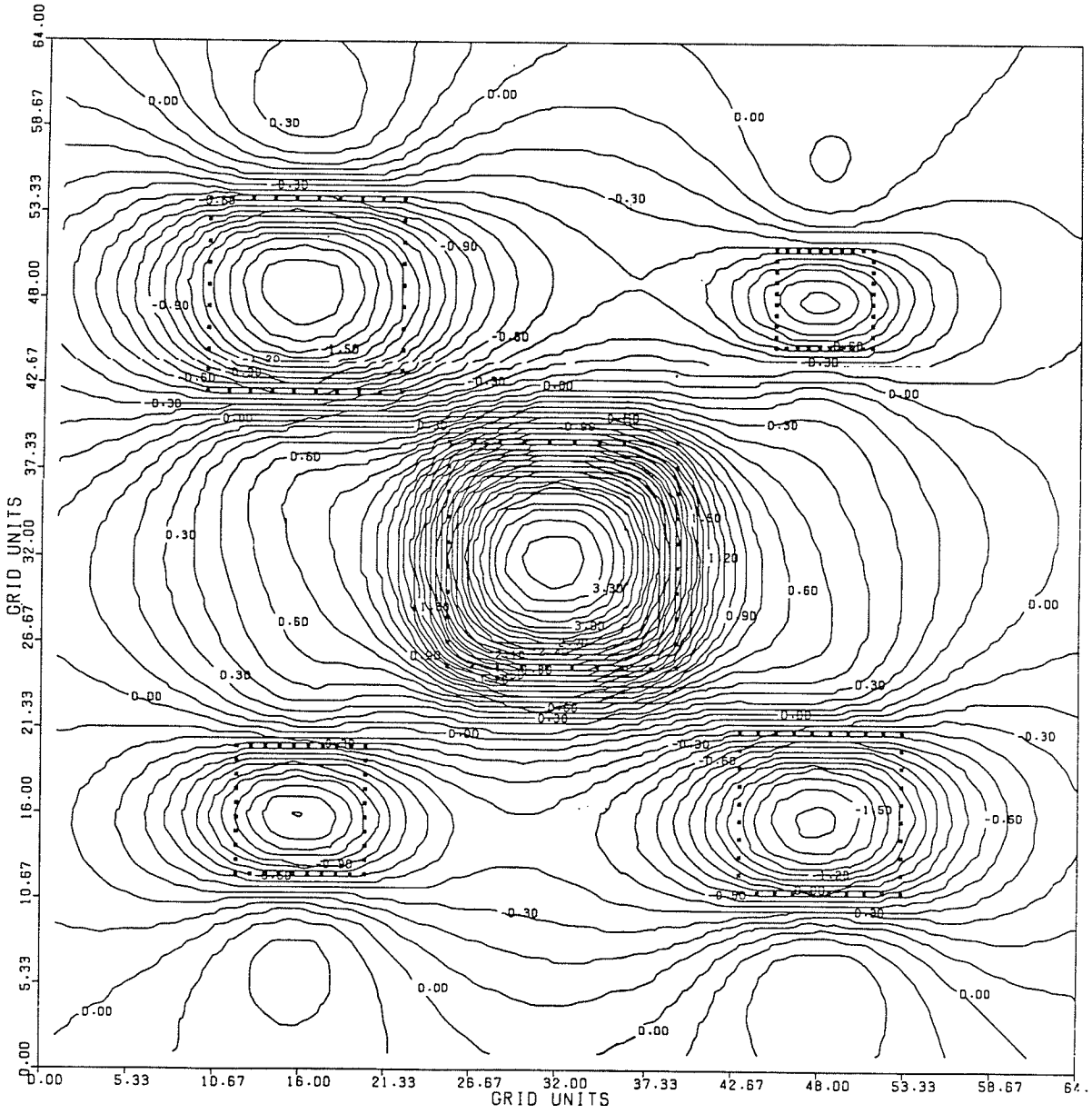


Fig. 7.11a Contour diagram of the total field due to five prismatic bodies when $I=I_0= 60^0$, $D= 0^0$, $D_0=180^0$, $h = 3$ for all the prisms ( arbitrary unit ).

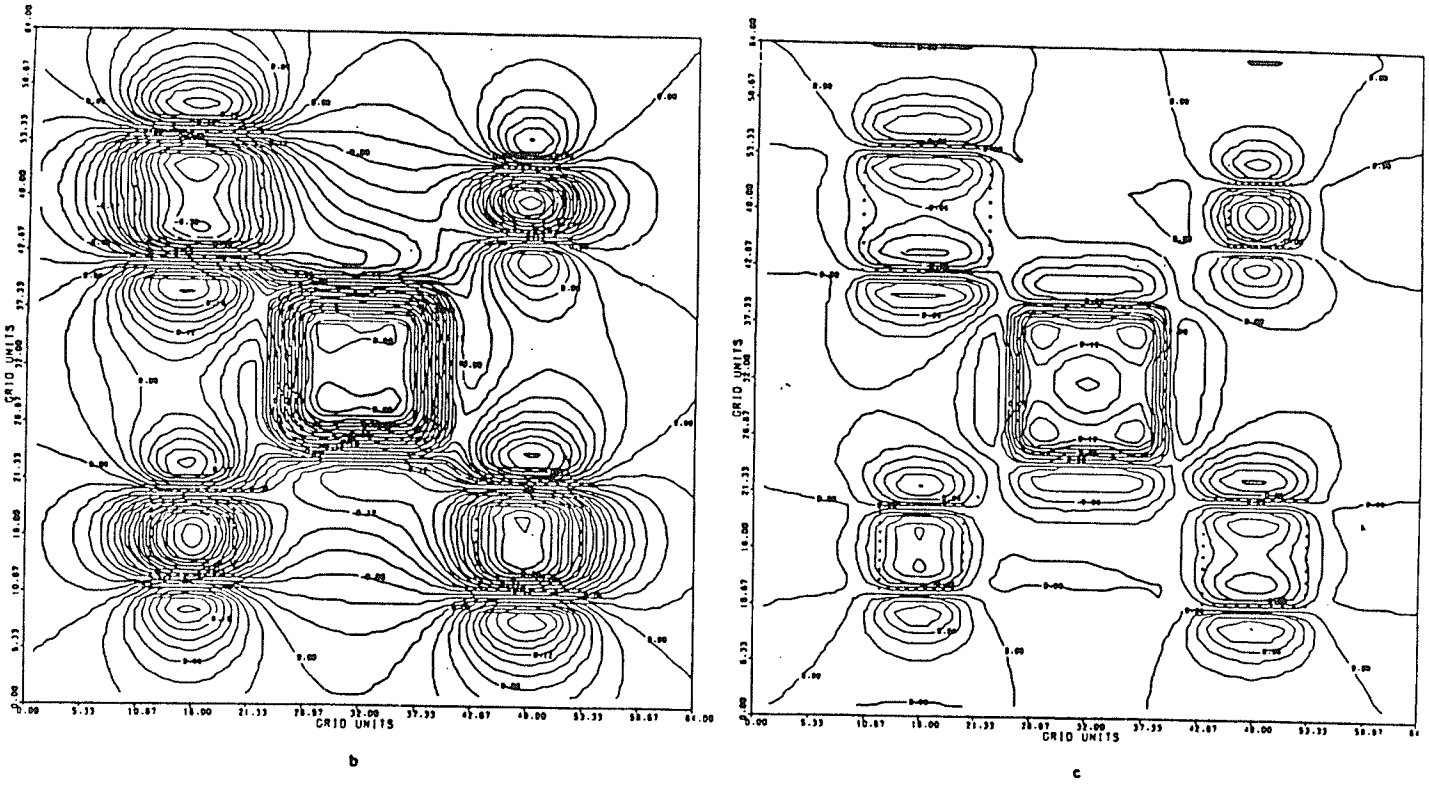


Fig. 7.11 (b) Vertical first derivative of the total field obtained by using 2-D Hilbert transform.
(c) Vertical second derivative of the total field obtained by using 2-D Hilbert transform

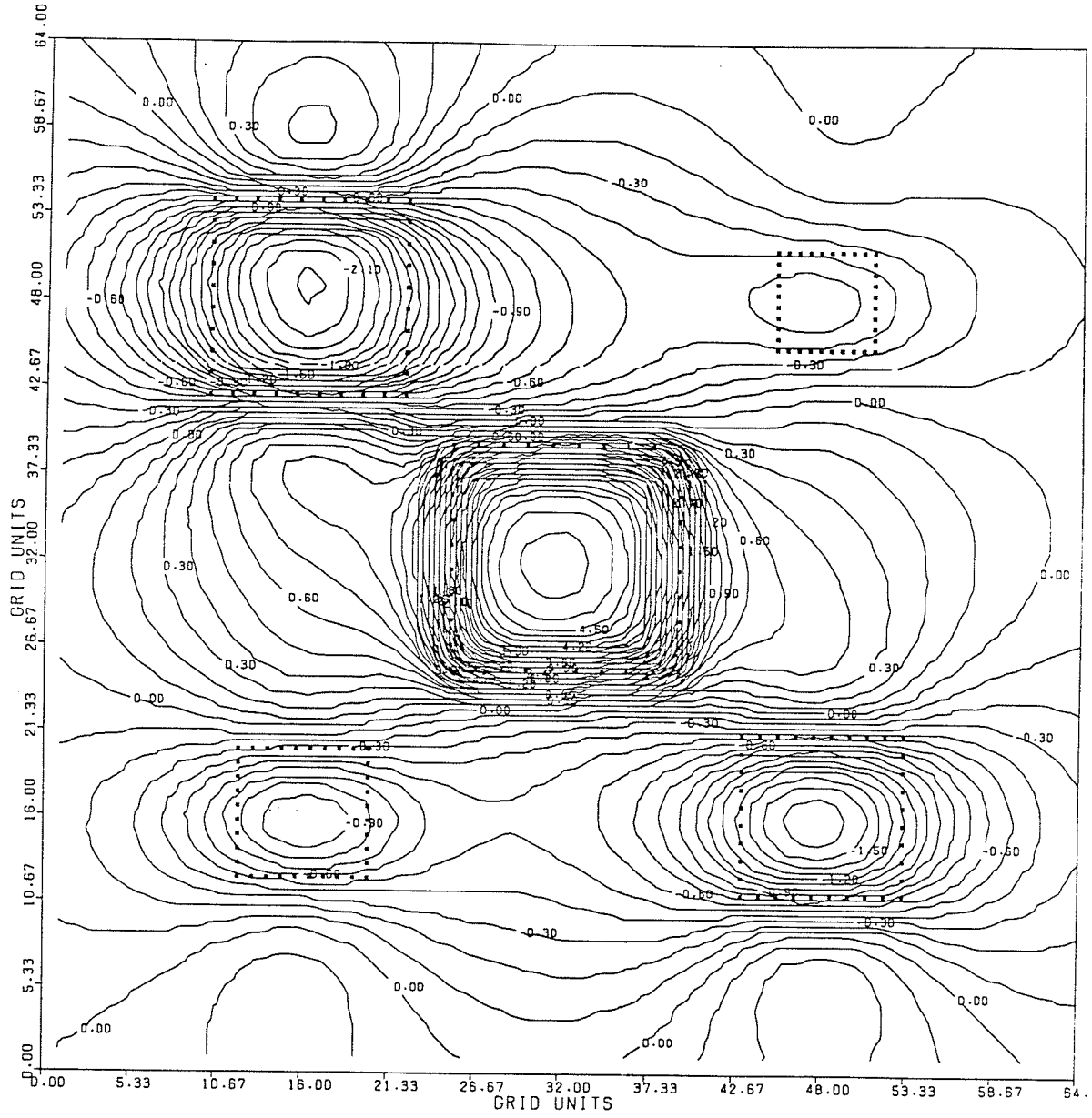


Fig. 7.12a Contour diagram of the total field due to five prismatic bodies when $I=I_0=60^0$, $D=0^0$, $D_0=180^0$, h for prism1= 1, prism2= 2, prism3= 3, prism4= 4 and prism5= 5 ( arbitrary units ).

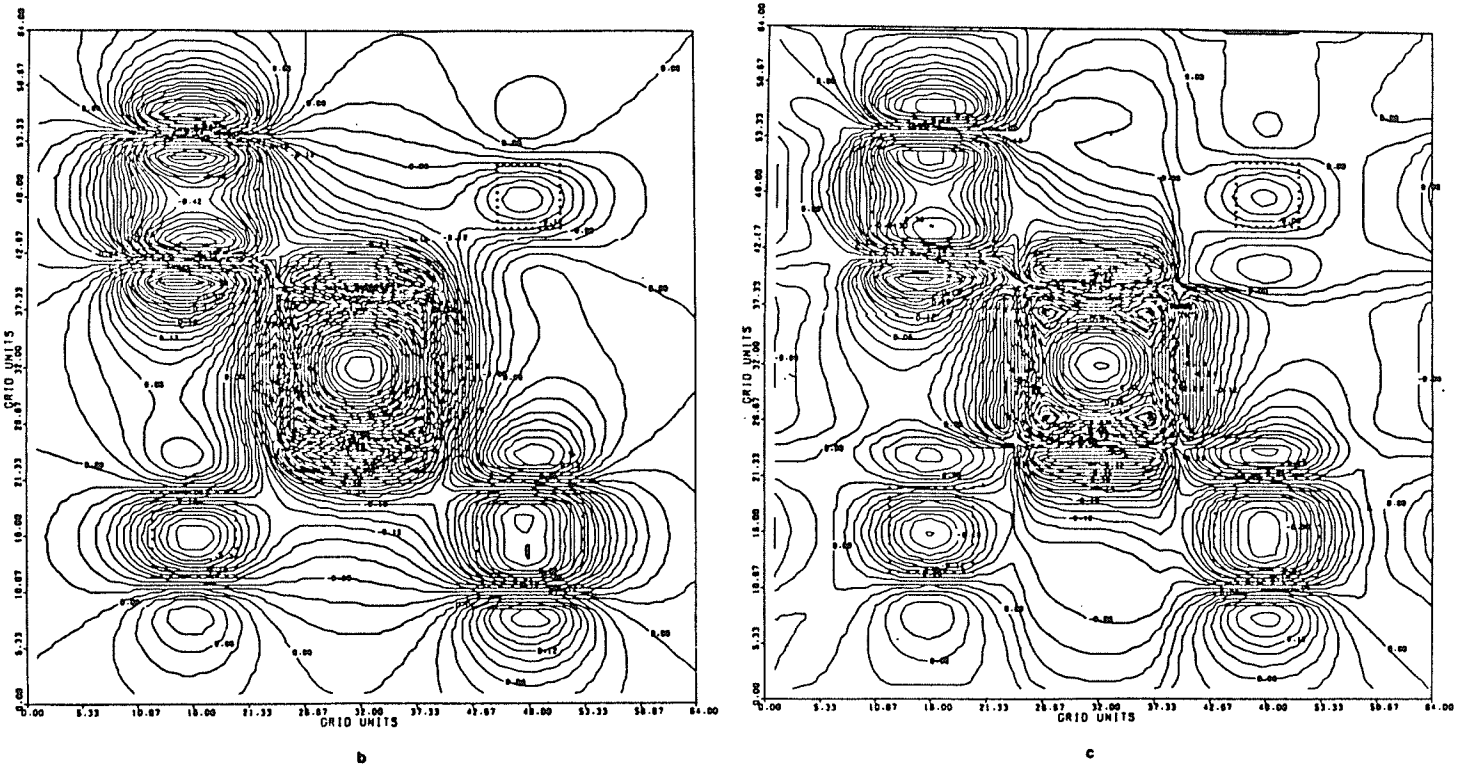


Fig. 7.12a Contour diagram of the total field due to five prismatic bodies when $I=I_0=60^0$, $D=0^0$, $D_0=180^0$, h for prism1= 1, prism2= 2, prism3= 3, prism4= 4 and prism5= 5 ( arbitrary units ).

examples, the vertical derivatives which are obtained by 2-D Hilbert transform can be used to outline each body separatly.

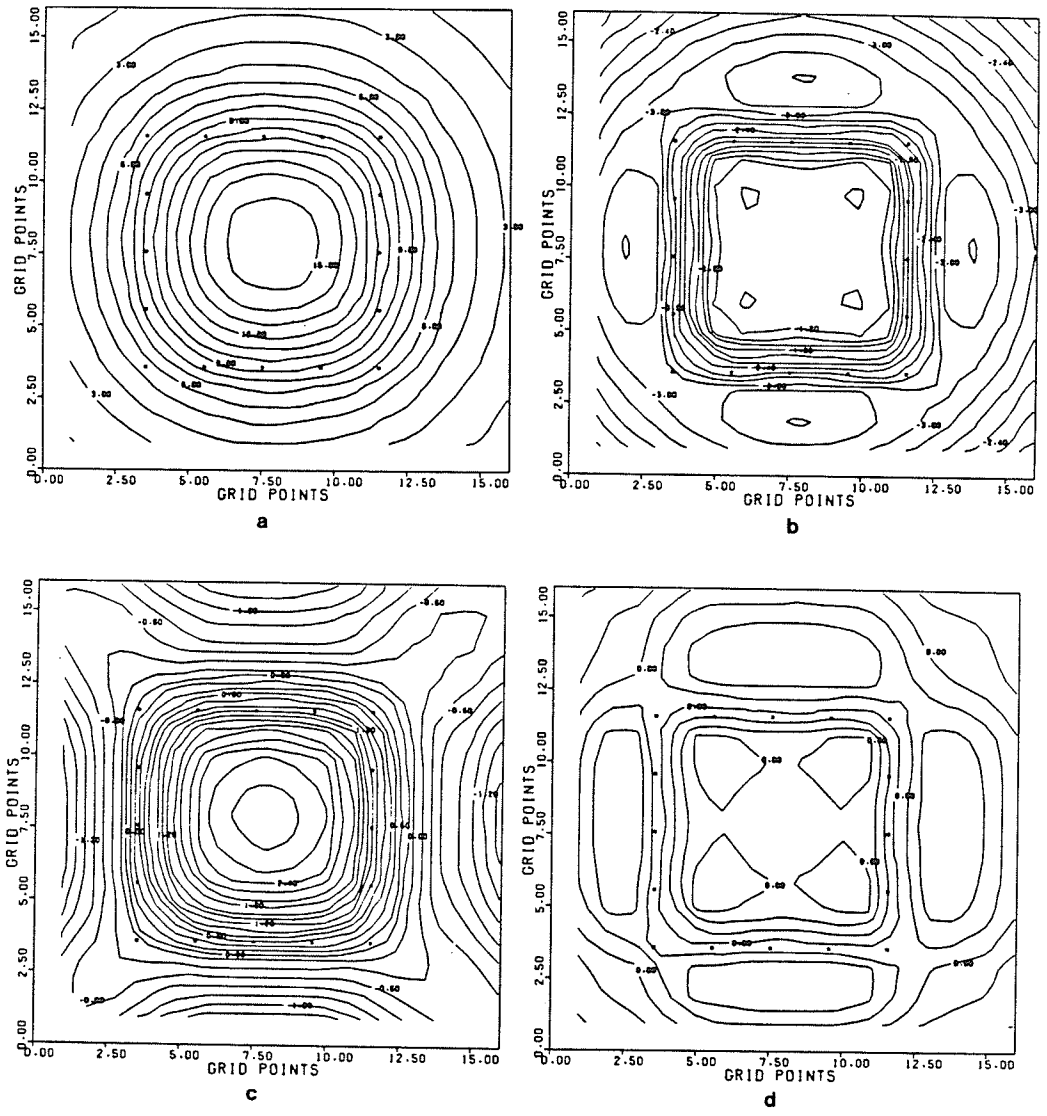


Fig. 7.13 (a) Contour diagram of the theoretical gravity effect due to Prismatic body; the field is contoured in arbitrary units, $h_1$= 1, $h_2$= 9 ( arbitrary unit ).
(b) Vertical first derivative of the gravity effect without using 2-D Hilbert transform.
(c) Vertical first derivative of the gravity effect obtained by using 2-D Hilbert transform.
(d) Vertical second derivative of the gravity effect obtained by using 2-D Hilbert transform.

## 7.4 SOME EXAMPLES OF GRAVITATIONAL ATTRACTION OF A PRISM

The anomaly of the vertical component of the attraction of a prism in Fig. 7.13a is obtained by using equation ( 6.4-9b ). The sides of the prism are assumed to be parallel to the x-and y-axis, respectively. The prism extends from -4.0 to 4.0 units in each horizontal direction( x and y ), and from 1.0 to 9 units in the z-direction.

The first and second vertical derivatives are shown in the Figs. 7.13b-d. The first vertical derivative is much smoother than the second derivative, for which reason it is recommended that the second derivative can be used in the quantitative interpretation for the boundaries of the prism. The stars in the figures denote the exact location of the prism, which is symetrical about the center of contour map.

The theory of multiprismatic bodies in gravity is simpler than the magnetic case, where equation (6.3-3) is still valid in gravity if we neglect the terms wich are related to the polarization vector and change the intensity of magnetization with gravitational constant.

Fig. 7.14a represents a contour diagram of the theoretical gravity effect due to five prismatic bodies, the field is contoured in arbitrary units, the contour interval is 1 unit. The sizes and centers of the prisms are the same as given in Fig. 7.10, the depth to the top of all the prisms in this model is equal 2 units below the surface of the

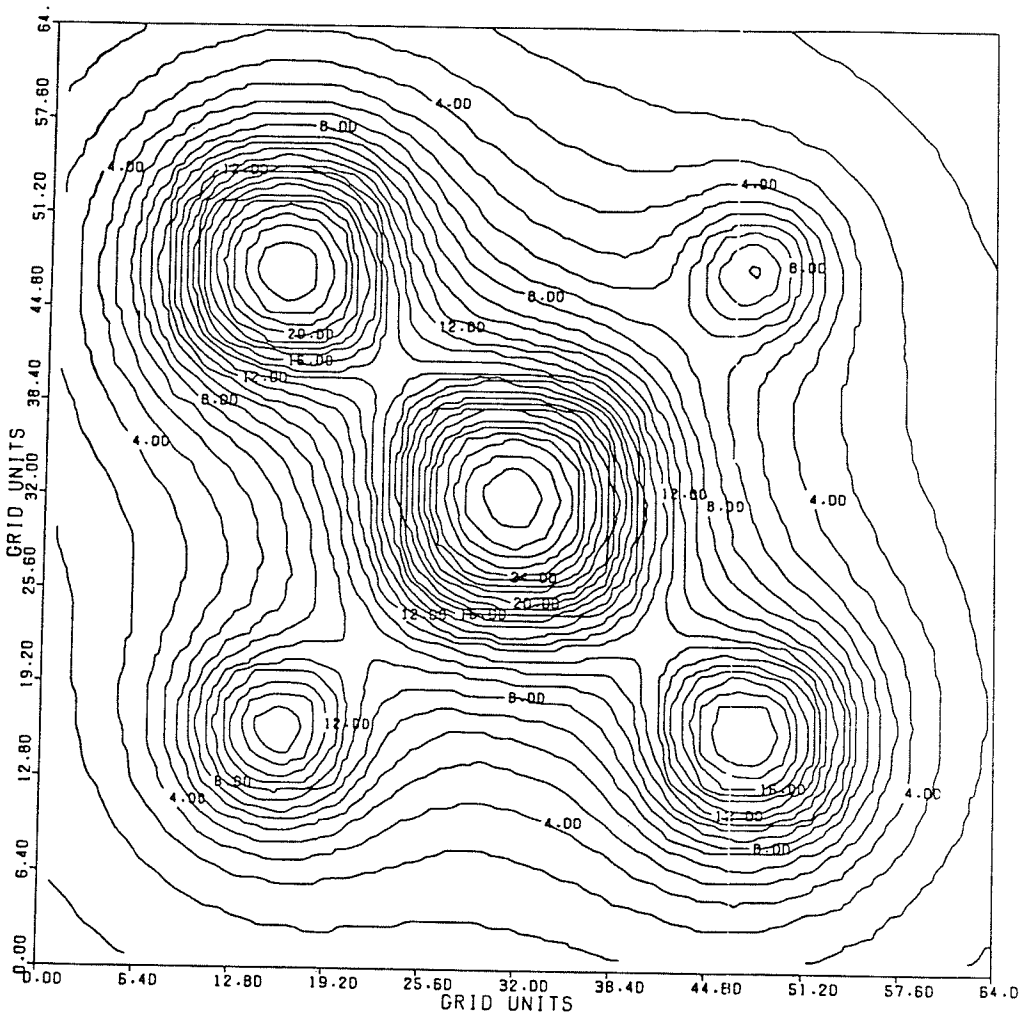


Fig. 7.14a Contour diagram of the theoretical gravity effect due to five prismatic bodies, the field is is contoured in arbitrary units. $h_1$= 2.0 for all the prisms.

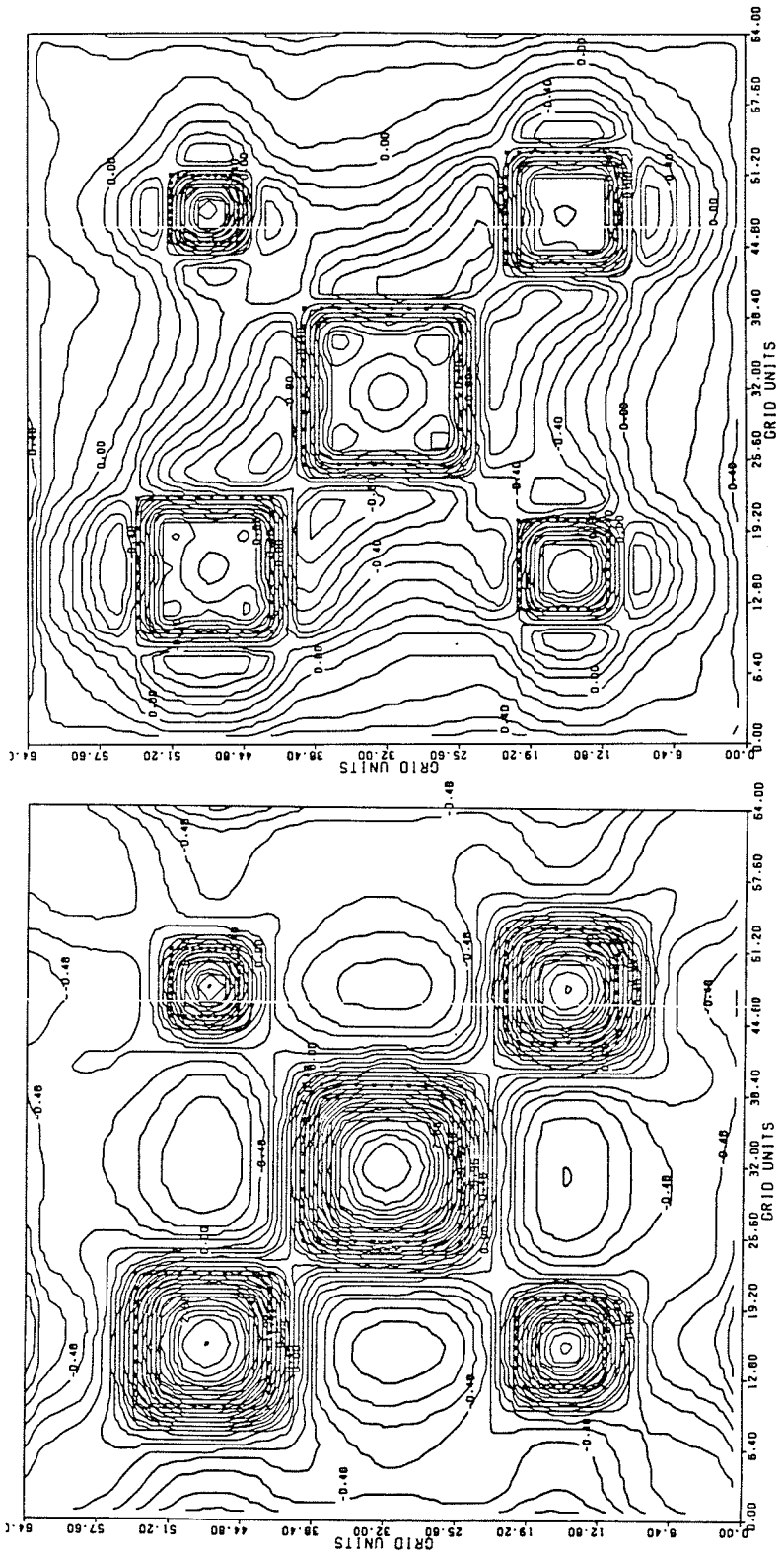


Fig. 7.14 (b) Vertical first derivative of the gravity effect obtained by using 2-D Hilbert transform.
(c) Vertical second derivative of the total field obtained by using 2-D Hilbert transform.

observation. Figs. 7.14b-c represent first and second vertical derivatives which obtained by using 2-D Hilbert transform, from these figures the boundaries of the prisms in the model are very clear and easily can be determined from the second vertical derivative ( Fig.7.14c ).

Several examples are tested by increasing the depths of all the prisms upto 8 units. Also we gave another example where the depths are not same for each prism. Some of these examples are presented in Figs.7.15a-c and 7.16a-c, from which experiments one can say the techniques of using 2-D Hilbert transform in multiprismatic bodies in gravity are not only valid to outline the vertical projection of the shallow subsurface bodies, but also can be used at various depths.

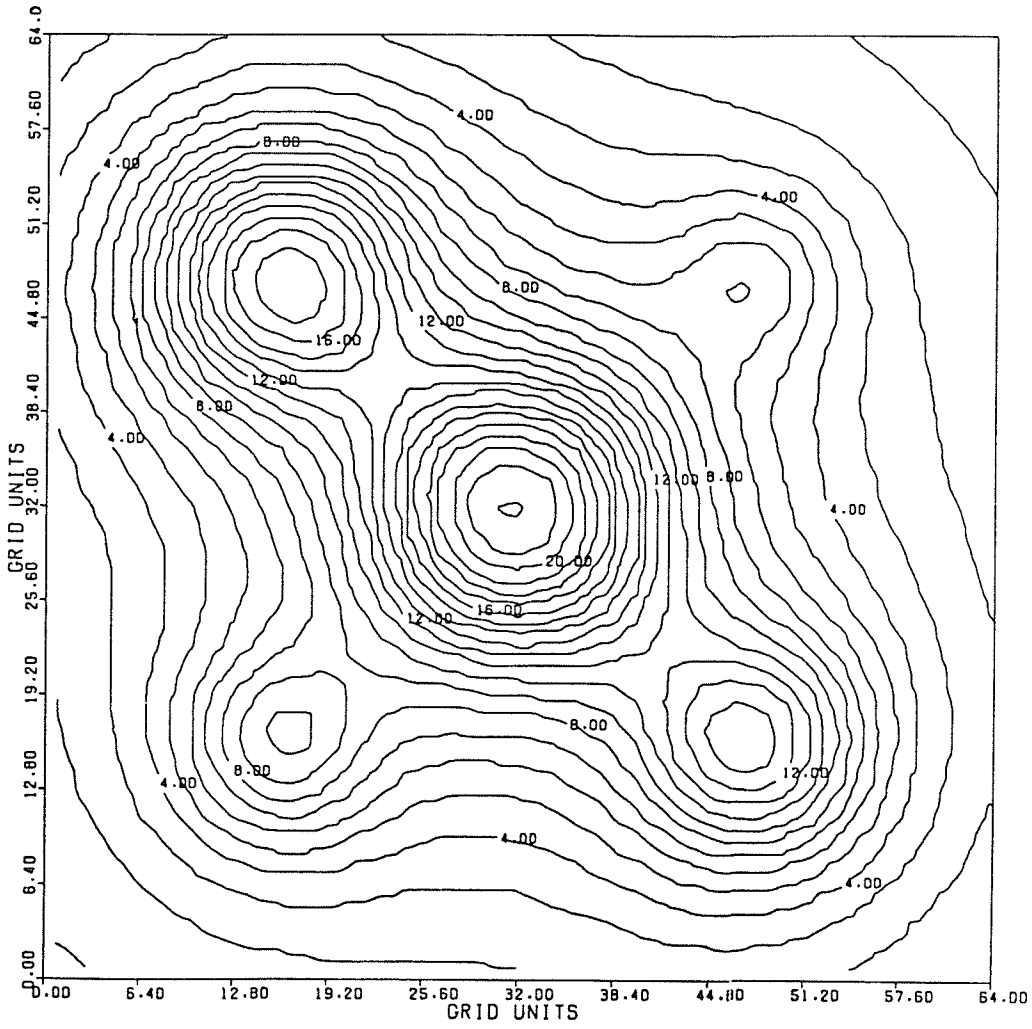


Fig. 7.15a Contour diagram of the theoretical gravity effect due to five prismatic bodies, the field is is contoured in arbitrary units. $h_1$= 4.0 for all the prisms.

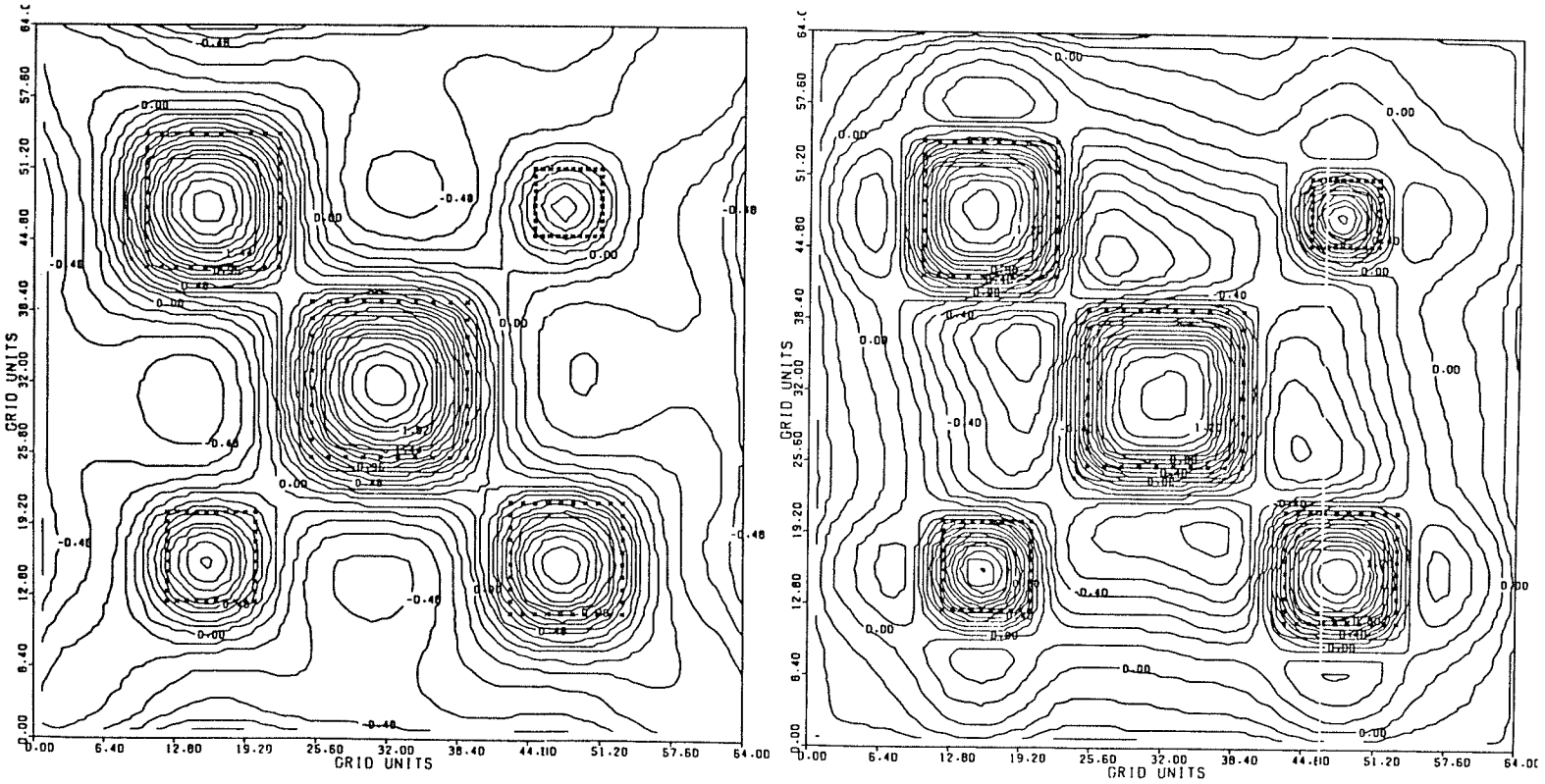


Fig. 7.15 (b) Vertical first derivative of the gravity effect obtained by using 2-D Hilbert transform.
(c) Vertical second derivative of the total field obtained by using 2-D Hilbert transform.

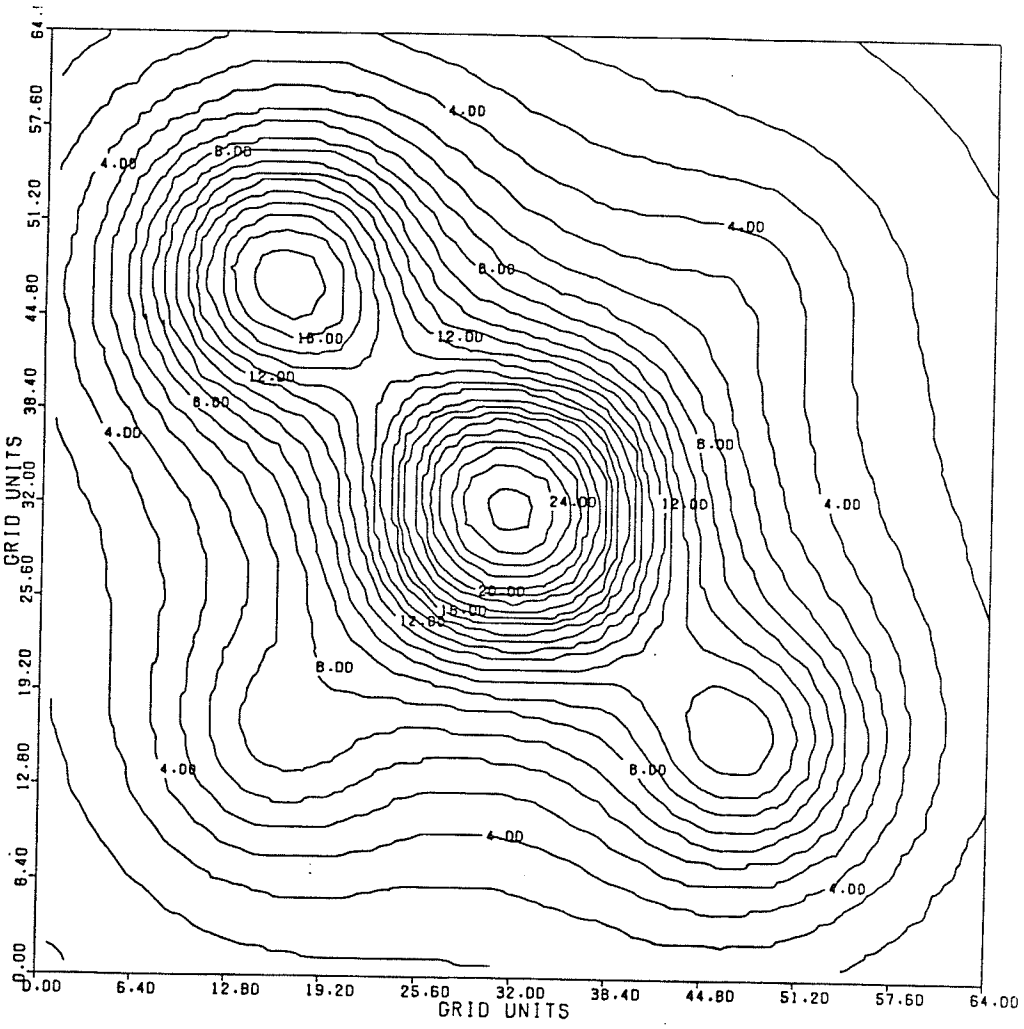


Fig. 7.16a Contour diagram of the theoretical gravity effect due to five prismatic bodies, the field is is contoured in arbitrary units. for prism1 $h_1$= 3 , prism2 $h_1$= 4, prism3 $h_1$= 5, prism4 $h_1$=6 and prism5 $h_1$= 7 ( arbitrary unit ).

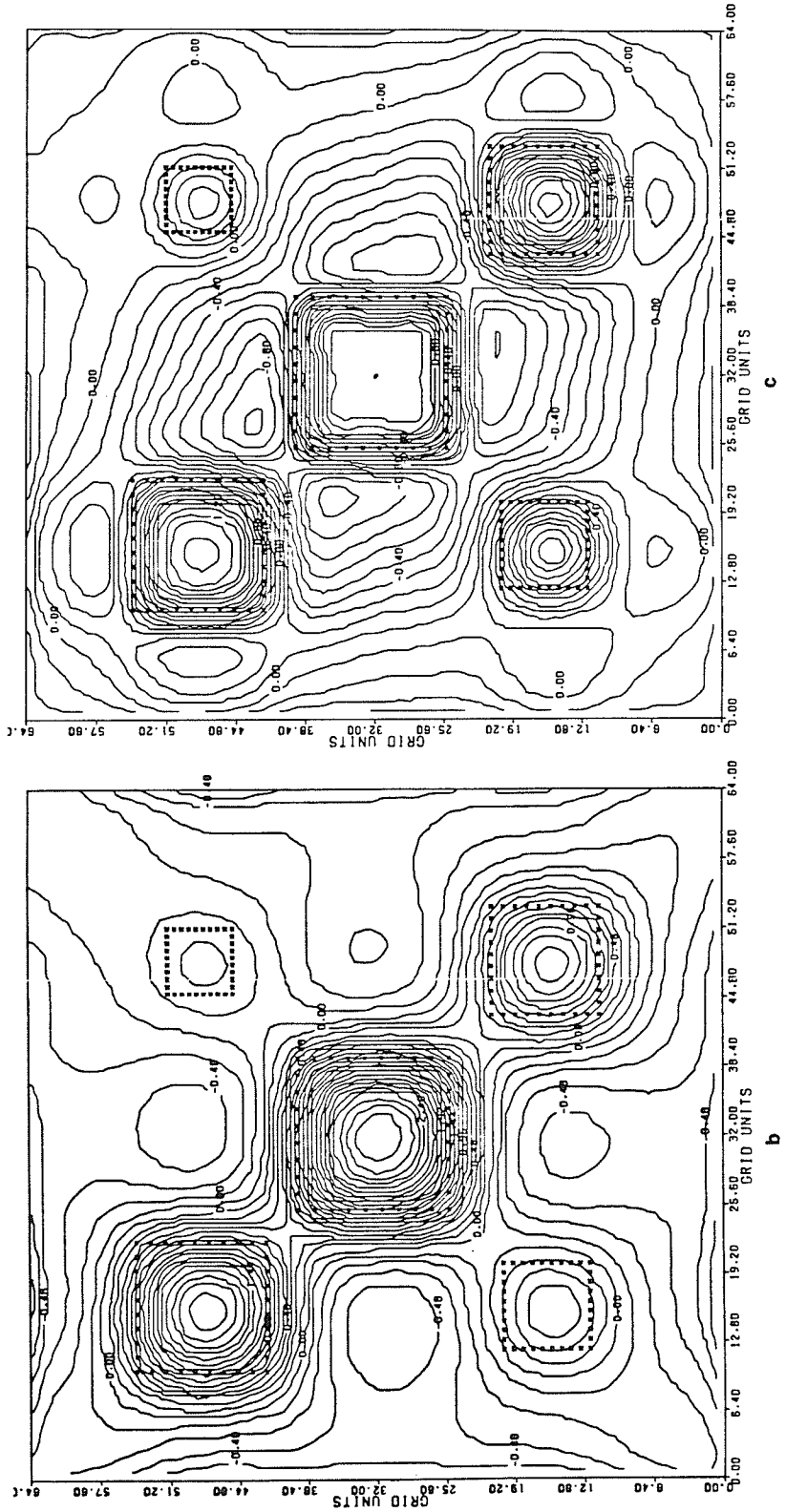


Fig. 7.16 (b) Vertical first derivative of the gravity effect obtained by using 2-D Hilbert transform.
(c) Vertical second derivative of the total field obtained by using 2-D Hilbert transform.

## 7.5 GRAVITY ANOMALY DATA OF THE SUDBURY BASIN

The Sudbury basin located in a unique geological setting near the junction of the Superior, Southern and Grenville Structural provinces of the Canadian Shield . It is located also at the junction of two regional fault systems.

According to the stratigraphic studies of the Huronian rocks outside the basin indicate that the area now occupied by the Sudbury structure was a positive element which influnced Huronian deposition. Paleocurrents in the Chelmsford Formation of the Whitewater Group inside the basin trend southwest parallel to the long axis of the basin, suggesting that the elliptical basin shape was established at an early stage atop the major domal structure.

The deflection of paleocurrent trends and important facies change in the lower Huronian formations reflect a positive element in the Sudbury area and suggest that it was a center of "eugeosynclinal" volcanic activity. Paleocurrent data suggest that the Chelmsford Formation was deposited in a basin which had a north easterly trending axis and a southwest paleoslope. The structural data indicate that the depositional basin was less elliptical than the present basin and the axis of that basin was probably rectilinear and located somewhat southeast of the acute axis of the present basin.

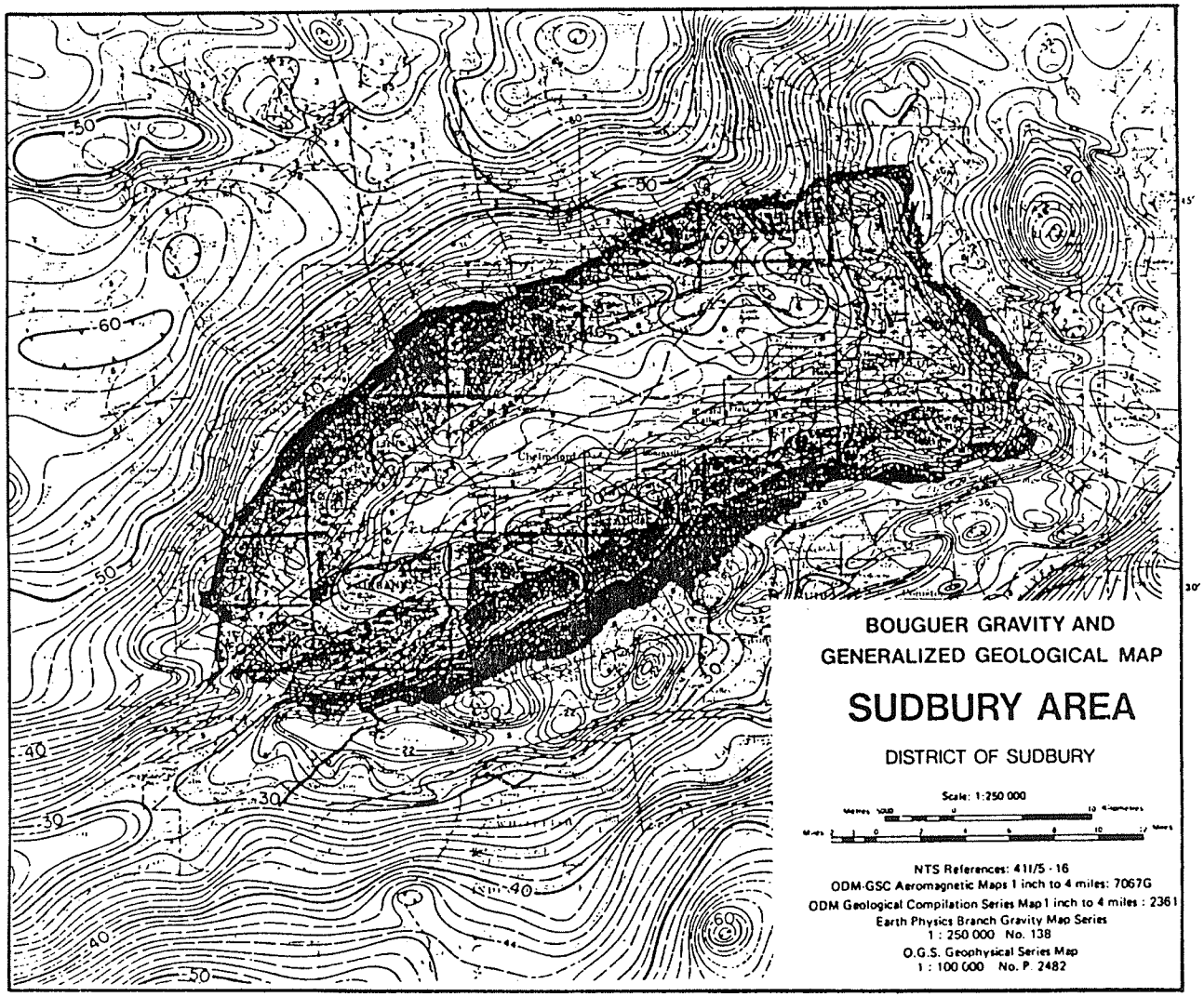


Fig. 7.17 The Bouguer gravity anomalies of the Sudbury area ( orignal map ).

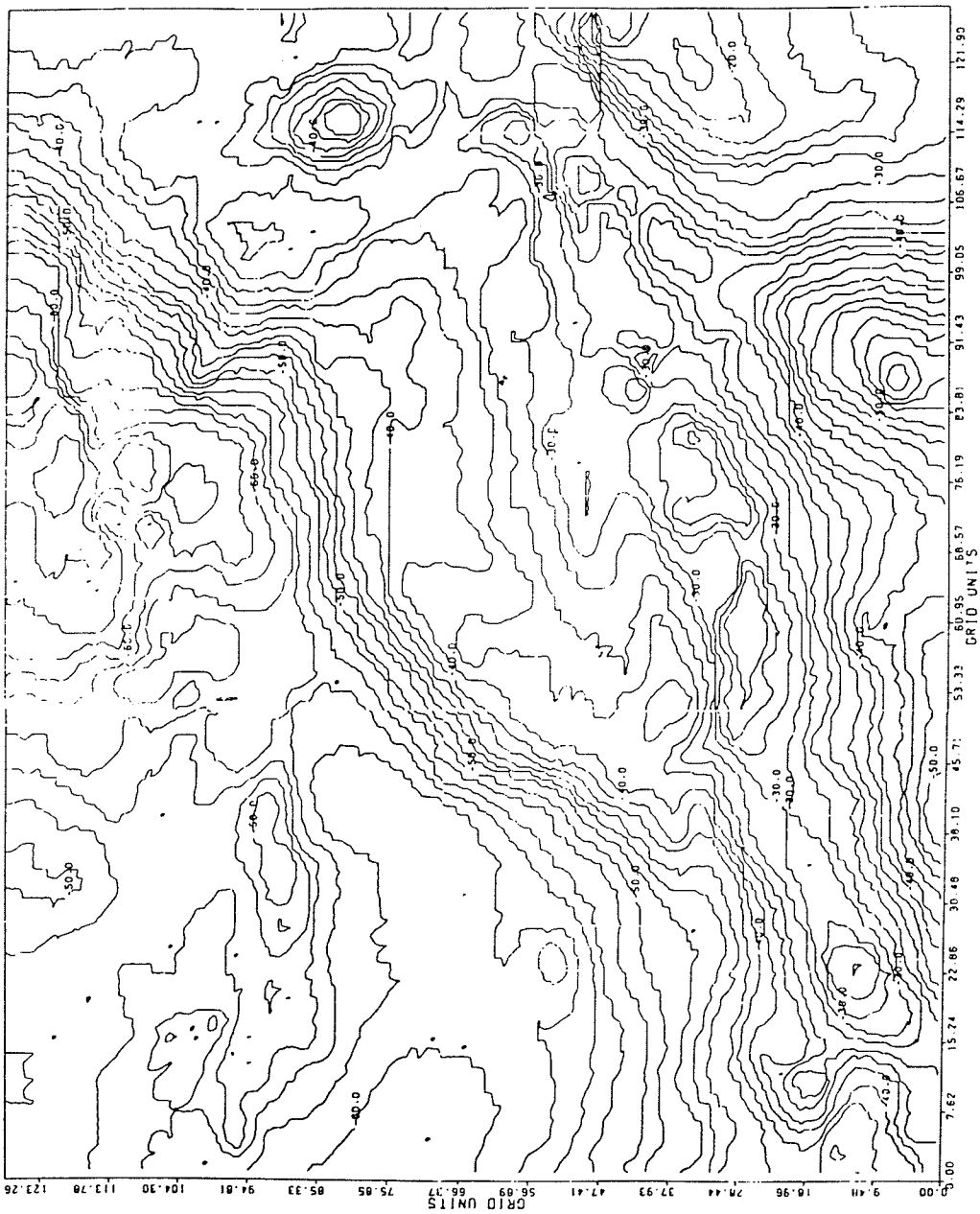


Fig. 7.18 The Bouguer gravity anomalies of the Sudbury area is digitized to 128 by 128 grid units from the orignal map ( Fig. 7.17 ). The contour interval is 2mgal.

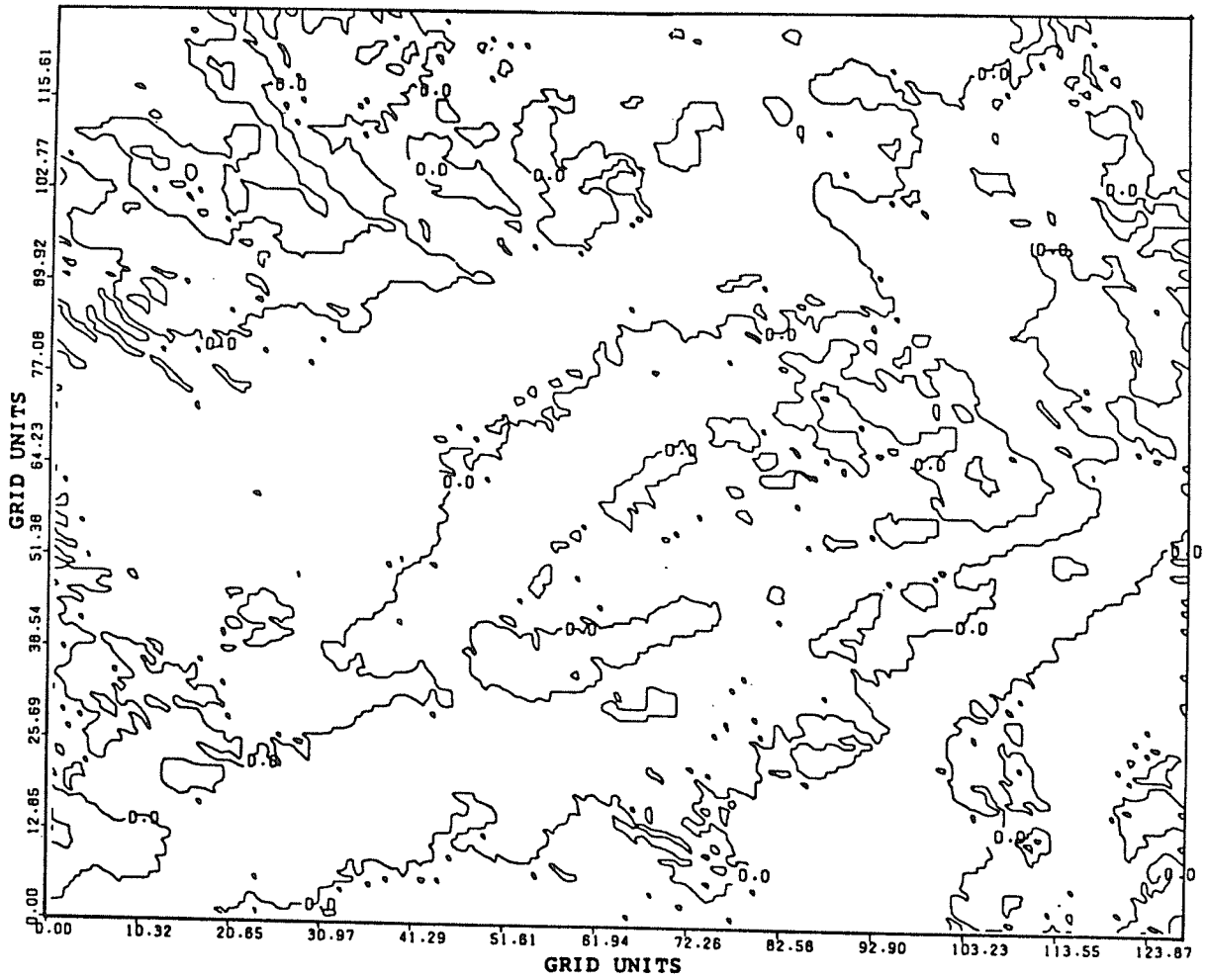


Fig. 7.19 The zero contoured values of the vertical gravity derivative of Fig. 7.18.

In general, the gravity anomaly reflects actual density distribution of rocks where the average density for the Sudbury area is about 2.77 g/cc, and hence its geological interpretation can, under favourable circumstances, contribute to investigation of the present state of geological structure.

The method of using the 2-D Hilbert transform of horizontal derivative of the Bouguer gravity anomaly ( Figs. 7.17, 7.18 ) has proved to be useful for gradual separation of the local gravity features. The "zero contour" in Fig.( 7.19 ) separates the positive and negative vertical gradient, where the positive anomalies believed to be caused by the norite, and other mafic magmatic and metamorphic rocks.

The zero contour map in Fig. 7.19 represents the vertical derivative of Fig. 7.18. The horizontal derivatives are computed by the 2-D central difference method. The zero contour lines closely identify some of the geological boundaries of the basin.

## 7.6 MAGNETIC ANOMALY DATA OF THE SUDBURY BASIN

The magnetic data on the digitized map ( Fig. 7.20a ) were compiled from information recorded along the flight lines. The anomalies expressed by the magnetic contours are dependent on the variable magnetic intensities of the underlying rocks, and may be due to conditions near, or at unknown depths below the surface. High magnetic anomalies normally indicate the presence of basic rocks, such as diabase gabbro, or serpentinite, which have a relatively high iron content, but in special instances may be due, or partly due, to concentrations of magnetic minerals. By means of the magnetic anomalies, various rock bodies or structural features, such as faults or folds, may be traced into, or across, areas of few or no outcrops.

A positive regional magnetic anomaly of the digitized map ( Fig. 7.20a ) occupies the western part of the Sudbury structure with the maximum in the northwest. The intense local anomalies corresponding to the South Range norite have nearly disappeared. This indicates that the South Range norite is probably separated at depth from the main magnetic mass which underlies the northwestern part of the structure. It extends as far south as the Fairbank Lake fault and is controlled by the Sandcherry Greek fault to the east.

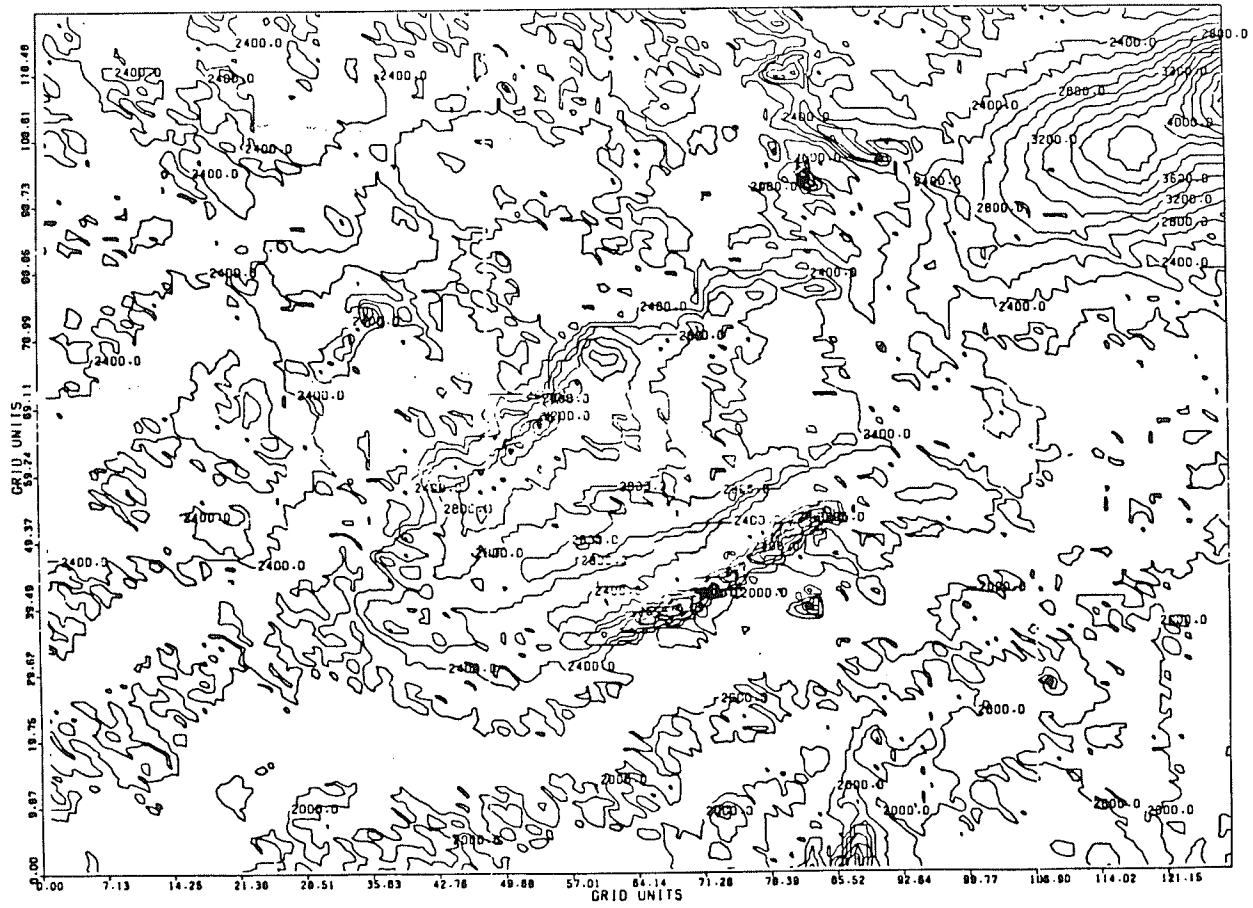


Fig. 7.20a The magnetic anomalies map of the Sudbury area is digitized to 128 by 128 grid units from the orignal maps. The contour interval is 200γ.

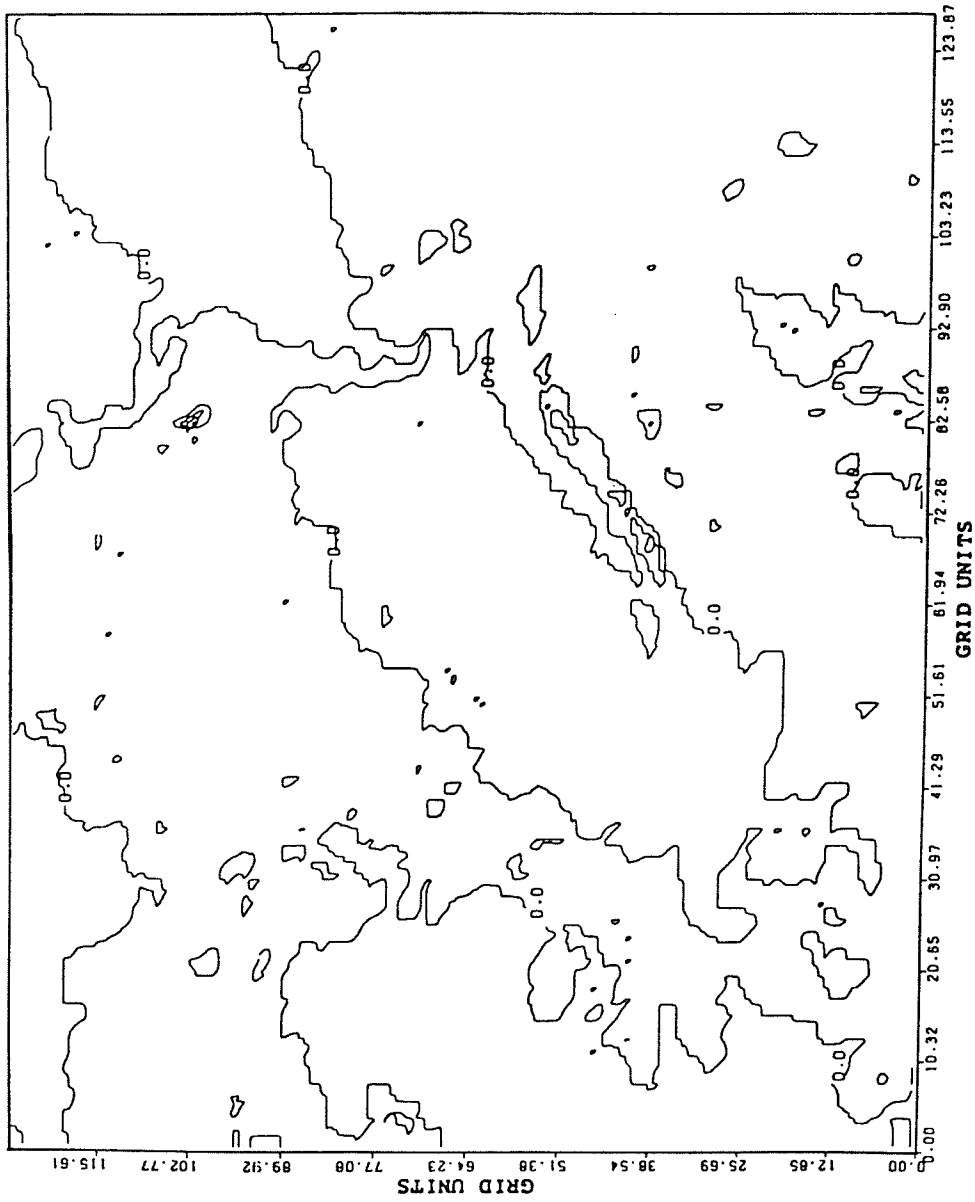


Fig. 7.20b The zero contoured values of the vertical magnetic derivative of Fig. 7.20a

The application of using 2-D Hilbert transform in quantitative interpretation of magnetic data in Sudbury can be considered as additional source of Geophysical information in that area. The vertical derivative of the digitized map ( Fig. 7.20b ) is obtained by using 2-D Hilbert transform techniques, the main zero contour line approximately outlines the real boundary of the Sudbury basin. The combined interpretation of the vertical derivative of gravity and magnetic maps provides important information for detailed studies of the Sudbury structure. The norite of the Sudbury Irruptive is characterized mostly by positive anomalies. The variations of both the gravity and the magnetic anomalies are remarkably similar and indicate that the norite is not a single homogeneous unit.

## 7.7 2-D HILBERT TRANSFORM AND HORIZONTAL DERIVATIVES

As we know from previous sections, the Hilbert transform can be very successfully used to find the vertical derivative from horizontal derivatives. In this section I want to reverse the process, i.e. I want to experiment and estimate the horizontal derivatives from the first vertical derivative by using the 2-D Hilbert transform techniques.

Figs. 7.21 and 7.22 represent the contour diagrams of horizontal derivative of the magnetic field and the gravity effect, respectively, due to a prismatic body. These are obtained numerically by using the 2-D central difference meth-

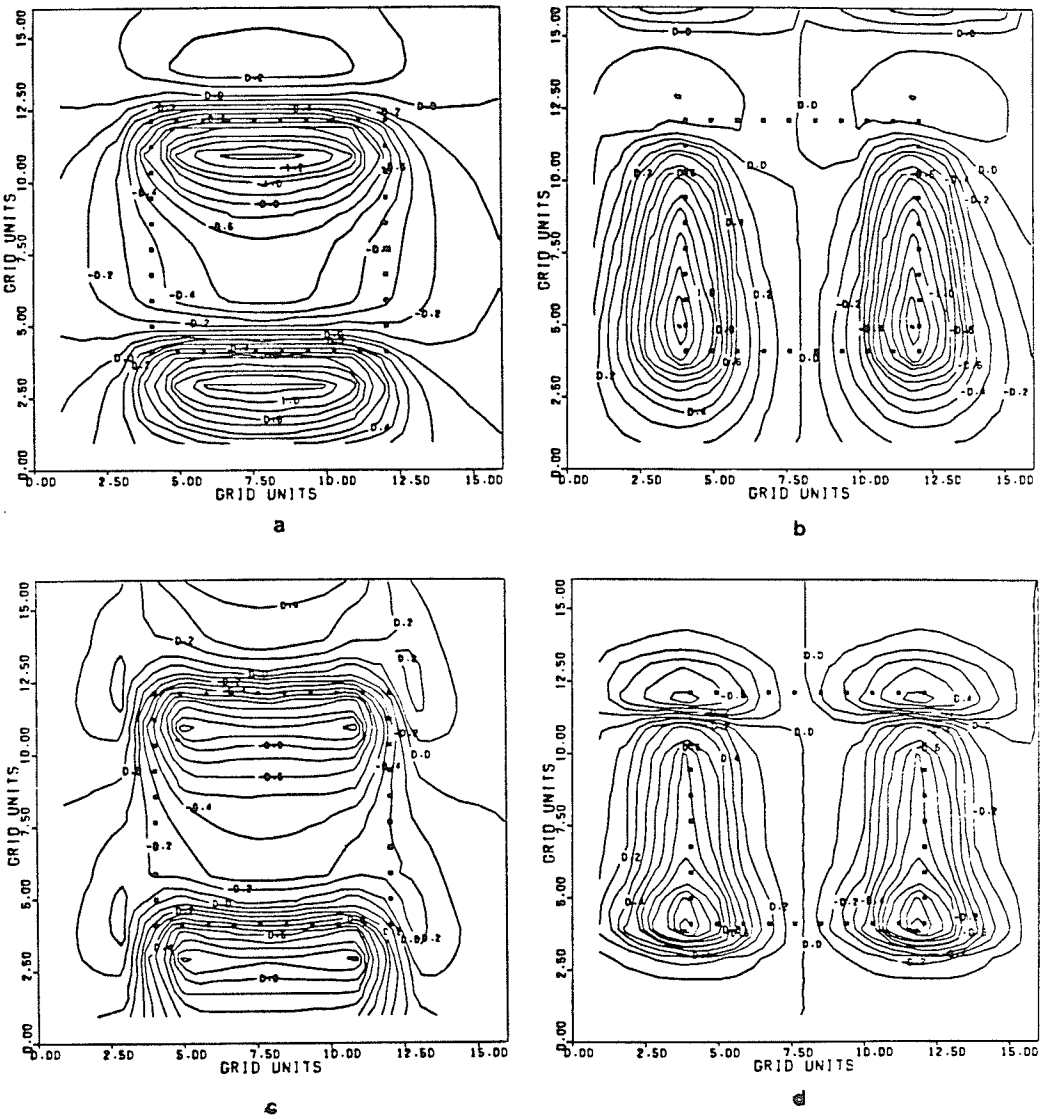


Fig. 7.21 Contour diagram of the horizontal derivatives of the total field when; $D=D_0= 0^0$, $I=I_0= 60^0$, and $h= 1$ unit.
(a) and (b) represent the horizontal derivatives with respect to x and y, respectively, obtained from the total field by using 2-D central difference formula.
(c) and (d) represent the horizontal derivatives with respect to x and y, respectively, obtained from the vertical derivative of the total field by using 2-D Hilbert transform.

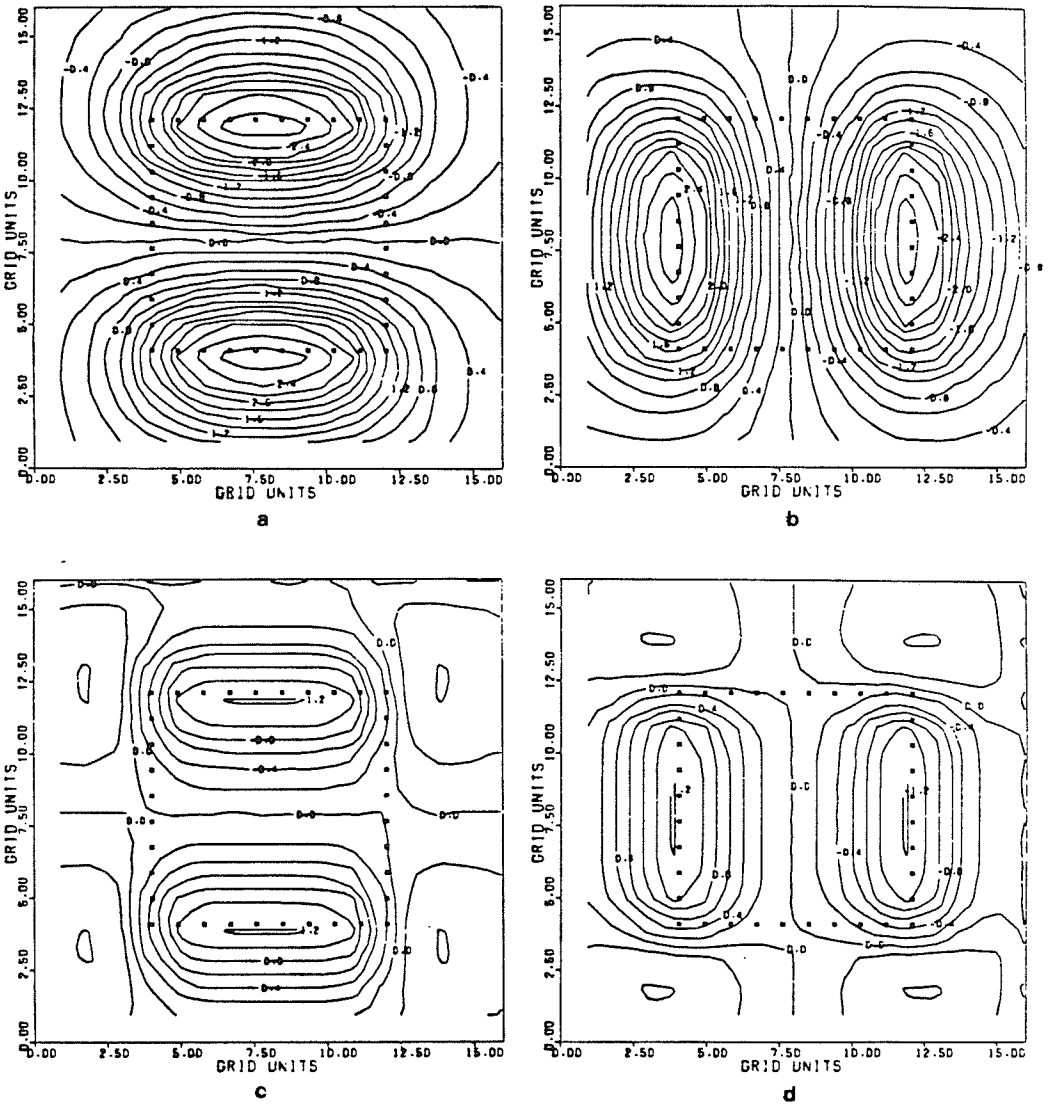


Fig. 7.22 Contour digram of the horizontal derivatives of the theoretical gravity effect due to prismatic body; $h_1$ = 1, and $h_2$ = 9 ( arbitrary units ).
(a) and (b) represent the horizontal derivatives with respect to x and y, respectively, obtained from the total field by using 2-D central difference formula.
(c) and (d) represent the horizontal derivatives with respect to x and y, respectively, obtained from the vertical derivative of the total field by using 2-D Hilbert transform.

od and the 2-D discrete Hilbert transform. In Figs. 7.21a-b and 7.22a-b, the horizontal derivatives with respect to x and y, respectively, are obtained directly from the expression of the field formula by using the 2-D central difference formula. Figs. 7.21c-d and 7.22c-d are obtained by applying the 2-D Hilbert transform on the vertical derivative of the field formula.

In quantitative interpretation of magnetic and gravity field data, the horizontal derivative with respect to x is used to locate the two sides of the prism which are parallel to the X-axis. The horizontal derivative with respect to y can be used to locate the other two sides which are parallel to the Y -axis. It is however apparent that we need further improvement and testing for the application 2-D horizontal derivatives.

## 7.8 SOME GENERAL COMMENTS

In all the contour diagrams presented in this chapter, the prisms have been taken to be rectangular with equal sides. Some figures show that, whether a side of the prism increases or decreases in length, the shape of the anomaly bulges out or shrinks in the direction of the same side. However there is no consistent relationship between the physical dimensions of the prism and the shape of the magnetic anomaly mainly due to independent multiple parameters. As the depth to the top of a body increases, the first and second vertical derivatives become much smoother as expected.

In this chapter I have not presented the second vertical derivative with direct method ( without using 2-D Hilbert transform ), because an example of the direct method already was given in reference 4.

# CHAPTER 8

## CONCLUSION

The Hilbert transform can be defined in different ways, and through different mathematical relations, but essentially it is a quadrature filter which introduces a $90^0$ phase shift. The real and imaginary components of a complex function, or the even and odd parts of a real function, are related through the Hilbert transform relationships. The integral equations of the transform are reviewed in this thesis as a first step towards, the application discrete Hilbert transform relations.

The 1-D Hilbert transform has many applications in Geophysics, especially in seismology, gravity and magnetics. From the relations discussed in this thesis, I have found that the Blackman window provides an optimum result in the design of a 1-D digital Hilbert transform.

In the field of magnetics, the 1-D Hilbert transform was tested with several examples for interpreting vertical anomalies of sheet structures( finite and infinite depth extent ), dikes, and horizontal circular cylinders. The problem arising in the Mohan's ( 1982 ) approach, for a polarization angle $Q=45^0$ was also resolved. In addition, the Green ( 1976 ) and Izzeldin ( 1983 ) methods were examined with different examples such as a dipping fault, a semi-infinte

dike, and a horizontal cylinder. Given the same examples, the first method (Mohan) appears to give less reliable solutions, especially when the discrete Hilbert transform is used instead of the continuous Hilbert transform. In general the first method appears to be less accurate than the second one. However, each geophysical potential field problem should be studied independently for the best result.

Application of the Hilbert transform to find the complex envelope of real seismic signal can give more insight into the composition of a time series signal than is apparent in the original form. One of the major advantages becomes obvious when the amplitude envelope and phase can be separated from the complex envelope. This type of information is very useful in seismic signal analysis and deserves further attention.

The extension of the 1-D Hilbert transform to the 2-D case may be achieved in several ways. The usefulness of the 2-D Hilbert transform ranges from seismic problems such as 2-D recursive filters and stability problems and 2-D minimum phase, to the theory of horizontal and vertical derivatives of 3-D potential field functions. The first and second vertical derivatives caused by prismatic and multiprismatic bodies with arbitrary magnetic polarization can be obtained either directly or by using 2-D Hilbert transform techniques. The same procedure can be extended to gravity data in determining the first and second vertical derivatives.

Unlike the magnetic anomaly patterns, which are functions of declination, inclination, and inducing remanence magnetization, the gravity anomaly patterns are much simpler. The major contributing factor in each gravity anomaly is density contrast. For this reason, the vertical second derivative of a gravity anomaly closely outlines the surface geological boundaries. In processing of the field data ( digital gravity and magnetic maps of the Sudbury area ), the technique of using the 2-D Hilbert transform has proved to be very fast and effective in separating the local gravity and magnetic features.

The 2-D Hilbert transform process can also be reversed to estimate the horizontal derivatives from the vertical derivative. The vertical and horizontal derivatives can be used in quantitative interpretation and/or in detection of the vertical projection of the subsurface bodies.

## BIBLIOGRAPHY


1. Bhattacharyya B.K.1980. A generalized multibody model for inversion of magnetic anomalies. Geophysics, Vol. 45, No. 2, 255-270.

2. Bhattacharyya, B.,K. and M. E. Navolio, 1975. Digital convolution for computing gravity and magnetic anomalies due to arbitrary bodies Geophysics, Vol. 40, No. 6, 981-922.

3. Bhattacharyya B.K. 1965. Two-dimensional harmonic analysis as a tool for magnetic interpretation. Geophysics, Vol.XXX, No. 5, 829-57.

4. Bhattacharya B.K. 1964. Magnetic anomalies due to Prism-shaped bodies with arbitrary polarization. Geophysics, Vol.XXIX, No. 4, 517-531.

5. Blackman, R.B., and Tukey, J.W. 1959 The Measurment of Power Spectra. Dover Publications, New York , 190.

6. Bracewell, 1965. The Fourier transform and its applications. McGraw-Hill Book Co., New York, 268-271.

7. Bose N.K. and Prabhu K.A. 1979. Two-Dimensional Discrete Hilbert transform and computational complexity aspects in its Implementation. IEEE Transactions on Acoutics, Speech, and Signal Processing, Vol. Assp-27, No.4., 356-360.

8. Cain G.D. 1972. Hilbert transform description of linear filtering. Electronics Letters, Vol. 8, No. 15, 380-382.

9. Cizek V. 1970. Discrete Hilbert transform. IEEE Trans. on Audio and Electroacoustics, V. AU-18, 340-343.

10. Claerbout Jon F. 1976. Fundamentals of Geophysical Data Processing with applications to petroleum prospecting McGraw-Hill, Book Company, New York.

11. Gerald C.F. 1980. Applied Numerical Analysis. California Polytechnic State University San Luis Obispo, Addison-Wesley publishing Company.

12. Farnbach John S. 1975. The complex envelope in seismic signal analysis. Bulletin of Seismological Society of America, Vol. 65, No. 4, 951-962.

13. Gabor D. 1968. Theory of Communic. J. Inst. Elect. Eng.93, Part 1, 429-441.

14. Gold B. and Rader C.' 1969. Digital Processing of signals. New York, Mc Graw-Hill Book Co., Inc..

15. Goodacre A.K. 1973. Some comments on the calculation of the gravitational and magnetic attraction of a homogeneous Rectangular Prism. Geophysical Prospecting, Vol. 21, 66-69.

16. Grant F. S. and West G.F. 1965. Interpretation theory in applied Geophysics. New York: Mc Graw-Hill Book Company.

17. Green R. and Stanley J. M. 1975. Application of Hilbert transform method to the interpretation of surface-vehicle magnetic data. Geophysical Prospecting, Vol. 23, 18-27.

18. Gupta V., Grant F.S. and Card K.D. 1984. Gravity and Magnetic characteristics of the Sudbury structure, the Geology and Ore Deposits of the Sudbury structure. Ontario Geological Survey Special Volume # 1, 381-410.

19. Guy-Bray J.V. 1972. New developments in Sudbury Geology, special paper No. 10.

20. Hamid N. Al-Sadi, 1982. Seismic Exploration Iraq National Oil Company.

21. Huag T. S. 1981. Topics in applied physics. Vol. 43.

22. Izzeldin A.Y. 1983. An automatic direct method of interpretation of magnetic anomalies using the Hilbert transform. Bollettino di Geofisica, Vol. XXV. No. 98.

23. Jeffreys H. and Lapwood E.R. 1957. The reflection of a pulse within a sphere. Proc. Roy. Soc.( London ), Ser, A, 241, 455-479.

24. Jung K. 1961. Schwerkraftverfahren in der angewandten Geophysik, Geest and Portig.

25. Kanasewich E. R. 1981. Time sequence analysis in Geophysics. Edmonton: The University of Alberta Press.

26. Kulhanek O. and Klima K, 1970. The reliable frequency band for amplitude spectra corrections. Geophysics.J. 21, 235-242.

27. Mohan N.L., Sundararajan, and Seshagiri Rao S.V. 1982. Interpretation of some two-dimensional magnetic bodies using Hilbert transforms. Geophysics, Vol. 47, No. 3, 376-387.

28. Nabighian M.N. 1984. Toward a three-dimensional automatic interpretation of Potential field data via generalized Hilbert transforms: Fundamental relations. Geophysics, Vol. 49, No. 6, 780-786.

29. Nabighian M.N. 1972. The analytic signal of two dimensional magnetic bodies with polygonal cross section, its properties and use for automated anomaly interpretation. Geophysics 37, 507-512.

30. Nagy D. 1966. The Gravitational attraction of a Right Rectangular Prism. Geophysics, Vol. 21, 362-371.

31. Oppenheim Alan V. 1975. Digital Signal Processing. United States of America: PRENTICE-HALL, INC., Englewood Cliffs, New Jersey.

32. Read R.R. and Treitel S. 1973. The stabilization of two-dimensional Recursive filters via the discrete Hilbert transform. IEEE Transactions on Geoscience Electronics, GE 11, 153-160.

33. Shuey R.T. 1972. Application of Hilbert transforms to magnetic profiles. Geophysics 37, 1043-1045.

34. Stanley R. and Green J.M. 1976. Gravity gradients and the interpretation of the truncated plate. Geophysics 41, 1270-1276.

35. Stanley J. M. 1977. Simplified gravity interpretation by gradients. Geophysics 42, 1230-1235.

36. Stark Peter A. 1970. Introduction to numerical methods Macmillan Publishing Co.,Inc., New York.

## APPENDIX A: LIST OF COMPUTER PROGRAMS

1) DESIGNING OF 1-D HILBERT TRANSFORM

a- SUBROUTINE ABDU. b- SUBROUTINE 1-D FFT.

c- SUBROUTINE USHAH. c- SUBROUTINE GRAPH.

d- SUBROUTINE FIGER.

2) QUANTITATIVE INTERPRETATION OF 2-D MAGNETIC ANOMALY USING 1-D HILBERT TRANSFORMS

a- SUBROUTINE ROOT. b- SUBROUTINE VESH.

c- SUBROUTINE INTRVS. d- SUBROUTINE HZCCYL.

e- SUBROUTINE DIKE. f- SUBROUTINE HILB2.

3) 3-D POTENTIAL FIELD DUE TO MULTIPRISMATIC BODIES

a- SUBROUTINE MAG. b- SUBROUTINE G3.

c- SUBROUTINE DERIVE. d- SUBROUTINE HIL2D.

e- SUBROUTINE CNTOUR. f- SUBROUTINE BOUND.

Listing above programs may be available from the author or Dr. Wooil Moon, Department of geological Sciences, University of Manitoba, Winnipeg, Canada R37 2N2.